



Cairo University

VOLTAGE AND FREQUENCY CONTROL OF STAND-
ALONE DOUBLY-FED INDUCTION GENERATORS
FOR VARIABLE SPEED WIND ENERGY
CONVERSION SYSTEMS

By

Mohamed Mahmoud Anwar Mohamed Sharawy

A Thesis Submitted to the
Faculty of Engineering at Cairo University
in Partial Fulfillment of the
Requirements for the Degree of
MASTER OF SCIENCE
in
ELECTRICAL POWER AND MACHINES ENGINEERING

FACULTY OF ENGINEERING, CAIRO UNIVERSITY
GIZA, EGYPT
2016

VOLTAGE AND FREQUENCY CONTROL OF STAND-
ALONE DOUBLY-FED INDUCTION GENERATORS
FOR VARIABLE SPEED WIND ENERGY
CONVERSION SYSTEMS

By
Mohamed Mahmoud Anwar Mohamed Sharawy

A Thesis Submitted to the
Faculty of Engineering at Cairo University
in Partial Fulfillment of the
Requirements for the Degree of
MASTER OF SCIENCE
in
ELECTRICAL POWER AND MACHINES ENGINEERING

Under the Supervision of

Prof. Dr. Adel Shaltout

Prof. Dr. Naser M. B. Abdel-Rahim

.....
Professor
Electrical Power and Machines Engineering
Department
Faculty of Engineering
Cairo University

.....
Professor
Electrical Engineering Department
Faculty of Engineering at Shoubra
Benha University

FACULTY OF ENGINEERING, CAIRO UNIVERSITY
GIZA, EGYPT
2016

VOLTAGE AND FREQUENCY CONTROL OF STAND-
ALONE DOUBLY-FED INDUCTION GENERATORS
FOR VARIABLE SPEED WIND ENERGY
CONVERSION SYSTEMS

By
Mohamed Mahmoud Anwar Mohamed Sharawy

A Thesis Submitted to the
Faculty of Engineering at Cairo University
in Partial Fulfillment of the
Requirements for the Degree of
MASTER OF SCIENCE
in
ELECTRICAL POWER AND MACHINES ENGINEERING

Approved by the
Examining Committee

Prof. Dr. Adel Shaltout, Thesis Main Advisor

Prof. Dr. Naser M. B. Abdel-Rahim, Member

Prof. Dr. Mahmoud Mohamed Mahmoud Abdel-Hakim, Internal Examiner

Prof. Dr. Fahmy Metwally Ahmed Bendary, External Examiner
Prof. of Electrical Power Systems and Automatic Control – Electrical Engineering
Department – Faculty of Engineering at Shoubra – Benha University.

FACULTY OF ENGINEERING, CAIRO UNIVERSITY
GIZA, EGYPT
2016

Engineer's Name: Mohamed Mahmoud Anwar Mohamed Sharawy
Date of Birth: 28 / 12 / 1987
Nationality: Egyptian
E-mail: eng.mohamed.sharawy@gmail.com
Phone: 01220313358
Address: 14 El Fady St. – Dr. Lasheen St. – Faysal - Giza
Registration Date: 1 / 10 / 2011
Awarding Date: / / 2016
Degree: Master of Science
Department: Electrical Power and Machines Engineering



Supervisors:

Prof. Adel Shaltout
Prof. Naser M. B. Abdel-Rahim (Prof. of Power Electronics –
Electrical Engineering Department – Faculty of Engineering at
Shoubra – Benha University)

Examiners:

Prof. Fahmy Metwally Ahmed Bendary, (External examiner)
(Prof. of Electrical Power Systems and Automatic Control –
Electrical Engineering Department – Faculty of Engineering at
Shoubra – Benha University)
Prof. Mahmoud Mohamed Mahmoud Abdel-Hakim (Internal
examiner)
Prof. Adel Shaltout (Thesis main advisor)
Prof. Naser M. B. Abdel-Rahim (Member) (Prof. of Power
Electronics – Electrical Engineering Department – Faculty of
Engineering at Shoubra – Benha University)

Title of Thesis:

Voltage and Frequency Control of Stand-Alone Doubly-Fed Induction Generators for
Variable Speed Wind Energy Conversion Systems

Key Words:

Stand-Alone Wind Energy Conversion Systems; Aerodynamics of Wind Turbine;
Dynamic Modeling of Doubly-Fed Induction Generator; Indirect Vector Control;
Maximum Power Point Tracking

Summary:

Self-excited induction generators usually suffer from variable output voltage frequency and magnitude with variation of wind speed when they are used in stand-alone variable speed Wind Energy Conversion Systems (VSWECS). The doubly-fed induction generators (DFIGs) have been used in stand-alone VSWECS applications. Controlling the magnitude and frequency of the stator output voltage for DFIG achieved by controlling the rotor input voltage, magnitude and frequency. The maximum power point tracking control technique is applied to DFIG for optimum operating point.

Acknowledgments

First, I would like to thank ALLAH the beneficent, the Merciful. Praise be to ALLAH, lord of the world. ALLAH guides me along the way.

I would like to thanks my two supervisors **Prof. Dr. Adel Diaa El Din Shaltot**, Department of Electrical Power and Machines Engineering, Faculty of Engineering, Cairo University and Prof. **Dr. Naser M. B. Abdel-Rahim**, Department of Electrical Power and Machines Engineering, Faculty of Engineering at Shoubra, Benha University, for their guidance, support, motivation and encouragement to work on this thesis. Their readiness for consultation at all times, their educative comments, their concern and assistance have been invaluable.

Special thanks to the examiners who accepted arbitration this thesis and I welcome all constructive comments about this thesis.

I am very thankful to my **parent** and my **wife** for providing constant encouragement during my studies and assisting me in completion of the thesis and pushing me to be better. They have great sources of inspiration to me and I thank them from the bottom of my heart.

At last but not least, I would like to thank the staff of electrical engineering department, faculty of engineering – Cairo University, for constant support and providing place to work during thesis period. I would also like to extend my gratitude to our faculty, faculty of engineering at Shoubra- Benha University, who are with me during thick and thin.

Table of Contents

ACKNOWLEDGMENTS	I
TABLE OF CONTENTS.....	II
LIST OF TABLES	IV
LIST OF FIGURES	V
NOMENCLATURE.....	VIII
ABSTRACT	XII
CHAPTER 1 : INTRODUCTION.....	1
1.1. INTRODUCTION	1
1.2. INTRODUCTION TO WIND ENERGY CONVERSION SYSTEM.....	1
1.3. TYPES OF WIND TURBINES USED IN WECS.....	2
1.3.1. Vertical Axis Wind Turbine (VAWT)	2
1.3.2. Horizontal Axis Wind Turbine (HAWT).....	3
1.4. COMPONENTS OF HAWT USED IN WECS	4
1.5. TYPES OF ELECTRICAL GENERATORS USED IN FIXED AND VARIABLE SPEED WECS	7
1.5.1. Direct Current Generators	7
1.5.2. AC Synchronous Generators (SGs)	7
1.5.3. AC Asynchronous (Induction) Generators.....	8
1.5.3.1. Squirrel- Cage Induction Generators (SCIGs)	9
1.5.3.2. Wound-Rotor (Slip Ring) Induction Generator.....	10
1.5.3.2.1. Limited Speed WECS Mode of Operation	10
1.5.3.2.2. Variable Speed WECS Mode of Operation.....	11
1.6. STAND-ALONE WIND ENERGY CONVERSION SYSTEM	12
1.7. THESIS OBJECTIVES	13
1.8. THESIS ORGANIZATION	13
CHAPTER 2 : MODELLING OF WIND TURBINE.....	15
2.1. INTRODUCTION	15
2.2. AERODYNAMIC MODEL	16
2.3. MATLAB/ SIMULINK OF WIND TURBINE	19
CHAPTER 3 : MODELLING OF DOUBLY-FED INDUCTION GENERATOR	23
3.1. INTRODUCTION	23
3.2. DFIG MODEL EXPRESSED IN THE ABC REFERENCE FRAME	23
3.3. DFIG MODEL EXPRESSED IN THE D-Q REFERENCE FRAME	29
3.4. MATLAB/ SIMULINK MODEL FOR DFIG	38
CHAPTER 4 : CONTROL AND MPPT OF STAND-ALONE DFIG USED IN WECS	43
4.1. INTRODUCTION	43

4.2.	EFFECTS OF ROTOR INPUT VOLTAGE OF DFIG	43
4.2.1.	Sub-Synchronous Speed Mode of Operation	44
4.2.2.	Super-Synchronous Speed Mode of Operation.....	45
4.3.	FUNDAMENTALS OF VECTOR CONTROL OF INDUCTION MACHINES ...	47
4.4.	VECTOR CONTROL IMPLEMENTATION OF DFIG.....	50
4.5.	MAXIMUM POWER POINT TRACKING FOR DFIG USED IN WECS	53
4.5.1.	Characteristics of Wind Turbines for MPPT	53
4.5.1.1.	Low-Speed Region.....	54
4.5.1.2.	Moderate-Speed Region.....	54
4.5.1.3.	High-Speed Region.....	54
4.5.2.	Maximum Power Point Tracking Control Algorithms.....	55
4.5.2.1.	Algorithms Based on Wind Speed and Turbine Speed	55
4.5.2.2.	Algorithms Based on The Output Power Measurement and Calculation	56
4.5.2.3.	Algorithms Based on Power Characteristic Curve	57
CHAPTER 5 : MATLAB/SIMULINK AND SIMULATION RESULTS.....		58
5.1.	INTRODUCTION	58
5.2.	DFIG POWER FLOW.....	58
5.3.	SUB-SYNCHRONOUS SPEED MODE OF OPERATION	60
5.3.1.	Mechanical Calculations	60
5.3.2.	Electrical Calculations	61
5.3.3.	Simulation and Results.....	63
5.4.	SUPER-SYNCHRONOUS SPEED MODE OF OPERATION.....	70
5.4.1.	Mechanical Calculations	70
5.4.2.	Electrical Calculations	72
5.4.3.	Simulation and Results.....	73
5.5.	MPPT FOR DFIG BASED ON POWER CHARACTERISTIC CURVE CONTROL STRATEGY	79
5.5.1.	MATLAB/SIMULINK Model Implementation Using MPPT Algorithm	80
CHAPTER 6 : CONCLUSIONS AND FUTURE WORKS		88
6.1.	SUMMARY	88
6.2.	FUTURE WORKS.....	89
REFERENCES		90

List of Tables

Table 1.1: comparison between VAWT and HAWT	3
Table 2.1: Turbine main parameters.....	19
Table 3.1: DFIG Main Parameters	38

List of Figures

Figure 1.1: Block Diagram showing the components of WECS connected to grid (dashed item is architecture dependent)	2
Figure 1.2: Horizontal axis wind turbine (HAWT) and vertical axis wind turbine (VAWT) [3].....	4
Figure 1.3: Main Components of HAWT used in WECS	4
Figure 1.4: Contributions of main components for wind turbine in percentage terms to the overall cost.....	6
Figure 1.5: Schematic of a DC generator system	7
Figure 1.6: Configurations of synchronous generator used in variable speed WECS ((a) with gearbox and (b) without gearbox)	8
Figure 1.7: Grid connected-Fixed speed WECS using SCIGs	9
Figure 1.8: Grid connected-variable speed WECS using SCIGs	9
Figure 1.9: Stand-alone-variable speed WECS using SCIGs.....	10
Figure 1.10: Slip ring induction generator used in limited variable speed WECS.....	11
Figure 1.11: DFIG used in variable speed WECS.....	11
Figure 1.12: Proposed system of stand-alone DFIG used in variable-speed WECS.....	13
Figure 2.1: Block scheme of a variable speed wind turbine-generator systems model .	15
Figure 2.2: Different parts of wind turbine	16
Figure 2.3: Flow of air through wind turbine	16
Figure 2.4: Rotor blade and pitch angle of wind turbine.....	17
Figure 2.5: Betz Limit illustration	18
Figure 2.6: Schematic block diagram of the wind turbine MATLAB model system	20
Figure 2.7: The power Coefficient C_P as function of tip speed ratio λ and blades angle β at wind speed equal 5.5 m/s and rotor radius of 42 m	20
Figure 2.8: The power Coefficient C_P as function of tip speed ratio λ at $\beta = 0^\circ$	21
Figure 2.9: The wind turbine power P_t at low speed shaft with the rotor angular speed ω_t at different wind speed V_w	21
Figure 2.10: The wind turbine torque T_t at low speed shaft with the rotor angular speed ω_t at different wind speed V_w	22
Figure 2.11: The generator mechanical input torque T_G at high speed shaft with the rotor rotational speed N_G at different wind speed V_w	22
Figure 3.1: Ideal three-phase windings (stator and rotor) of the DFIG.....	24
Figure 3.2: DFIG electric equivalent circuit.....	25
Figure 3.3: Three phase winding machine representation.....	29
Figure 3.4: Transformed two-phase winding machine representation	29
Figure 3.5: Stationary frame a-b-c to d^s - q^s axes transformation	30
Figure 3.6: Stationary frame d^s - q^s to synchronously rotating frame d^e - q^e transformation	32
Figure 3.7: Dynamic d – q equivalent circuit of DFIG in synchronously rotating reference frame ((a) q-axis and (b) d-axis).....	37
Figure 3.8: Matlab M-file calculations for DFIG	39
Figure 3.9: Schematic block diagram for the dynamic modelling of DFIG using MATLAB/SIMULINK.....	40
Figure 3.10: Stator rms terminal output voltage V_t (V)	41
Figure 3.11: Stator output frequency F_s (Hz).....	41
Figure 3.12: Generator rotational speed N_g (rpm).....	42

Figure 3.13: Generator electromechanical torque T_g (N.m)	42
Figure 4.1: Transformation of rotor abc reference frame to d_r - q_r synchronously rotating reference frame at sub-synchronous speed	45
Figure 4.2: Transformation of rotor acb reference frame to d_r - q_r synchronously rotating reference frame at super-synchronous speed	46
Figure 4.3: Separately excited DC motor control	47
Figure 4.4: Vector-controlled induction machine	48
Figure 4.5: Implementation of vector control principle	49
Figure 4.6: Vector control of DFIG	50
Figure 4.7: Phasor diagram for stator flux oriented vector control	52
Figure 4.8: Mechanical power against rotor speed for different wind speeds	54
Figure 4.9: Ideal power curve of wind turbine	55
Figure 4.10: Tip speed ratio control of WECS	56
Figure 4.11: HCS Control Principle	56
Figure 4.12: WECS with hill climb search control	57
Figure 4.13: Power signal feedback control	57
Figure 5.1: Power flow diagram of DFIG	59
Figure 5.2: Turbine power with generator rotational speed at wind speed 5.5 m/s	60
Figure 5.3: Generator mechanical torque with rotational speed at wind speed 5.5 m/s	61
Figure 5.4: Control scheme for the stand-alone DFIG	63
Figure 5.5: SIMULINK /Model of DFIG connected to wind turbine	64
Figure 5.6: Quadrature axis of the rotor input current I_{qr} (A)	65
Figure 5.7: Direct axis of the rotor input current I_{dr} (A)	65
Figure 5.8: Instantaneous value of the rotor input voltage v_{abcr} (V)	66
Figure 5.9: Zoom view of Figure 5.8 between 24.5 and 27 second	66
Figure 5.10: Frequency of the rotor input voltage F_r (Hz)	67
Figure 5.11: Generator rotational speed N_g (rpm)	67
Figure 5.12: Rotor power P_r (W)	68
Figure 5.13: Instantaneous stator output voltage v_{abcs} (V) of DFIG	68
Figure 5.14: Stator rms terminal output voltage V_t (V)	69
Figure 5.15: Stator output frequency F_s (Hz)	69
Figure 5.16: Stator output and reference power (W)	70
Figure 5.17: Generator electromechanical torque T_g (N.m)	70
Figure 5.18: Turbine power with generator rotational speed at wind speed 7.5 m/s	71
Figure 5.19: Generator mechanical torque with rotational speed at wind speed 7.5 m/s	71
Figure 5.20: Quadrature axis of the rotor input current I_{qr} (A)	73
Figure 5.21: Direct axis of the rotor input current I_{dr} (A)	74
Figure 5.22: Instantaneous value of the rotor input voltage v_{abcr} (V)	74
Figure 5.23: Zoom view of Figure 5.22 between 25 and 30 second	75
Figure 5.24: Frequency of the rotor input voltage F_r (Hz)	75
Figure 5.25: Generator rotational speed N_g (rpm)	76
Figure 5.26: Rotor power P_r (W)	76
Figure 5.27: Instantaneous stator output voltage v_{abcs} (V) of DFIG	77
Figure 5.28: Stator rms terminal output voltage V_t (V)	77
Figure 5.29: Stator output frequency F_s (Hz)	78
Figure 5.30: Stator output and reference power (W)	78
Figure 5.31: Generator electromechanical torque T_g (N.m)	79
Figure 5.32: The wind turbine power P_t with the rotor angular speed ω_t	80
Figure 5.33: MPPT based on Power characteristic curve (Regulation of power)	80

Figure 5.34: PSF control strategy and lookup table	81
Figure 5.35: Wind speed profile	82
Figure 5.36: Quadrature axis of the rotor input current I_{qr} (A)	82
Figure 5.37: Direct axis of the rotor input current I_{dr} (A)	83
Figure 5.38: Instantaneous value of the rotor input voltage v_{abcr} (V)	83
Figure 5.39: Zoom view of Figure 5.38 between 61 and 62 second	84
Figure 5.40: Frequency of the rotor input voltage F_r (Hz)	84
Figure 5.41: Generator rotational speed N_g (rpm)	85
Figure 5.42: Rotor power P_r (W)	85
Figure 5.43: Instantaneous stator output voltage v_{abcs} (V) of DFIG	86
Figure 5.44: Stator rms terminal output voltage V_t (V)	86
Figure 5.45: Stator output frequency F_s (Hz)	87
Figure 5.46: Stator output and reference power (W)	87

Nomenclature

A	The swept surface area = πR^2 (m^2).
C_p	The power coefficient.
DFIG	Doubly-fed induction generator.
EESG	Electrically excited synchronous generator.
GSC	Grid side converter.
HAWT	Horizontal axis wind turbine.
HCS	Hill-climb search.
i_{as} , i_{bs} and i_{cs}	The stator currents of phases a, b, and c (A).
i_{ar} , i_{br} and i_{cr}	The rotor currents of phases a, b, and c (A).
i_{qs} , i_{ds} , i_{qr} , i_{dr}	The stator and rotor currents component respectively (A).
I_a	The armature current of separately excited DC motor (A)
I_f	The field current of separately excited DC motor (A).
J	The rotor inertia (Kg.m^2).
K	The machine constant (N.m/A.Wb).
LSC	Load side converter.
L_{ls}	The stator leakage inductance per phase (H).
L_{ms}	The stator magnetizing inductance per phase (H).
L_{asbs} , L_{ascs} , L_{bsas} , L_{bscs} , L_{csas} and L_{csbs}	The stator-to-stator mutual inductance per phase (H).
L_{arar} , L_{brbr} and L_{crer}	The rotor self-inductances per phase (H).
L_{lr}	The rotor leakage inductance per phase (H).
L_{mr}	The rotor magnetizing inductance per phase (H).
L_{arbr} , L_{arcr} , L_{brar} , L_{brcr} , L_{crar} and L_{crbr}	The rotor-to-rotor mutual inductance per phase (H).
L_{sr}	The peak value of mutual inductance between a stator and a rotor winding per phase (H).
MPPT	Maximum power point tracking.
mmf	Magnetomotive force.
N_G	Rotational speed of the generator shaft (rpm).
n_s	DFIG stator winding number of turns per phase.
n_r	DFIG rotor winding number of turns per phase.

PMSG	Permanent magnet synchronous generator.
PSF	Power signal feedback.
PWM	Pulse width modulation.
P_t	The extracted mechanical power from the turbine (W)
p	The number of poles of DFIG.
P	The number of pole pairs of DFIG.
P_o	The output power from doubly-fed induction generator (W)
P_s	The stator power (W).
P_r	The rotor power (W).
P_s	The stator electrical output power (W)
P_r	The rotor electrical (in/out) power (W)
P_{cus}	The stator copper losses (W).
P_{cur}	The rotor copper losses (W).
P_m	The mechanical input power (W).
P_{max}	The optimum or maximum power extracted from a wind turbine (W).
Q_s	The stator reactive power respectively (VAR).
Q_r	The rotor reactive power respectively (VAR).
RSC	Rotor side converter.
R	The radius of rotor blades (m).
R_s	The stator winding resistance per phase (Ω).
R_r	The rotor winding resistance per phase (Ω).
R_L	The load resistance per phase (Ω).
SCIG	Squirrel cage induction generator.
SG	Synchronous generator.
s	The slip.
TSR	Tip speed ratio.
T_t	The turbine torque (N.m).
T_e	The electromagnetic torque developed by the DFIG (N.m).
T	the electro-magnetic torque of separately excited DC motor (N.m).
VAWT	Vertical axis wind turbine.
VSCF	Variable speed constant frequency.

V_w	The wind speed (m/s).
v_{as}, v_{bs} and v_{cs}	The applied stator voltages (V).
v_{ar}, v_{br} and v_{cr}	The applied rotor voltages (V).
$v_{qs}, v_{ds}, v_{qr}, v_{dr}$	The stator and rotor voltages component respectively (V).
v_{ar}, v_{br}, v_{cr}	The instantaneous value of the rotor input voltages per phase (V).
V_m	The amplitude of the rotor input voltage per phase (V).
V_{cut-in}	The cut-in wind speed of wind turbine.
$V_{cut-out}$	The cut-out wind speed of wind turbine.
β	The pitch angle of the rotor blades (degree).
θ_m	The angle between the magnetic axes of stator phase winding, A, and rotor phase winding (electrical degree).
θ_e	The angle between the q-axis of the stationary reference frame fixed on the stator and rotating q-d axes (electric degree).
θ_r	The angle between the q-axis of the stationary reference frame fixed on the rotor and rotating q-d axes (electric degree).
λ	The tip speed ratio.
λ_{opt}	The optimum tip speed ratio.
ρ	The air density = 1.225 kg/m ³ at 15°C and normal pressure.
Φ	The phase shift angle (in degrees).
ψ_{as}, ψ_{bs} and ψ_{cs}	The stator fluxes (Wb. turn). The stator side electric variables.
ψ_{ar}, ψ_{br} and ψ_{cr}	The rotor fluxes (Wb. turn).
ψ_a	The armature flux of separately excited DC motor (Wb).
ψ_f	The field flux of separately excited DC motor (Wb).
ψ_{ds}	The d-axis component of the stator flux.
ψ_s	The stator flux.
WECS	Wind energy conversion system.
WRIG	Wound rotor induction generator.
ω_t	The rotor angular velocity of the turbine (mechanical rad/sec).
ω_s	The angular frequency of the voltages and currents of the stator windings (elec.rad/s).
ω_r	The angular frequency of the voltages and currents of the rotor windings (elec.rad/s).
ω_m	The rotor angular frequency of the generator (elec.rad/s).

ω_{opt}

The optimum turbine rotor speed (mec.rad/sec).

Ω_m

The mechanical angular speed of the rotor (mech.rad/s).

Abstract

Self-excited induction generators usually suffer from some problems when they are used in stand-alone variable speed Wind Energy Conversion Systems (WECS). The most prominent of these problems are the variable output voltage frequency and magnitude as the wind speed variation.

In this thesis these problems are discussed and it is shown that in order to overcome these problems the doubly-fed induction generators have been used instead of self-excited induction generators as stand-alone variable speed wind energy conversion system applications.

Firstly, the wind energy and aerodynamics of the wind turbine are studied and modelled by equations and simulated by the help of MATLAB/SIMULINK. Then the characteristics and performance of wind turbine parameters such as speed, torque and wind power are examined when it be connected with the electrical generators. Also the dynamic modelling of doubly-fed induction generator is presented by its electric equations and simulated by using the MATLAB/SIMULINK to study the electrical characteristics and performance as an electrical generator.

Secondly, both wind turbine and electric generator are connected with each other in one system. Then the performance of the system is studied for wind speed variation and associated output voltage, magnitude and frequency, power and other electric quantities of the generator. It is shown that to control the output voltage magnitude, frequency, and power, the rotor currents, frequency, and phase sequence must be controlled continuously according to wind speed variations. Indirect vector control algorithm on the rotor's electric quantity is applied to maintain both constant output voltage magnitude and frequency throughout the whole range of wind speed variations.

Finally, as the wind speed changes there is a value of maximum power that can be obtained from the doubly-fed induction generator at each value of wind speed corresponding to the maximum power curve of wind turbine. So for optimum operating point of stand-alone doubly-fed induction generator is always sought. The MATLAB/SIMULINK results of the maximum power point tracking are presented and the proposed control scheme is verified.

Keywords:

Stand-Alone Wind Energy Conversion Systems; Aerodynamics of Wind Turbine; Dynamic Modeling of Doubly-Fed Induction Generator; Indirect Vector Control; Maximum Power Point Tracking.

Chapter 1 : Introduction

1.1. Introduction

The increase of the level of environmental pollution and energy problems due to combustion of fossil fuels for electricity generation in the recent years become a major concern in people daily life. Using fossil fuel have adverse impact on the environment such as increasing CO₂ emissions, smog, acid rains, and other environmental hazards caused by usage of fossil fuels.

This problem has attracted many researchers to find new technologies to use renewable and clean energy sources for generating electricity and limit the usage of fossil fuel-based systems. Renewable energy sources are sustainable, inexhaustible and cost-effective, and cost less for remote areas.

The main types of possible renewable energy sources for an environmentally-friendly energy solutions are:

- 1- Wind energy.
- 2- Solar energy.
- 3- Tidal energy.
- 4- Biomass energy.
- 5- Hydro energy.

Wind power is one of the most important, promising renewable energy source [1]. In the past decades, electricity generation using wind power has experienced a very fast development. This thesis focuses on stand-alone wind energy conversion system employing doubly-fed induction generators.

1.2. Introduction to Wind Energy Conversion System

The wind power can be obtained by converting wind energy into another suitable form of useful energy. This method is called wind energy conversion system (WECS). It can be used for other energy requirements such as electricity generation by using wind turbine, producing mechanical power by using windmills and powering water pumping by using wind pumps. The total amount of economically extractable power available from the wind is considerably more than present human power use from all sources.

For electricity generation purposes, the WECS employs wind turbines in which the wind energy is converted to mechanical energy and is later on used as a prime mover to drive the electrical generators. WECS basically consist of three sections as shown in Figure (1.1) [2]:

- 1- Aerodynamic
- 2- Mechanical
- 3- Electrical

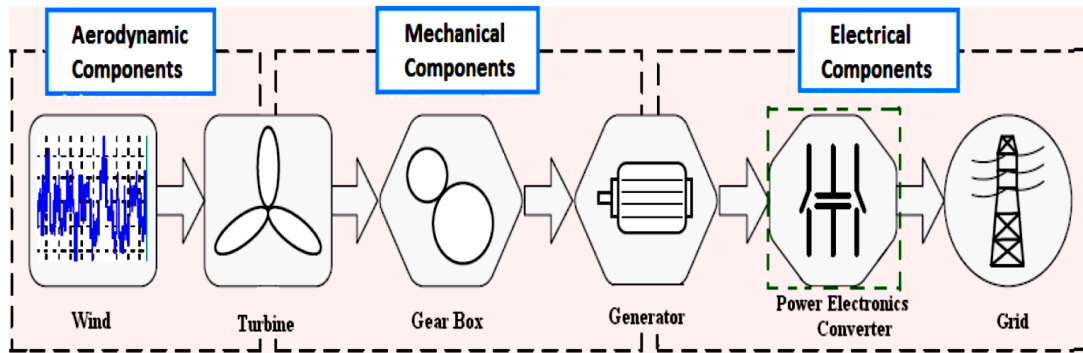


Figure 1.1: Block Diagram showing the components of WECS connected to grid (dashed item is architecture dependent)

Wind power has the following characteristics:

- 1- It is abundant, renewable, widely spread, clean, and produces no greenhouse gas emissions during operation. A one megawatt (1 MW) wind turbine for one year can displace over 1,500 tons of carbon dioxide, 6.5 tons of sulphur dioxides, 3.2 tons of nitrogen oxide, and 60 pounds of mercury (based on the U.S. average utility generation fuel mix).
- 2- Wind plants can provide a firm flow of income to landowners who lease their land for wind development, while increasing property tax revenues for local communities.
- 3- Wind applications can take many forms, including large wind farms, distributed generation, and single end-use systems. Utilities can use wind resources tactically to help reduction of load forecasting risks and trapped costs.
- 4- Energy price stability by further diversifying the energy mixture, wind energy reduces dependence on conventional fuels that are subject to price and supply instability.
- 5- Reduced dependence on imported fuels. Wind energy expenditures don't need to obtain fuels from abroad, keeping funds closer to home, and lessening reliance on foreign governments that supply these fuels.

1.3. Types of Wind Turbines Used in WECS

Wind turbines used in WECS are classified into two types from the physical setup point of view as follows [3]:

1.3.1. Vertical Axis Wind Turbine (VAWT)

The designs of vertical axis were considered superior due to their expected advantages of yaw-system is not needed because the VAWT does not need to change its direction with the change in wind speed direction hence no additional cost is required.

Also their gears and generating equipment position at the base of the wind turbine tower hence the maintenance of such type of wind turbines is very simple. However, the VAWT is not used in the commercial market due to reduced aerodynamic efficiency since much of the blade surface is close to the axis.

1.3.2. Horizontal Axis Wind Turbine (HAWT)

The HAWT is the most popular and famous type of wind turbines which employed in modern wind farms because they are capable of extracting more wind energy. The blades of HAWT rotate around an axis parallel to the wind flow the ground. The main advantages of HAWT are:

- 1- Self-starting of operation.
- 2- Having wide range of rated output power.
- 3- Comparatively low cost.

However, unlike VAWT, HAWT must be redirected continuously with every change in the wind direction. Also the difficult degree of maintenance for gear box, control systems, electrical generator and other mechanical parts as they are located in the top of the wind turbine and not in the ground as in VAWT. Table (1.1) shows a comparison between VAWT and HAWT and Figure (1.2) illustrates the difference in physical setup [4].

Table 1.1: comparison between VAWT and HAWT

Compared Item	VAWT	HAWT
1- Starting	Need to starting means	Self-starting
2- redirection according to wind direction	Redirection not needed	Redirection needed
3- Location of mechanical parts and electrical generator	At the ground surface	At the top of the tower
4- Maintenance	Easy	Difficult
5- Output power	Limited range	Wide range
6- Cost	Lower	Higher
7- Efficiency	Higher	Lower

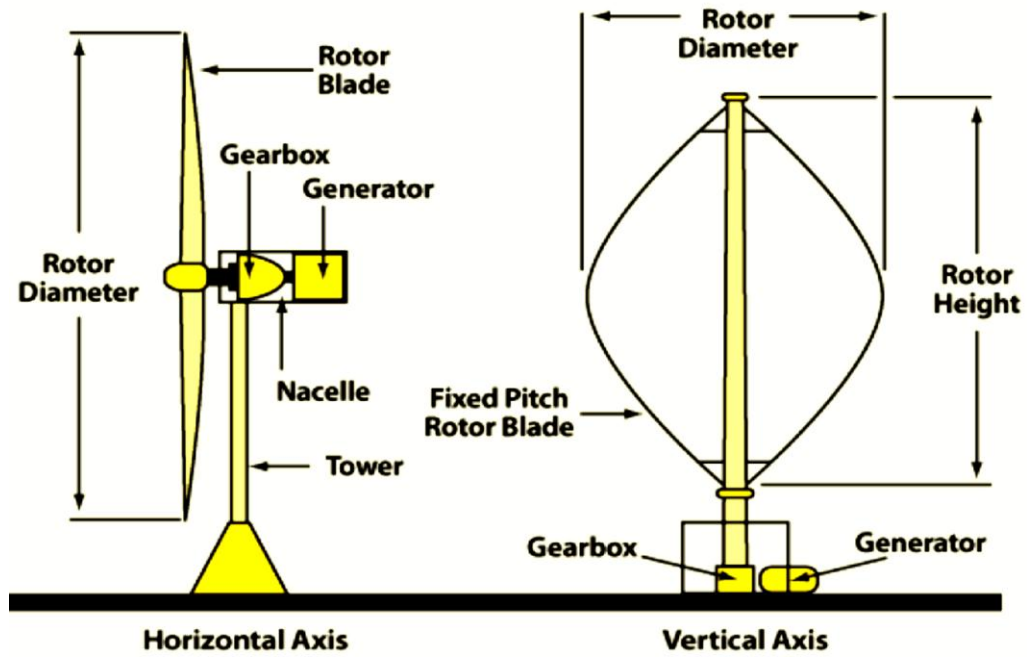


Figure 1.2: Horizontal axis wind turbine (HAWT) and vertical axis wind turbine (VAWT) [3]

1.4. Components of HAWT Used in WECS

The main components of HAWT used in WECS are shown in Figure (1.3) and important parts are listed as follows [5]:

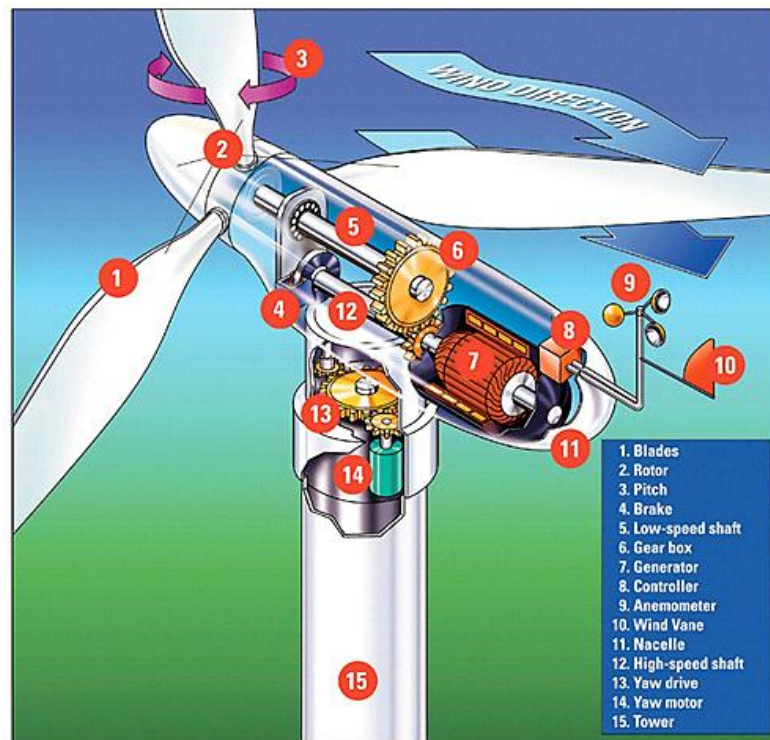


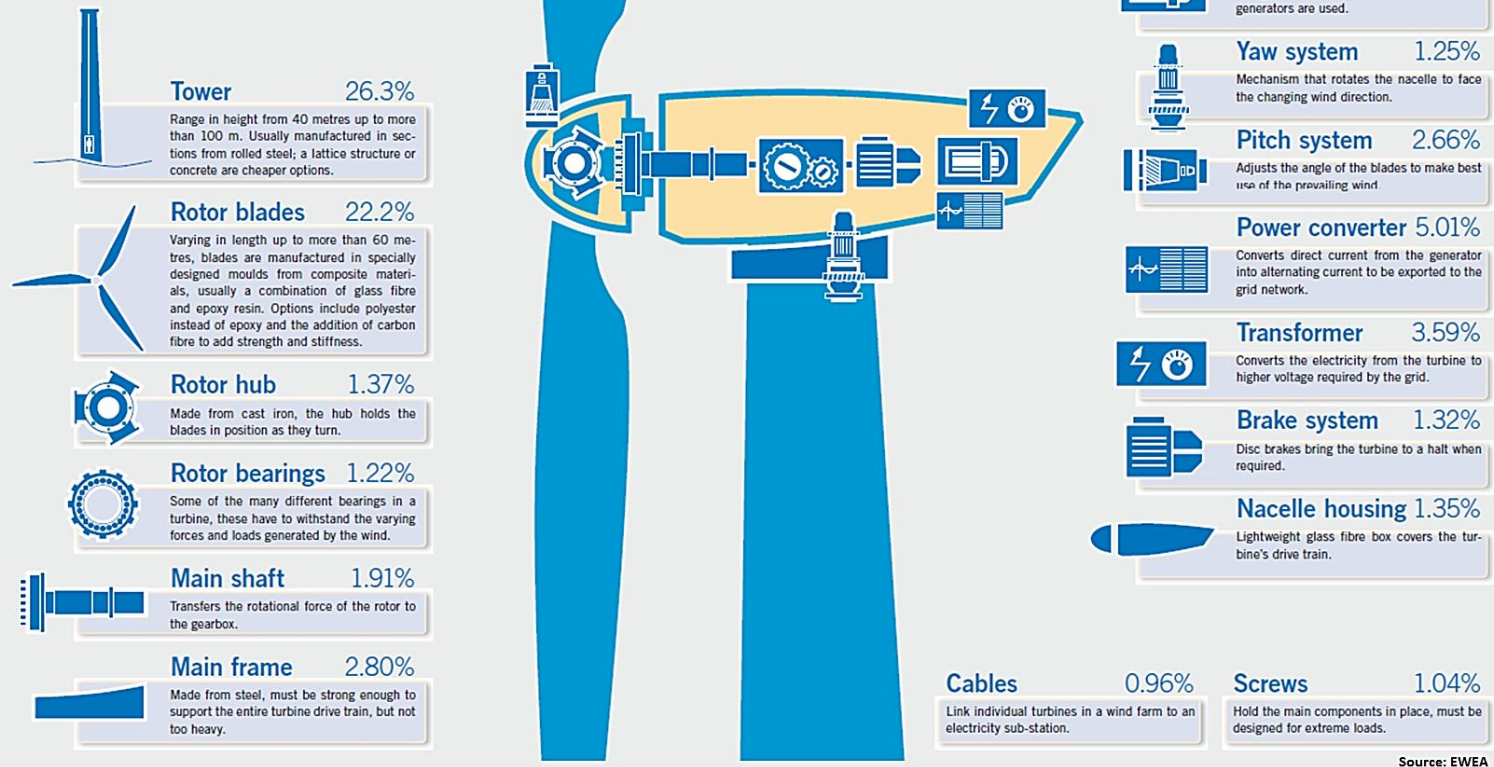
Figure 1.3: Main Components of HAWT used in WECS

- 1- Blades: They are stroked by the wind and extract power from the air stream.
- 2- Pitch and rotor: There are extensive on-board controllers which improving the efficiency of the power generation. Those controllers are called pitch angle and stall control. The control can be achieved by connecting the blades to the shaft through a hub with flanges which are designed and bolted to allow for rotor blades.
- 3- Gear box: It is used to obtain the operating speeds of the connected generators.
- 4- Drive-train (shafts, gearbox, couplings, mechanical brake, and electrical generator).
- 5- Anemometer and wind van: They are used to measure the wind direction and wind speed respectively. Hence the direction of wind turbine can be controlled according to wind direction by the mean of yaw control and when the turbine must start and stop according to wind speed.

Figure (1.4) shows the contributions of the main components for wind turbine in percentage terms to the overall cost [6].

How a wind turbine comes together

A typical wind turbine will contain up to 8,000 different components. This guide shows the main parts and their contribution in percentage terms to the overall cost. Figures are based on a REpower MM92 turbine with 45.3 metre length blades and a 100 metre tower.



Source: EWEA

Figure 1.4: Contributions of main components for wind turbine in percentage terms to the overall cost

1.5. Types of Electrical Generators Used in Fixed and Variable Speed WECS

Traditionally there are three main types of generators which can be used in fixed speed and variable speed WECS technologies [7-12]. This types are:

1.5.1. Direct Current Generators

The permanent magnet or shunt wound DC generators concept can be used in fixed and variable speed WECS. Figure (1.5) illustrates a WECS with DC generator which consists of a wind turbine, a DC generator, a full rated power inverter to convert the output electrical power from DC to AC, a controller, a transformer and the power grid. In general, because of the regular maintenance requirements and the relatively costly commutators and brushes for such that type of generator, their usage in WECS applications are limited in low power demand requirements where the load is physically near to the wind turbine place, in heating applications or in battery charging.

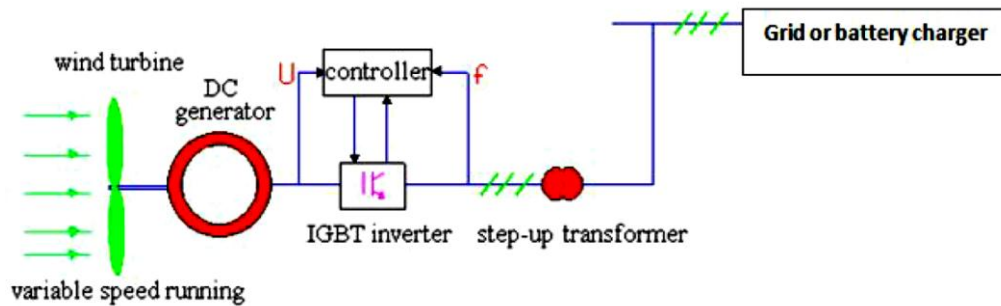


Figure 1.5: Schematic of a DC generator system

1.5.2. AC Synchronous Generators (SGs)

Because of the wide spread use of the wind turbines in recent decades, considerable efforts three-phase synchronous machines have considered as its electric generators. There are two types of AC synchronous generators which are most commonly used in variable speed WECS. The two types are: the permanent magnet synchronous generators (PMSGs) and the electrically excited synchronous generators (EESGs). The voltage and frequency in the PMSGs are controlled by the converter circuit which are connected to the output of the generators. In EESGs, The output voltage and frequency are controlled through field winding. The SGs can be connected to the wind turbine through the gear box or directly connected to the turbine as shown in Figure (1.6) (a) and (b) respectively.

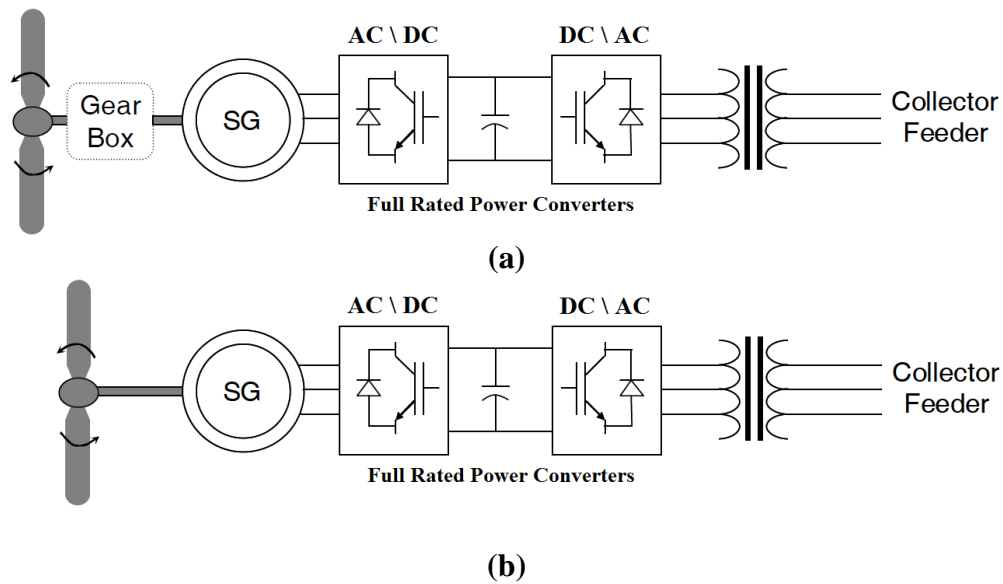


Figure 1.6: Configurations of synchronous generator used in variable speed WECS ((a) with gearbox and (b) without gearbox)

The main advantages and disadvantages of this system are listed as follows:

Advantages:

- 1- Aerodynamically efficient, can work without gearbox, less mechanical stress high power density and low mass.
- 2- Rugged, reliable and simple machines as the commutator, slip rings and brushes is eliminated in PMSGs.
- 3- The cost of PMSGs can be prohibitively high for large machines due to dispensing on the field winding and its associated power losses.
- 4- Good choice in small wind turbine generators.

Disadvantages:

- 1- Full rated power converters are needed which cause high losses and high cost.
- 2- Expensive, heavy and more complex generator.
- 3- In case PMSGs, high temperature causes demagnetization to the permanent magnets.

1.5.3. AC Asynchronous (Induction) Generators

Asynchronous generators or induction generators are the most common generators used in modern WECS. They have two main types:

- 1- Squirrel-cage induction generators (SCIGs).
- 2- Wound-rotor (slip ring) induction generator (WRIG).

These generators have the capability of using it in fixed speed or variable speed WECS. Another advantages which made those generators are suitable and more efficient from other types of generators are:

- 1- Ruggedness and simple in construction.
- 2- Low maintenance as brushes and commutators not exist (for SCIGs).
- 3- Low initial cost.
- 4- High power per unit mass of materials.

1.5.3.1. Squirrel- Cage Induction Generators (SCIGs)

When SCIGs are used in wind turbine applications, they can be used as fixed speed or variable speed WECS. Such that types of generators are not self-excited which consume rather than supplies reactive power from the system that are connected to it and supplies only real power to this system. For grid connected usage, the voltage and frequency will be provided by the grid. The reactive power requirement by the induction generators and the connected loads on the system is supplied the grid or static capacitors connected with the SCIGs. When SCIGs used in stand-alone WECS, the voltage and frequency are function of generator speed, connected capacitance (reactive power supplies) and loads. Figure (1.7) illustrates the configuration of SCIGs when they are used in grid connected or stand-alone with fixed speed (or nearly fixed) WECS.

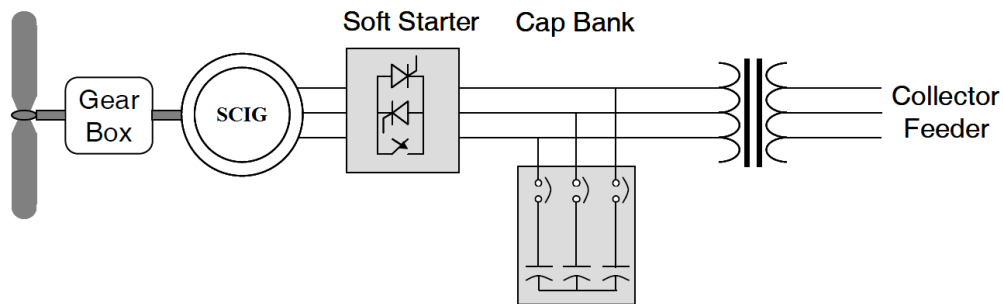


Figure 1.7: Grid connected-Fixed speed WECS using SCIGs

Operating the WECS at variable speed reduces the physical stress on the wind turbine blades and drive train, and hence improves system aerodynamic efficiency and torque transient behaviors. It can be achieved by using SCIGs with full rated power converters connected to them as shown in Figure (1.8) and Figure (1.9), [13], for grid connected and stand-alone WECS.

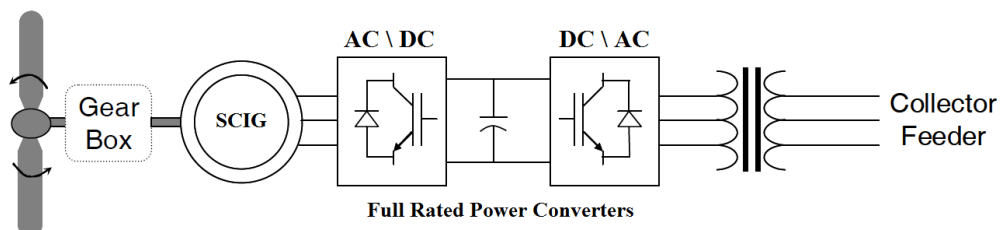


Figure 1.8: Grid connected-variable speed WECS using SCIGs

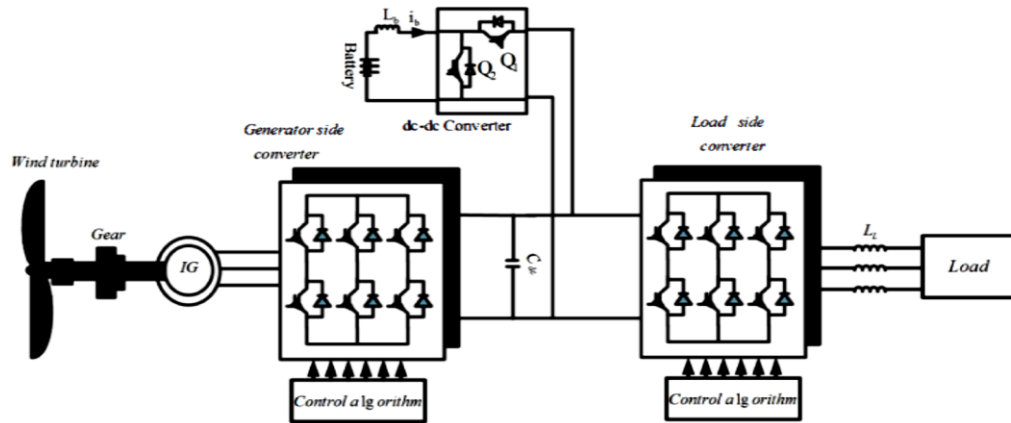


Figure 1.9: Stand-alone-variable speed WECS using SCIGs

The main drawbacks from using SCIGs in WECS are [14]:

- 1- Lower efficiency.
- 2- The large requirements of reactive power and high starting current which could be solved by using soft starter.
- 3- Maximum power can't be extracted with fixed speed operation.
- 4- Full rated power converters associated with variable speed operation.

1.5.3.2. Wound-Rotor (Slip Ring) Induction Generator

When wound-rotor or slip-ring induction generators are used in WECS, their configurations mainly depend on the mode of speed of operation, which is either limited variable speed or variable speed WECS. The two configurations are listed according to speed mode of operation as follows:

1.5.3.2.1. Limited Speed WECS Mode of Operation

In this configuration, the stator of the generator is directly connected to the grid transformer through the soft starter and capacitor bank for reactive power requirements by the generator. For the rotor circuit, variable external resistors are inserted into the rotor terminals as shown in Figure (1.10). The function of the variable resistors is to control the rotor currents in order to keep constant power operation even during gusting conditions. The variable resistors are also used to influence the machine's dynamic response during grid disturbances. This is achieved by:

- 1- A set of resistors and power electronics connected externally with the rotor to control the rotor power through the rotor currents flowing between the resistors and rotor via slip rings.
- 2- Using the Weier design, which mounts the resistors and electronics on the rotor, hence slip rings can be eliminated.

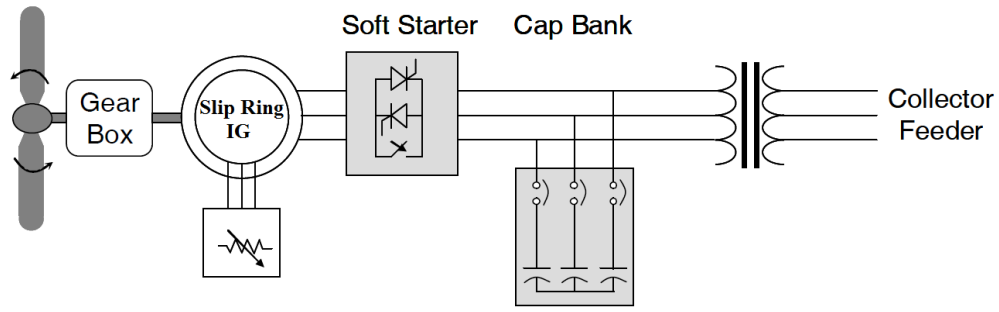


Figure 1.10: Slip ring induction generator used in limited variable speed WECS

This configuration is used when the speed of operation is variable but limited to 10% above synchronous speed.

1.5.3.2.2. Variable Speed WECS Mode of Operation

When the wound-rotor induction generator is used in WECS with a fractional rated scale power converters which are connected to the rotor circuit this machine is called Doubly Fed Induction Generator (DFIG). The stator of DFIG is directly connected to the grid or through power transformer, see Figure (1.11). The word (doubly fed) means that the active and reactive power transfer between the DFIG and the grid is done directly by the stator and by the rotor through the bidirectional power converters.

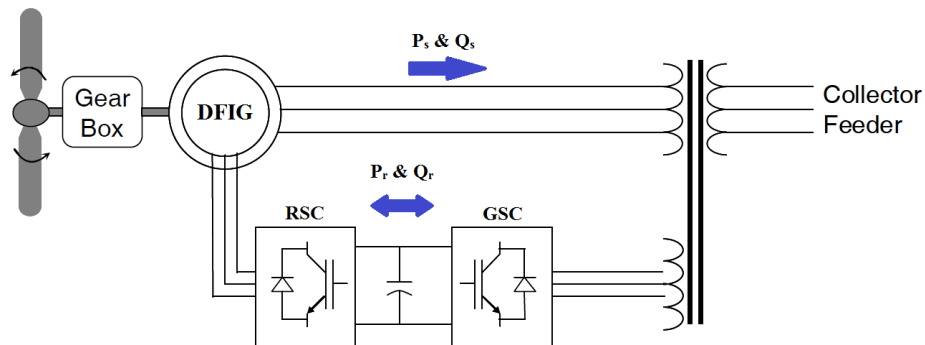


Figure 1.11: DFIG used in variable speed WECS

Recently, DFIG becomes the most widely generators which are used in variable speed constant frequency (VSCF) wind energy conversion systems [15]. This importance is due to many advantages such as:

- 1- Variable speed operation rang in sub-synchronous and super-synchronous speed ($\pm 50\%$), although narrower ranges are more common.
- 2- The separation control for active and reactive power.
- 3- Small scale power converters (30% from generator rated power), hence cost and power losses are reduced.
- 4- During super-synchronous speed mode of operation the output power (P_o) from the DFIG are from stator and rotor.
- 5- Capability of power transfer to the grid directly from the stator and (from or to) rotor via grid side converter (GSC).

- 6- The active and reactive power requirements by the generator can be controlled through the rotor side converter (RSC).
- 7- Maximum power point tracking techniques can be applied on this system due to the variable speed operation.
- 8- Power factor controllable.

The disadvantages of DFIG used in WECS are

- 1- Need for slip-rings and associated high maintenance requirements.
- 2- Need for gearbox (normally a three-stage one).
- 3- Complex control system.

In this thesis the focusing will be on DFIG used in stand-alone variable speed wind energy conversion system. As it has many advantages make the WECS more efficient and effective when applied it in renewable energy applications.

1.6. Stand-Alone Wind Energy Conversion System

Stand-alone or isolated WECS are generally used in remote areas which does not have access to the main grid. In this case, this system is able to provide cost-effective energy services and potentially provide remote communities without electrical energy services. Main issues here are the quality assurance schemes for improving the reliability of systems and reducing life cycle costs such as maintenance and repair [16].

Due to the fluctuating nature of wind power, the electric generator used in and the stand-alone variable speed WECS must be able to generate constant voltage and frequency at the terminals regardless of the shaft speed [17].

There are different generators types as mentioned before can be used in stand-alone WECS. In some systems, such as self-excited squirrel cage induction generators, the generators are able to regulate the output voltage magnitude but only at a variable frequency. Other systems employ synchronous or doubly-fed induction generators, are capable of achieving voltage and frequency regulation under variable speed operation by means of PWM converter between the generator and the load [16]. The used power converters in WECS may be either full scale size or fraction scale size from the output generated power according to the type of used generator.

In the last decade, the DFIG is considered a suitable choice as an electrical generator in stand-alone variable speed WECS. They can create cheap electric system having constant frequency and constant voltage regardless to the variable speed of operation [19]. The capacity of the rotor connected power converters depends on the operational speed range. Compared with other generators which require full capacity power converters, this system is cheaper [20].

1.7. Thesis Objectives

In this thesis, stand-alone variable speed WECS is proposed which employs a DFIG. The proposed system is shown in Figure (1.12). It consists of a stand-alone DFIG which is connected to the isolated load through the stator. The rotor of DFIG connected to battery through a rotor side converter (RSC). Also the battery is connected to the load through load side converter (LSC).

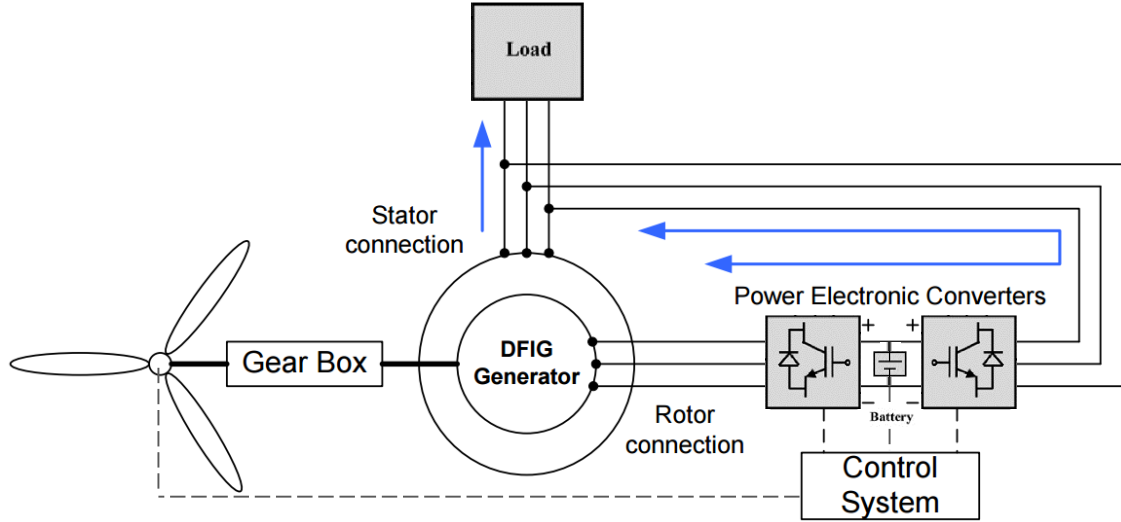


Figure 1.12: Proposed system of stand-alone DFIG used in variable-speed WECS

The objectives of this thesis are:

- 1- Obtaining constant magnitude and frequency of output voltage from DFIG irrespective of the wind speed variations.
- 2- Applying indirect vector control to control the power and voltage produced from the DFIG in both sub- and super-synchronous speed modes of operation.
- 3- Operating the DFIG at optimum operating point by using maximum power point tracking technique to extract the maximum output power available at each value of wind speed.

1.8. Thesis Organization

The thesis is organized into six chapters including the chapter of introduction. Each chapter is different from the other and is described along with the necessary theory required to comprehend it.

Chapter 1 (Introduction) presents the introduction of the renewable energy, components of wind energy conversion system, types of wind turbines, types of generators used in wind energy conversion system, stand-alone wind energy conversion system, thesis objectives and thesis organization.

Chapter 2 (Modelling of Wind Turbine) shows the aerodynamics of wind turbines, power, torque and speed equations, different characteristics of wind turbine, and modelling of the wind turbine using MATLAB/SIMULINK.

Chapter 3 (Modelling of Doubly-Fed Induction Generator) dealing with the DFIG in dynamic model. First, the equations of DFIG are expressed in **ABC** reference frame model. Then for simplifying they are expressed in d-q synchronously rotating reference frame model. Finally MATLAB/SIMULINK model is presented for DFIG.

Chapter 4 (Control and MPPT of Stand-Alone DFIG used in WECS) presents the effect of rotor input voltage and frequency in sub-synchronous and super-synchronous speed modes of operation, explains the indirect vector control method which applied to the stand-alone DFIG to control the magnitude and frequency of the output voltage and power transfer from the generator to the loads, discusses the characteristics of wind turbine for maximum power point tracking, different maximum point tracking control algorithms.

Chapter 5 (MATLAB/SIMULINK and Simulation Results), implements MATLAB/SIMULINK model for the controlling method in sub-synchronous and super-synchronous speed modes of operation and final results and figures are obtained finally the maximum power point tracking control is achieved by using power characteristic curve strategy by the help of MATLAB/SIMULINK model and the final results are obtained which shows that the tracking is achieved.

Chapter 7 (Conclusions and Future Works) concludes the work performed. The future works that can be done is mentioned.

Chapter 2 : Modelling of Wind Turbine

2.1. Introduction

The wind energy conversion systems (WECSs) are used to convert kinetic wind energy into electrical energy. Various types of electrical generators like doubly-fed induction generators (DFIGs) or squirrel cage induction generators (SCIGs) and feed this energy into the utility grid. Other configuration is used for isolated area and isolated loads in remote area. Research model of these systems comprises wind turbine, the electrical generator, grid or isolated loads system and control system which governs operation of these systems.

Referring to Figure (2.1), the WECS model comprises the following subsystems [10]:

- 1- Aerodynamic system model, which evaluates the turbine torque, T_t , as a function of wind speed (V_w) and the turbine angular speed (ω_t).
- 2- Electrical machine and power converters which transform the wind turbine power into electrical power.
- 3- Grid or isolated loads model which is connected at the generator terminals.
- 4- Control system, evaluates the generator torque, active and reactive power references as a function of wind speed and grid or load voltage.

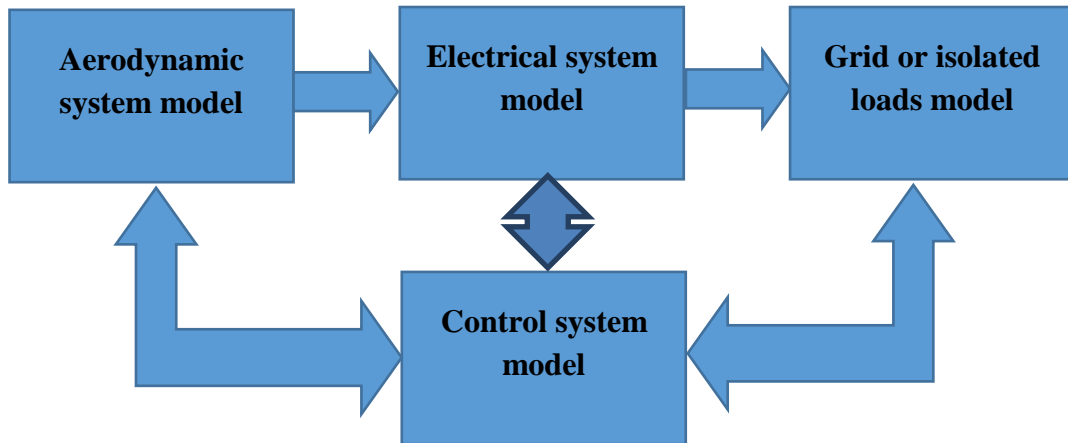


Figure 2.1: Block scheme of a variable speed wind turbine-generator systems model

In this chapter, the first subsystem is discussed and last three subsystems will be discussed in the next chapters in details.

2.2. Aerodynamic Model

The aerodynamic model represents how the power can be extracted from the wind turbine rotor, calculating the mechanical power and the output torque as a function of the air flow on the blades. The conversion of power takes place by the aerodynamic power extracted from the wind stream which causes the turbine blades to rotate and hence turning the rotor of the turbine. Then the electrical generator which is connected to the shaft of the turbine by the mean of gear box transforms the rotational mechanical power to electrical power as shown in Figures (2.2) and (2.3).

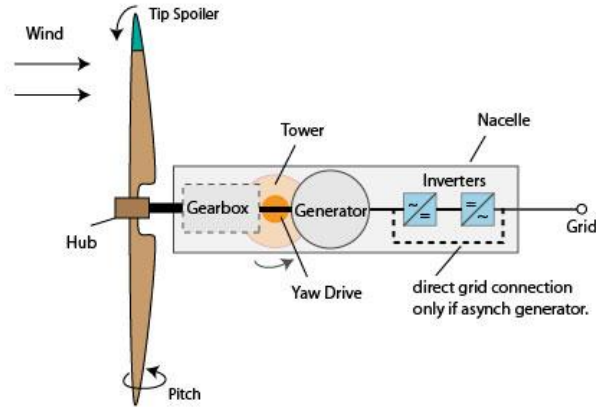


Figure 2.2: Different parts of wind turbine

The wind power is given by [10]:

$$P_w = \frac{1}{2} \rho A V_w^3 \quad (2.1)$$

Where

- V_w is the wind speed (m/s).
- A is the swept surface area = πR^2 (m²).
- R is the radius of rotor blades (m).
- ρ is the air density = 1.225 kg/m³ at 15°C and normal pressure.

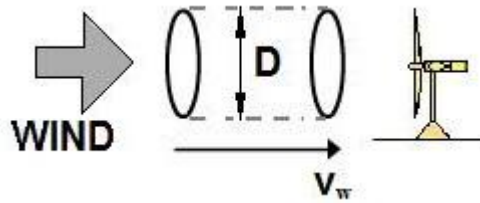


Figure 2.3: Flow of air through wind turbine

The effective power or mechanical power P_t (W) which is transferred to the wind turbine rotor is reduced by the power coefficient C_P [21, 22]. Then the extracted mechanical power from the turbine can thus be expressed follows [10, 18, 23, 24]:

$$P_t = \frac{1}{2} \rho \pi R^2 V_w^3 C_P \quad (2.2)$$

The power coefficient C_P is a dimensionless factor which indicates the ability of the wind turbine to convert the kinetic energy stored in the air to mechanical energy. For a certain wind turbine this coefficient is function of various factors such as wind speed, the speed of rotation of the wind turbine, and the pitch angle of the rotor blades which is defined as the angle between the plane of rotation and the blade cross-section chord β , see Figure (2.4). Usually the power coefficient C_P is determined as function of the tip speed ratio λ which is expressed as [21-23]:

$$\lambda = \frac{\omega_t R}{V_w} \quad (2.3)$$

Where

- ω_t is the rotor angular velocity of the turbine (mechanical rad/sec).
- R the rotor radius of the blades (m).
- V_w the wind speed (m/s).

The maximum value of C_P is defined by the Betz limit, which states that a turbine can never extract more than 59.3% of the power from an air stream as shown in Figure (2.5). In reality, wind turbine rotors have maximum C_P values in the range 25-45% [10].

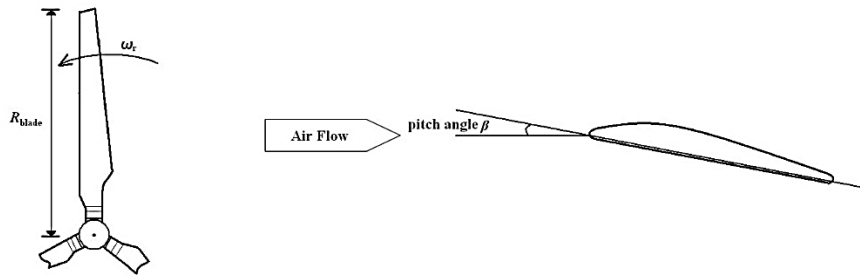


Figure 2.4: Rotor blade and pitch angle of wind turbine

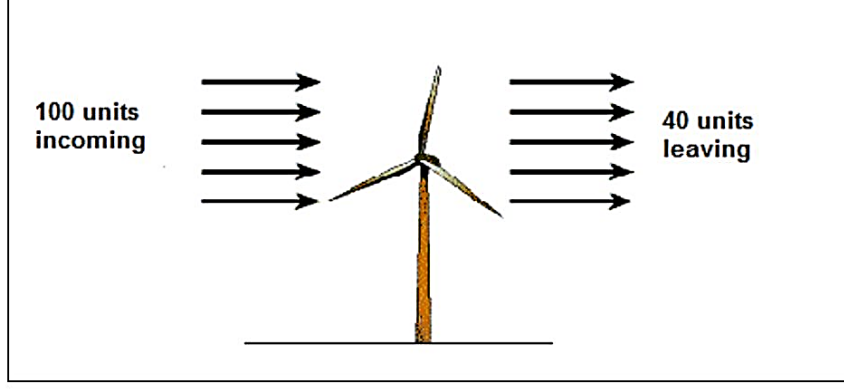


Figure 2.5: Betz Limit illustration

As mentioned in a previous section the C_P in a wind turbine mechanical equation can be approximated by means of analytical expressions and different possible non-linear equations as a function of tip speed ratio λ and the pitch angle of the blades β . For a wind turbine, the most simple and commonly used way to describe the $C_P(\lambda, \beta)$ as follows [10, 18, 22]:

$$C_P(\lambda, \beta) = C_1 (C_2 - C_3\beta - C_4\beta^2 - C_5) e^{-C_6} \quad (2.4)$$

Where

$C_1 = 0.5$, $C_2 = 116 * \lambda_i$, $C_3 = 0.4$, $C_4 = 0$, $C_5 = 5$, $C_6 = 21 * \lambda_i$ and:

$$\lambda_i = \frac{1}{\lambda + .08\beta} - \frac{0.035}{1 + \beta^3} \quad (2.5)$$

The last expressions depend mainly on the geometric characteristics of the blades. These are tailored to the particular site characteristics, the desired nominal power and control type (pitch or stall), and operation (variable or fixed speed) of the turbine [10]. The dependence of C_P on λ and β , the maximum value of C_P can be reached and maintained by controlling the pitch angle of the turbine blades and rotor speed for each wind speed.

The turbine torque can be expressed as follows [10, 23]:

$$T_t = \frac{P_t}{\omega_t} = \frac{\rho \pi R^2 V_w^3}{2 \omega_t} C_P \quad (2.6)$$

2.3. MATLAB/SIMULINK of Wind Turbine

The basic data for a 2.4 MW turbine used in simulation as follows [10]:

The radius of the blade is in the range of 40 - 45 meters, depending on the wind class of the turbine. The nominal power is extracted for a wind speed between 11 and 13 m/s. The rotor speed (low speed axis) is in the range of 8.5 to 20 rpm. . The gearbox ratio is around 100 for a two pole pairs and 50 Hz DFIG. The turbine parameters are listed in Table (2.1).

Table 2.1: Turbine main parameters

Parameter	Value
Radius of rotor blades	42 m
Nominal wind speed	12.5 m/s
Variable speed ratio (minimum–maximum turbine speed)	9 – 18 rpm
Optimum tip speed ratio λ_{opt}	7.2
Maximum power coefficient C_{pmax}	0.44
Air density ρ	1.1225 Kg/m ³

By using MATLAB/SIMULINK the wind turbine model can be presented as shown in Figure (2.6).

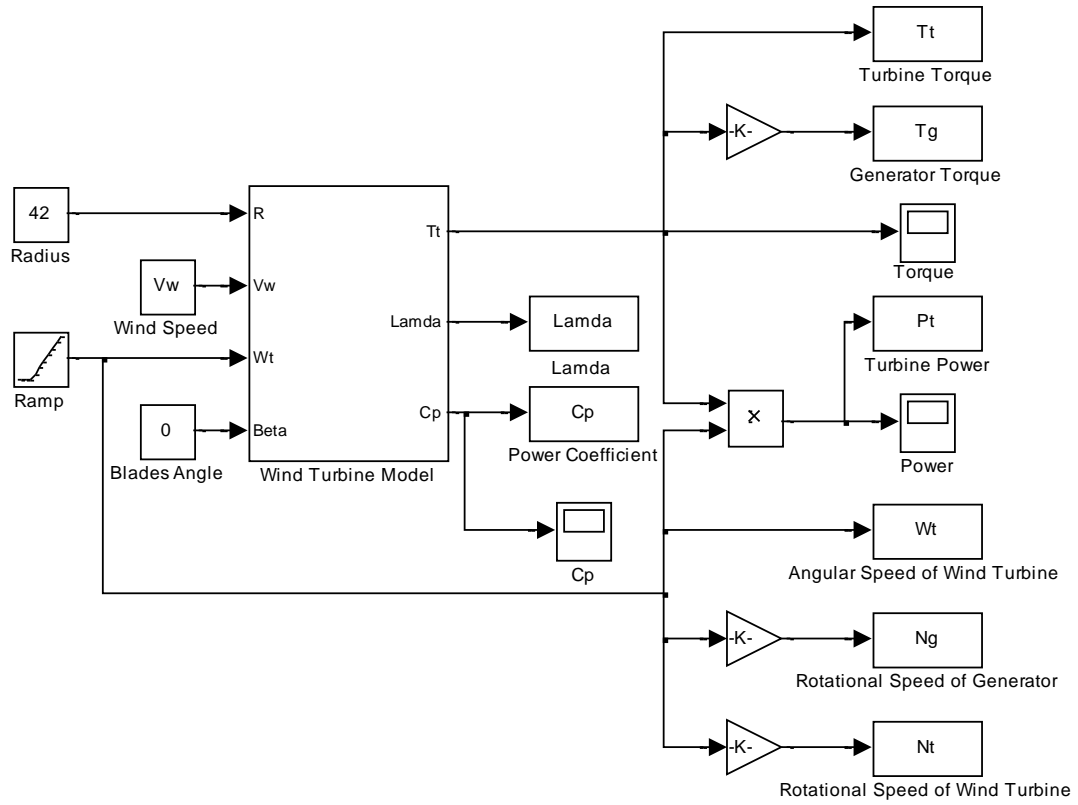


Figure 2.6: Schematic block diagram of the wind turbine MATLAB model system

Figure (2.7) shows a group of typical $C_p - \lambda$ curves for different values of β at wind speed equal 5.5 m/s and rotor radius of 42 m. There is always a maximum value for C_p at certain wind speed.

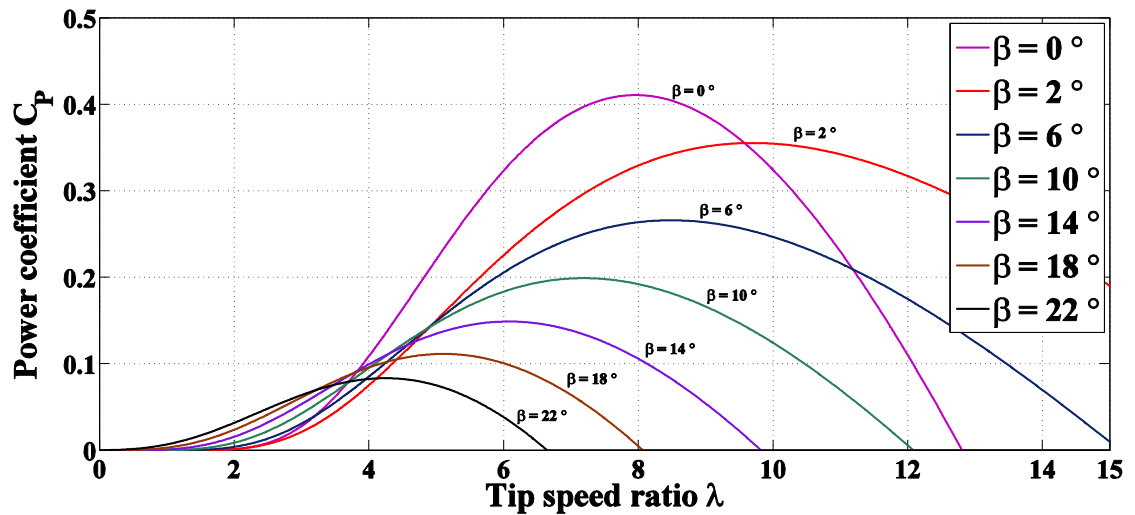


Figure 2.7: The power Coefficient C_p as function of tip speed ratio λ and blades angle β at wind speed equal 5.5 m/s and rotor radius of 42 m

Figure (2.8) shows the relationship between the power coefficient as a function of tip speed ratio from Equations (2.4) and (2.5) at $\beta = 0^\circ$ and wind speed of 5.5 m/s notice that the maximum power coefficient is about 0.411 and the optimum tip speed ratio is about 7.9.

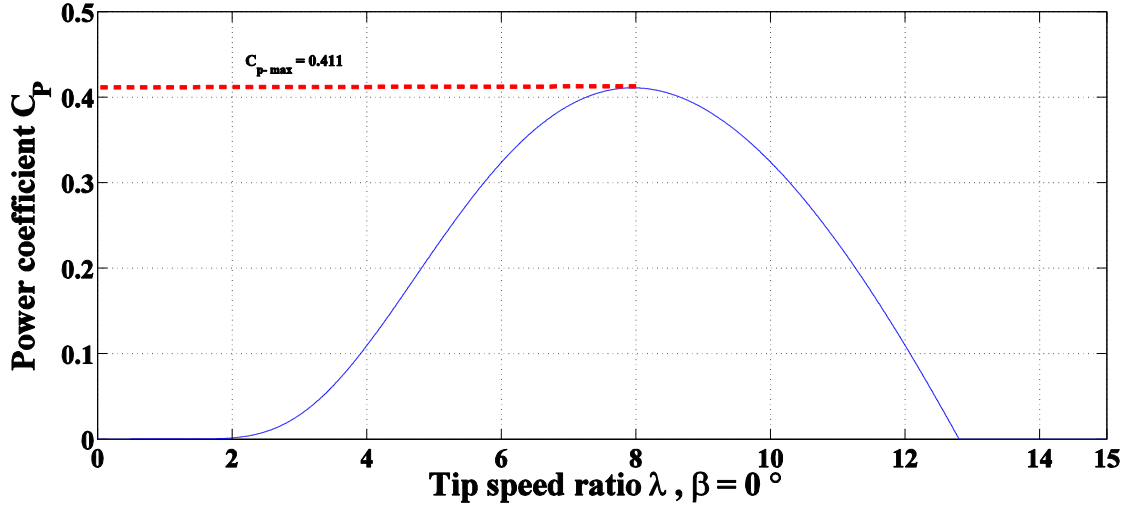


Figure 2.8: The power Coefficient C_P as function of tip speed ratio λ at $\beta = 0^\circ$

The curves in Figure (2.9) and Figure (2.10) shows the turbine power and torque as a function of rotor angular speed at different wind speed, along with the typical speed limits (9 and 18 rpm) and the nominal power (2.4 MW).

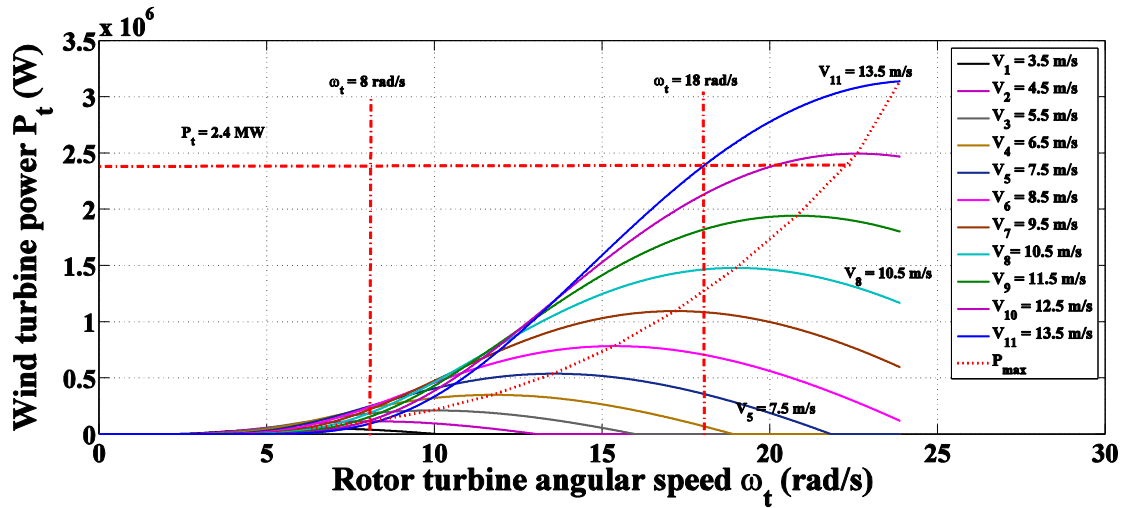


Figure 2.9: The wind turbine power P_t at low speed shaft with the rotor angular speed ω_t at different wind speed V_w

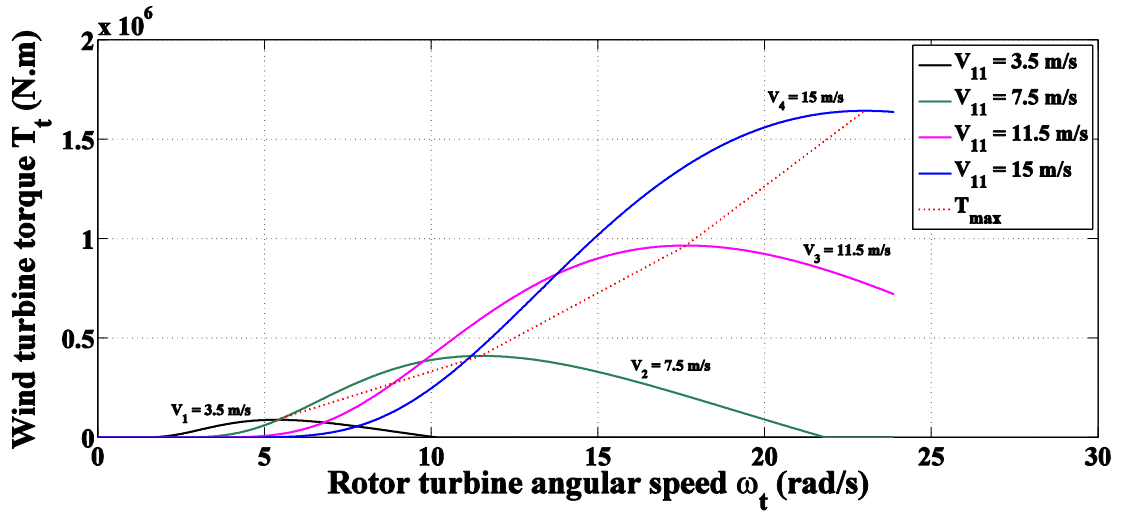


Figure 2.10: The wind turbine torque T_t at low speed shaft with the rotor angular speed ω_t at different wind speed V_w

The next curves in Figure (2.11) show the generator mechanical input torque as a function of rotational speed of the generator shaft N_G (rpm) at different wind speed, along with the typical speed limits (900 and 1800 rpm).

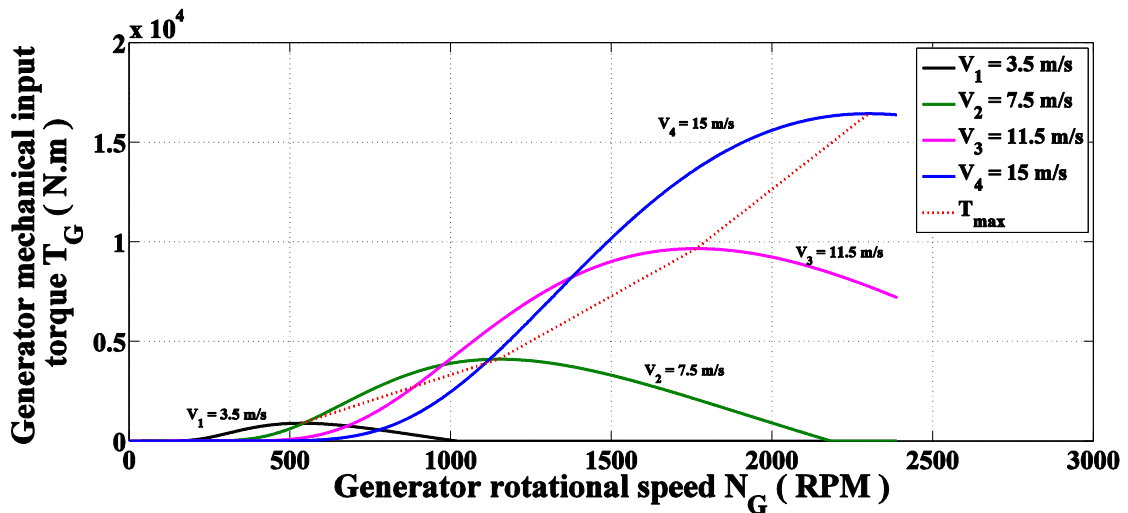


Figure 2.11: The generator mechanical input torque T_G at high speed shaft with the rotor rotational speed N_G at different wind speed V_w

Chapter 3 : Modelling of Doubly-Fed Induction Generator

3.1. Introduction

The d-q dynamic model of DFIG would be very beneficial in terms for studying the behavior under sub-synchronous and super-synchronous modes of operation and applying the vector control approach to control the output active and reactive power [25].

To achieve this, it is necessary to understand the behavior of the wound rotor induction machine. In this section, the winding arrangement, equivalent circuit and principle of operation of a wound rotor machine are described, along with the supporting equations. The equations show that in the stationary **abc** reference frame, machine parameters such as inductance are time-varying. The equivalent circuit in the stationary **abc** reference frame is transformed using the Park transform to the equivalent in the rotating q-d reference frame, to make the machine parameters such as inductance time-invariant. In the q-d reference frame, the q-axis and d-axis are 90° degrees apart and hence decoupled [26].

The following assumptions are made to derive the dynamic model [26]:

- 1- Uniform air gap.
- 2- Symmetrical rotor and stator windings. With sinusoidally distributed magnetomotive force (mmf).
- 3- Inductance vs. rotor position is sinusoidal.
- 4- Saturation and parameter changes are neglected.

3.2. DFIG Model Expressed in The ABC Reference Frame

Figure (3.1) shows a wound rotor induction generator with symmetrical three-phase, two pole pairs and star connected windings. The Figure shows the simplified and idealized DFIG model. It has three windings in the stator with n_s turns for each phase and are displaced by 120° electrical degrees from each other and three windings in the rotor have n_r turns for each phase and are also displaced by 120° electrical degrees from each other. The angle between the magnetic axes of stator phase winding, A, and rotor phase winding, a, is θ_m in electrical degree. Note that θ_m is the electrical rotor position at any instant obtained and is given by multiplying the mechanical rotor position by the number of pole pairs of the machine [26].

The relation between the stator angular frequency and the rotor angular frequency is:

$$\omega_s = \omega_r + \omega_m \quad (3.1)$$

Where

ω_s is the angular frequency of the voltages and currents of the stator windings (elec.rad/s).

ω_r is the angular frequency of the voltages and currents of the rotor windings (elec.rad/s).

ω_m is the rotor angular frequency of the generator (elec.rad/s) and given by:

$$\omega_m = P\Omega_m \quad (3.2)$$

Where

P is the number of pole pairs.

Ω_m is the mechanical angular speed of the rotor (mech.rad/s).

Figure (3.1) [10] indicate the direction of both ω_m and θ_m in the counter-clockwise direction. These windings are an ideal representation of the real machine, which helps to derive an equivalent electric circuit, as shown in Figure (3.2) [10].

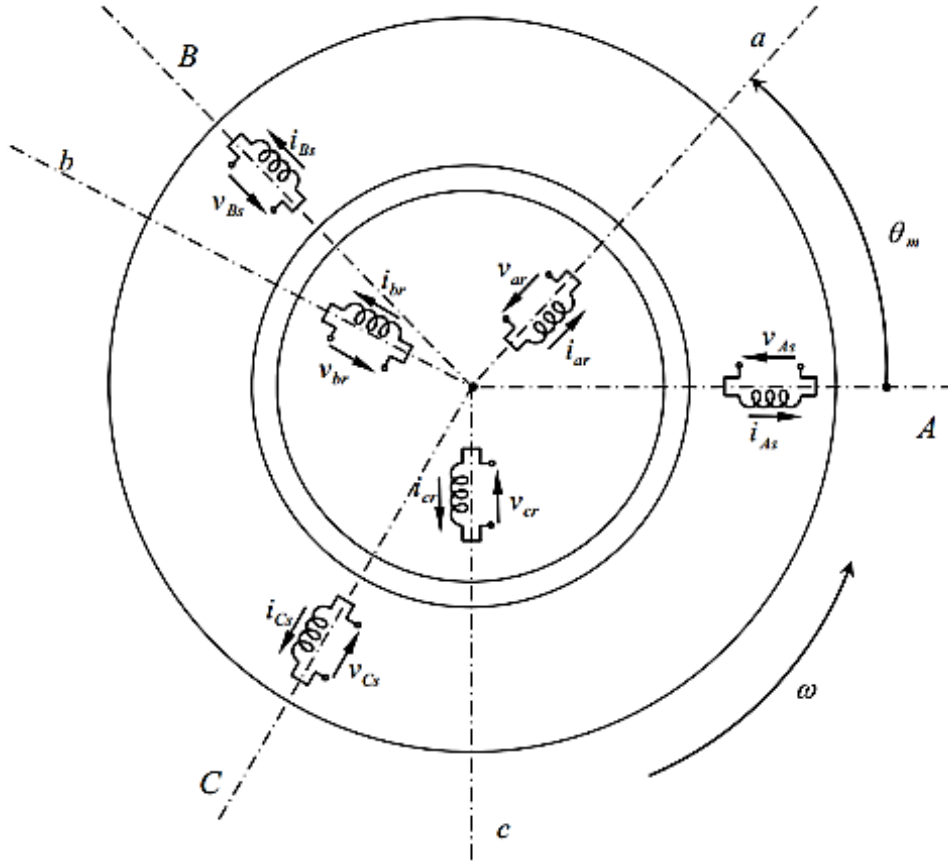


Figure 3.1: Ideal three-phase windings (stator and rotor) of the DFIG

Under this idealized model, the instantaneous stator voltages, current, and fluxes of the machine can be described by the Equations (3.3) to (3.8) [10]. As the DFIG has different turns in the stator and rotor, all parameters and variables of the rotor circuit are referred to the stator circuit.

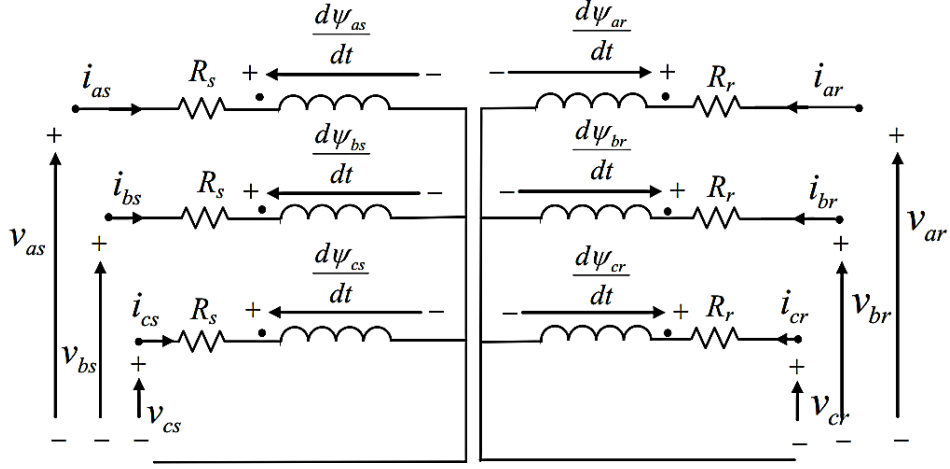


Figure 3.2: DFIG electric equivalent circuit

The terminal voltages of the stator and rotor windings can be expressed as the sum of the voltage drops in resistances and rates or change of flux linkages. The equations are expressed as follows in motor sign [27]:

Staror voltage equations

$$v_{as} = R_s i_{as} + \frac{d\psi_{as}}{dt} \quad (3.3)$$

$$v_{bs} = R_s i_{bs} + \frac{d\psi_{bs}}{dt} \quad (3.4)$$

$$v_{cs} = R_s i_{cs} + \frac{d\psi_{cs}}{dt} \quad (3.5)$$

Where

R_s is the stator winding resistance per phase (Ω).
 i_{as} , i_{bs} and i_{cs} are the stator currents of phases a, b, and c (A).
 v_{as} , v_{bs} and v_{cs} are the applied stator voltages (V)
 ψ_{as} , ψ_{bs} and ψ_{cs} are the stator fluxes (Wb. turn).

The stator side electric variables, at steady state, have a constant sinusoidal angular frequency, ω_s (elec.rad/s), which is the angular frequency imposed by the grid.

Rotor voltage equations

$$v_{ar} = R_r i_{ar} + \frac{d\psi_{ar}}{dt} \quad (3.6)$$

$$v_{br} = R_r i_{br} + \frac{d\psi_{br}}{dt} \quad (3.7)$$

$$v_{cr} = R_r i_{cr} + \frac{d\psi_{cr}}{dt} \quad (3.8)$$

Where

R_r is the rotor winding resistance per phase (Ω).
 i_{ar} , i_{br} and i_{cr} are the rotor currents of phases a, b, and c (A).
 v_{ar} , v_{br} and v_{cr} are the applied rotor voltages (V)
 ψ_{ar} , ψ_{br} and ψ_{cr} are the rotor fluxes (Wb. turn).

The rotor side electric magnitudes, at steady state, have a constant sinusoidal angular frequency, ω_r (elec.rad/s), the angular frequency imposed by the rotor side converter.

Stator flux linkage equations

$$\psi_{as} = L_{asas} i_{as} + L_{asbs} i_{bs} + L_{ascs} i_{cs} + L_{asar} i_{ar} + L_{asbr} i_{br} + L_{ascr} i_{cr} \quad (3.9)$$

$$\psi_{bs} = L_{bsas} i_{as} + L_{bsbs} i_{bs} + L_{bscs} i_{cs} + L_{bsar} i_{ar} + L_{bsbr} i_{br} + L_{bscr} i_{cr} \quad (3.10)$$

$$\psi_{cs} = L_{csas} i_{as} + L_{csbs} i_{bs} + L_{cses} i_{cs} + L_{csar} i_{ar} + L_{csbr} i_{br} + L_{cscr} i_{cr} \quad (3.11)$$

Rotor flux linkage equations

$$\psi_{ar} = L_{aras} i_{as} + L_{arbs} i_{bs} + L_{arcs} i_{cs} + L_{arar} i_{ar} + L_{arbr} i_{br} + L_{arcr} i_{cr} \quad (3.12)$$

$$\psi_{br} = L_{bras} i_{as} + L_{brbs} i_{bs} + L_{brcs} i_{cs} + L_{brar} i_{ar} + L_{brbr} i_{br} + L_{brcr} i_{cr} \quad (3.13)$$

$$\psi_{cr} = L_{cras} i_{as} + L_{crbs} i_{bs} + L_{crcs} i_{cs} + L_{crar} i_{ar} + L_{crbr} i_{br} + L_{crer} i_{cr} \quad (3.14)$$

L_{asas} , L_{bsbs} and L_{cses} are the stator self-inductances per phase which are the same as follows:

$$L_{asas} = L_{bsbs} = L_{cses} = L_{ls} + L_{ms} \quad (3.15)$$

Where

L_{ls} is the stator leakage inductance per phase (H) which is about 5% to 10% of the maximum self-inductance.

L_{ms} is the stator magnetizing inductance per phase (H).

$L_{asbs}, L_{ascs}, L_{bsas}, L_{bscs}, L_{csas}$ and L_{csbs} are the stator-to-stator mutual inductance per phase which are as follows:

$$L_{asbs} = L_{ascs} = L_{bsas} = L_{bscs} = L_{csas} = L_{csbs} = -\frac{1}{2}L_{ms} \quad (3.16)$$

L_{arar}, L_{brbr} and $L_{cr cr}$ are the rotor self-inductances per phase which are the same as follows:

$$L_{arar} = L_{brbr} = L_{cr cr} = L_{lr} + L_{mr} \quad (3.17)$$

Where

L_{lr} is the rotor leakage inductance per phase which about 5% to 10% of the maximum self-inductance (H).

L_{mr} is the rotor magnetizing inductance per phase (H).

$L_{arbr}, L_{arcr}, L_{brar}, L_{brcr}, L_{crar}$ and L_{crbr} are the rotor-to-rotor mutual inductance per phase which are the same as follows:

$$L_{arbr} = L_{arcr} = L_{brar} = L_{brcr} = L_{crar} = L_{crbr} = -\frac{1}{2}L_{mr} \quad (3.18)$$

The mutual inductances per phase between a stator and a rotor winding function of rotor position, θ_m , and they are assumed to be sinusoidal functions because of the assumption of sinusoidal distributed mmf in winding [26]. Due to the symmetry in the windings and construction, the mutual inductances between one stator and one rotor winding to be the same whether they are viewed from the stator or the rotor [26]. They can be expressed as follows:

$$L_{asar} = L_{bsbr} = L_{cs cr} = L_{sr} \cos \theta_m \quad (3.19)$$

$$L_{asbr} = L_{bscr} = L_{cs ar} = L_{sr} \cos(\theta_m + 120^\circ) \quad (3.20)$$

$$L_{ascr} = L_{bsar} = L_{cs br} = L_{sr} \cos(\theta_m - 120^\circ) \quad (3.21)$$

$$L_{aras} = L_{brbs} = L_{cr cs} = L_{sr} \cos \theta_m \quad (3.22)$$

$$L_{arbs} = L_{brcs} = L_{cr as} = L_{sr} \cos(\theta_m - 120^\circ) \quad (3.23)$$

$$L_{arcs} = L_{bras} = L_{cr bs} = L_{sr} \cos(\theta_m + 120^\circ) \quad (3.24)$$

Where

L_{sr} is the peak value of mutual inductance between a stator and a rotor winding per phase (H). The equations previous can be simplified as follows:

$$\begin{bmatrix} v_{abcs} \\ v_{abcr} \end{bmatrix} = \begin{bmatrix} R_{ss} & 0 \\ 0 & R_{rr} \end{bmatrix} \begin{bmatrix} i_{abcs} \\ i_{abcr} \end{bmatrix} + \frac{d}{dt} \begin{bmatrix} L_{ss} & L_{sr} \\ L_{rs} & L_{ss} \end{bmatrix} \begin{bmatrix} i_{abcs} \\ i_{abcr} \end{bmatrix} \quad \text{V} \quad (3.25)$$

Where

$$\mathbf{R}_{ss} = \begin{bmatrix} R_s & 0 & 0 \\ 0 & R_s & 0 \\ 0 & 0 & R_s \end{bmatrix} \quad \Omega \quad (3.26)$$

$$\mathbf{R}_{rr} = \begin{bmatrix} R_r & 0 & 0 \\ 0 & R_r & 0 \\ 0 & 0 & R_r \end{bmatrix} \quad \Omega \quad (3.27)$$

$$\mathbf{L}_{ss} = \begin{bmatrix} L_{ls} + L_{ms} & -\frac{1}{2}L_{ms} & -\frac{1}{2}L_{ms} \\ -\frac{1}{2}L_{ms} & L_{ls} + L_{ms} & -\frac{1}{2}L_{ms} \\ -\frac{1}{2}L_{ms} & -\frac{1}{2}L_{ms} & L_{ls} + L_{ms} \end{bmatrix} \quad \mathbf{H} \quad , \quad (3.28)$$

$$\mathbf{L}_{rr} = \begin{bmatrix} L_{lr} + L_{mr} & -\frac{1}{2}L_{mr} & -\frac{1}{2}L_{mr} \\ -\frac{1}{2}L_{mr} & L_{lr} + L_{mr} & -\frac{1}{2}L_{mr} \\ -\frac{1}{2}L_{mr} & -\frac{1}{2}L_{mr} & L_{lr} + L_{mr} \end{bmatrix} \quad \mathbf{H} \quad (3.29)$$

$$\mathbf{L}_{sr} = L_{ms} \begin{bmatrix} \cos \theta_m & \cos(\theta_m + 120^\circ) & \cos(\theta_m - 120^\circ) \\ \cos(\theta_m - 120^\circ) & \cos \theta_m & \cos(\theta_m + 120^\circ) \\ \cos(\theta_m + 120^\circ) & \cos(\theta_m - 120^\circ) & \cos \theta_m \end{bmatrix} \quad \mathbf{H} \quad (3.30)$$

$$\mathbf{L}_{rs} = [\mathbf{L}_{sr}]^T \quad \mathbf{H} \quad (3.31)$$

From Eq. (3.25), the inductance matrix in the **abc** model of DFIG depends on the instantaneous rotor position, θ_m , and hence time dependent. The time varying inductances increases the mathematical complexity of the machine model and computation time needed to solve for the system drastically increases because the inductance matrix needs to be calculated at each time step. In order to eliminate this complexity, the variables in the stator and rotor associated with the three phase **abc** reference frame can be transformed into a common arbitrary reference frame called d-q (direct and quadrature axes) frame. The d-q reference frame can be fixed to the stator winding, the rotor winding, or to a synchronously rotating quantity.

3.3. DFIG Model Expressed in The d-q Reference Frame

The dynamic model of DFIG is set up in the form of the d-q synchronously rotating reference frame. Hence the time varying of the inductance matrix in the a-b-c reference frame model can be eliminated. In order to obtain the d-q reference frame two transformation steps are performed. First step, by using Clark's transformation to transform three phase time variant a-b-c frame, see Figure (3.3) [25], into equivalence two-phase time-variant d^s - q^s stationary reference frame on the stator and fixed on the rotor [28], see Figure (3.4) [25].

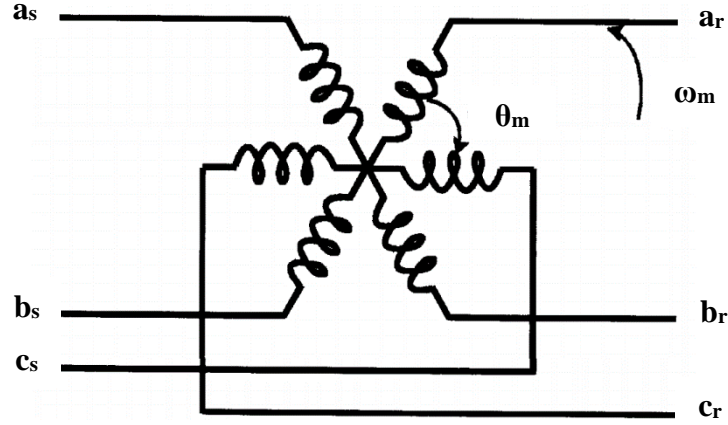


Figure 3.3: Three phase winding machine representation

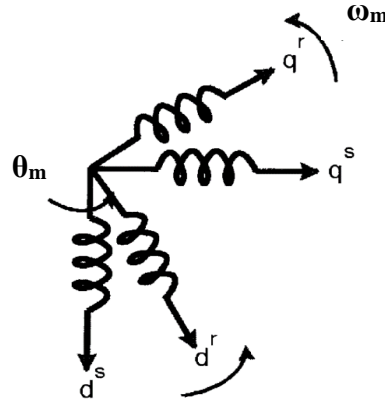


Figure 3.4: Transformed two-phase winding machine representation

The transformed frame is chosen where the d^s -axis lead q^s -axis by 90° electric degree. This equivalence is done so that the mmf produced by the two phase winding system and three phase winding system are equal and equal current magnitudes in each system. Note that, for mmf equality, if each of the three-phase windings has number of turns equal (n_s) and equal current magnitudes, then each of transformed two-phase windings must has number of turns equal $(3n_s/2)$ [26]. Assume a symmetrical DFIG

with three-phase stationary windings a, b and c. Each phase has an axes is placed at 120° angle to the other phase as shown in Figure (3.5) [25].

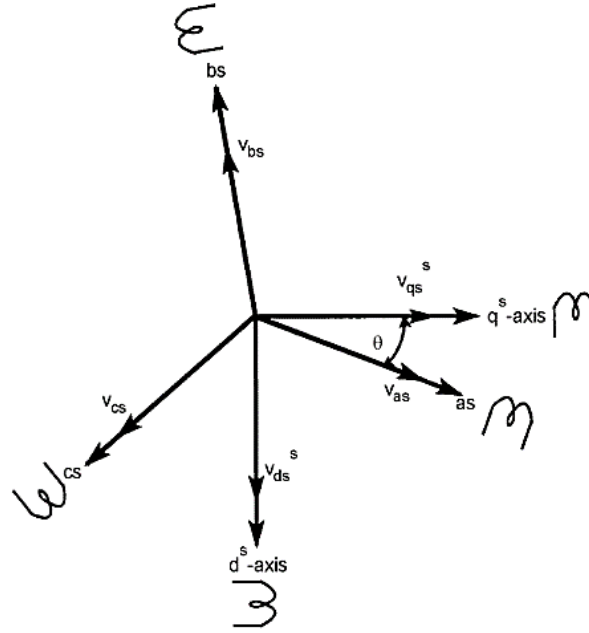


Figure 3.5: Stationary frame a-b-c to d^s-q^s axes transformation

The voltages, currents and flux linkage in the 3-phase **abc** frame can be expressed in the d^s-q^s stationary reference frame in the stator and fixed on the rotor as follows [28]:

$$[f_{qdo}^s] = T_{qdo}^s [f_{abc}] \quad (3.32)$$

$$\begin{bmatrix} f_q^s \\ f_d^s \\ f_o^s \end{bmatrix} = \frac{2}{3} \begin{bmatrix} \cos \theta & \cos(\theta - 120^\circ) & \cos(\theta + 120^\circ) \\ \sin \theta & \sin(\theta - 120^\circ) & \sin(\theta + 120^\circ) \\ 0.5 & 0.5 & 0.5 \end{bmatrix} \begin{bmatrix} f_a \\ f_b \\ f_c \end{bmatrix} \quad (3.33)$$

Where

f denotes to either phase voltages, phase currents, or flux linkages of the machine stator and rotor winding.

s denotes to stationary reference frame on the stator.

θ the displacement angle between **abc** frame and d^s-q^s frame.

The third component f_o^s is added which is known as the zero-sequence component in order for the transformation to be invertible. If the θ is considered to be equal zero hence the q^s axis is aligned with a_s axis. Then the transformation matrix can be obtained as:

$$\mathbf{T}_{qdo}^s = \frac{2}{3} \begin{bmatrix} 1 & -\frac{1}{2} & -\frac{1}{2} \\ 0 & -\frac{\sqrt{3}}{2} & \frac{\sqrt{3}}{2} \\ \frac{1}{2} & \frac{1}{2} & \frac{1}{2} \end{bmatrix} \quad (3.34)$$

Where the inverse transformation matrix is

$$[\mathbf{T}_{qdo}^s]^{-1} = \begin{bmatrix} 1 & 0 & 1 \\ -\frac{1}{2} & \frac{\sqrt{3}}{2} & 1 \\ -\frac{1}{2} & -\frac{\sqrt{3}}{2} & 1 \end{bmatrix} \quad (3.35)$$

The equation in **abc** frame can be transformed into d^s-q^s frame using Clark's transformation as follows:

$$\begin{bmatrix} v_{abcs} \\ v_{abcr} \end{bmatrix} = \begin{bmatrix} \mathbf{R}_{ss} & 0 \\ 0 & \mathbf{R}_{rr} \end{bmatrix} \begin{bmatrix} i_{abcs} \\ i_{abcr} \end{bmatrix} + \frac{d}{dt} \left[\begin{bmatrix} \mathbf{L}_{ss} & \mathbf{L}_{sr} \\ \mathbf{L}_{rs} & \mathbf{L}_{ss} \end{bmatrix} \begin{bmatrix} i_{abcs} \\ i_{abcr} \end{bmatrix} \right] \quad (3.36)$$

$$\begin{aligned} [\mathbf{T}_{qdo}^s]^{-1} \begin{bmatrix} v_{qdos}^s \\ v_{qdor}^s \end{bmatrix} &= \begin{bmatrix} \mathbf{R}_{ss} & 0 \\ 0 & \mathbf{R}_{rr} \end{bmatrix} [\mathbf{T}_{qdo}^s]^{-1} \begin{bmatrix} i_{qdos}^s \\ i_{qdor}^s \end{bmatrix} + \\ \frac{d}{dt} \left[\begin{bmatrix} \mathbf{L}_{ss} & \mathbf{L}_{sr} \\ \mathbf{L}_{rs} & \mathbf{L}_{ss} \end{bmatrix} [\mathbf{T}_{qdo}^s]^{-1} \begin{bmatrix} i_{qdos}^s \\ i_{qdor}^s \end{bmatrix} \right] \end{aligned} \quad (3.37)$$

$$\begin{aligned} [\mathbf{T}_{qdo}^s]^{-1} \begin{bmatrix} v_{qdos}^s \\ v_{qdor}^s \end{bmatrix} &= \begin{bmatrix} \mathbf{R}_{ss} & 0 \\ 0 & \mathbf{R}_{rr} \end{bmatrix} [\mathbf{T}_{qdo}^s]^{-1} \begin{bmatrix} i_{qdos}^s \\ i_{qdor}^s \end{bmatrix} + \\ [\mathbf{T}_{qdo}^s]^{-1} \frac{d}{dt} \left[\begin{bmatrix} \mathbf{L}_{ss} & \mathbf{L}_{sr} \\ \mathbf{L}_{rs} & \mathbf{L}_{ss} \end{bmatrix} \begin{bmatrix} i_{qdos}^s \\ i_{qdor}^s \end{bmatrix} \right] \end{aligned} \quad (3.38)$$

Multiply Eq. (3.38) by \mathbf{T}_{qdo}^s :

$$\begin{bmatrix} v_{qdos}^s \\ v_{qdor}^s \end{bmatrix} = \begin{bmatrix} \mathbf{R}_{ss} & 0 \\ 0 & \mathbf{R}_{rr} \end{bmatrix} \begin{bmatrix} i_{qdos}^s \\ i_{qdor}^s \end{bmatrix} + \frac{d}{dt} \left[\begin{bmatrix} \mathbf{L}_{ss} & \mathbf{L}_{sr} \\ \mathbf{L}_{rs} & \mathbf{L}_{ss} \end{bmatrix} \begin{bmatrix} i_{qdos}^s \\ i_{qdor}^s \end{bmatrix} \right] \quad (3.39)$$

(3.40)

Where

(3.41)

(3.42)

(3.43)

(3.44)

The second step by using Park's transformation to transform the two phase time-variant reference frames on the stator and rotor to two phase time-invariant d-q synchronously rotating reference frame, as shown in Figure (3.6) [25].

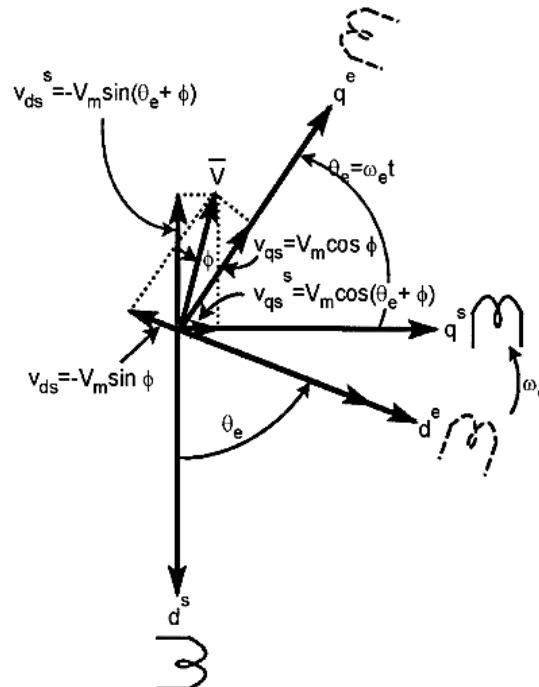


Figure 3.6: Stationary frame d^s - q^s to synchronously rotating frame d^e - q^e transformation

If zero-sequence component is neglected, the voltages, currents and flux linkage in the two-phase d^s-q^s stationary reference frame in the stator and rotor can be expressed in the d-q synchronously rotating reference frame as follows [25, 28]:

Stator axes transformation:

$$\begin{bmatrix} f_{qds} \end{bmatrix} = T_{\theta_e} \begin{bmatrix} f_{qds}^s \end{bmatrix} \quad (3.45)$$

$$\begin{bmatrix} f_{qs} \\ f_{ds} \end{bmatrix} = \begin{bmatrix} \cos \theta_e & -\sin \theta_e \\ \sin \theta_e & \cos \theta_e \end{bmatrix} \begin{bmatrix} f_{qs}^s \\ f_{ds}^s \end{bmatrix} \quad (3.46)$$

Where

f denotes to the phase voltages, the phase currents and the flux linkages of the stator winding machine.

s denotes to stationary reference frame.

θ_e is the angle between the q-axis of the stationary reference frame fixed on the stator and rotating q-d axes. It's value can be expressed as a function of the angular speed, $\omega_e(t)$, of the synchronously rotating d-q reference frame as follows:

$$\theta_e = \int \omega_e(t) dt = \omega_e t \quad (3.47)$$

The equations in d^s-q^s frame can be transformed into d-q frame using Park's transformation as follows:

$$\begin{bmatrix} v_{qds}^s \end{bmatrix} = [\mathbf{R}_{ss}] \begin{bmatrix} i_{qds}^s \end{bmatrix} + \frac{d}{dt} \begin{bmatrix} \psi_{qds}^s \end{bmatrix} \quad (3.48)$$

$$[\mathbf{T}_{\theta_e}]^{-1} \begin{bmatrix} v_{qds} \end{bmatrix} = [\mathbf{R}_{ss}] [\mathbf{T}_{\theta_e}]^{-1} \begin{bmatrix} i_{qds} \end{bmatrix} + \frac{d}{dt} \left[[\mathbf{T}_{\theta_e}]^{-1} \begin{bmatrix} \psi_{qds} \end{bmatrix} \right] \quad (3.49)$$

$$\begin{aligned} [\mathbf{T}_{\theta_e}]^{-1} \begin{bmatrix} v_{qds} \end{bmatrix} &= [\mathbf{R}_{ss}] [\mathbf{T}_{\theta_e}]^{-1} \begin{bmatrix} i_{qds} \end{bmatrix} + \left[\frac{d}{dt} [\mathbf{T}_{\theta_e}]^{-1} \right] \begin{bmatrix} \psi_{qds} \end{bmatrix} + \\ &[\mathbf{T}_{\theta_e}]^{-1} \left[\frac{d}{dt} \begin{bmatrix} \psi_{qds} \end{bmatrix} \right] \end{aligned} \quad (3.50)$$

Multiply Eq. (3.50) by T_{θ_e} :

$$\begin{bmatrix} v_{qds} \end{bmatrix} = [\mathbf{R}_{ss}] \begin{bmatrix} i_{qds} \end{bmatrix} + [\mathbf{T}_{\theta_e}] \left[\frac{d}{dt} [\mathbf{T}_{\theta_e}]^{-1} \right] \begin{bmatrix} \psi_{qds} \end{bmatrix} + \left[\frac{d}{dt} \begin{bmatrix} \psi_{qds} \end{bmatrix} \right] \quad (3.51)$$

Where

$$\left[\frac{d}{dt} [\mathbf{T}_{\theta_e}]^{-1} \right] = \omega_e \begin{bmatrix} -\sin \theta_e & \cos \theta_e \\ -\cos \theta_e & -\sin \theta_e \end{bmatrix} \quad (3.52)$$

And

$$\begin{bmatrix} \mathbf{T}_{\theta_e} \end{bmatrix} \begin{bmatrix} \frac{d}{dt} \begin{bmatrix} \mathbf{T}_{\theta_e} \end{bmatrix}^{-1} \end{bmatrix} = \omega_s \begin{bmatrix} 0 & 1 \\ -1 & 0 \end{bmatrix} \quad (3.53)$$

Then

$$\begin{bmatrix} v_{qs} \\ v_{ds} \end{bmatrix} = \begin{bmatrix} \mathbf{R}_s & 0 \\ 0 & \mathbf{R}_s \end{bmatrix} \begin{bmatrix} i_{qs} \\ i_{ds} \end{bmatrix} + \frac{d}{dt} \begin{bmatrix} \psi_{qs} \\ \psi_{ds} \end{bmatrix} + \omega_s \begin{bmatrix} \psi_{ds} \\ -\psi_{qs} \end{bmatrix} \quad (3.54)$$

Rotor axes transformation:

$$\begin{bmatrix} f_{qdr} \end{bmatrix} = \mathbf{T}_{\theta_r} \begin{bmatrix} f_{qdr}^s \end{bmatrix} \quad (3.55)$$

$$\begin{bmatrix} f_{qr} \\ f_{dr} \end{bmatrix} = \begin{bmatrix} \cos \theta_r & -\sin \theta_r \\ \sin \theta_r & \cos \theta_r \end{bmatrix} \begin{bmatrix} f_{qr}^s \\ f_{dr}^s \end{bmatrix} \quad (3.56)$$

Where

f denotes to the phase voltages, the phase currents and the flux linkages of the rotor winding machine.

s denotes to stationary reference frame.

θ_r is the angle between the q-axis of the stationary reference frame fixed on the rotor and rotating q-d axes. Its value can be expressed as follows:

$$\theta_r = \int (\omega_e(t) - \omega_m(t)) dt = (\omega_e - \omega_m)t \quad (3.57)$$

The equations in d^s - q^s frame can be transformed into d-q frame using Park's transformation as follows:

$$\begin{bmatrix} v_{qdr}^s \end{bmatrix} = \begin{bmatrix} \mathbf{R}_{rr} \end{bmatrix} \begin{bmatrix} i_{qdr}^s \end{bmatrix} + \frac{d}{dt} \begin{bmatrix} \psi_{qdr}^s \end{bmatrix} \quad (3.58)$$

$$\begin{bmatrix} \mathbf{T}_{\theta_r} \end{bmatrix}^{-1} \begin{bmatrix} v_{qdr} \end{bmatrix} = \begin{bmatrix} \mathbf{R}_{rr} \end{bmatrix} \begin{bmatrix} \mathbf{T}_{\theta_r} \end{bmatrix}^{-1} \begin{bmatrix} i_{qdr} \end{bmatrix} + \frac{d}{dt} \left[\begin{bmatrix} \mathbf{T}_{\theta_r} \end{bmatrix}^{-1} \begin{bmatrix} \psi_{qdr} \end{bmatrix} \right] \quad (3.59)$$

$$\begin{bmatrix} \mathbf{T}_{\theta_r} \end{bmatrix}^{-1} \begin{bmatrix} v_{qdr} \end{bmatrix} = \begin{bmatrix} \mathbf{R}_{rr} \end{bmatrix} \begin{bmatrix} \mathbf{T}_{\theta_r} \end{bmatrix}^{-1} \begin{bmatrix} i_{qdr} \end{bmatrix} + \left[\frac{d}{dt} \begin{bmatrix} \mathbf{T}_{\theta_r} \end{bmatrix}^{-1} \right] \begin{bmatrix} \psi_{qdr} \end{bmatrix} + \begin{bmatrix} \mathbf{T}_{\theta_r} \end{bmatrix}^{-1} \left[\frac{d}{dt} \begin{bmatrix} \psi_{qdr} \end{bmatrix} \right] \quad (3.60)$$

Multiply Eq. (3.62) by T_{θ_r} :

$$\begin{bmatrix} v_{qdr} \end{bmatrix} = \begin{bmatrix} R_{rr} \end{bmatrix} \begin{bmatrix} i_{qdr} \end{bmatrix} + \begin{bmatrix} T_{\theta_r} \end{bmatrix} \left[\frac{d}{dt} \begin{bmatrix} T_{\theta_r} \end{bmatrix}^{-1} \right] \begin{bmatrix} \psi_{qdr} \end{bmatrix} + \left[\frac{d}{dt} \begin{bmatrix} \psi_{qdr} \end{bmatrix} \right] \quad (3.61)$$

Where

$$\left[\frac{d}{dt} \begin{bmatrix} T_{\theta_r} \end{bmatrix}^{-1} \right] = (\omega_e - \omega_m) \begin{bmatrix} -\sin \theta_r & \cos \theta_r \\ -\cos \theta_r & -\sin \theta_r \end{bmatrix} \quad (3.62)$$

And

$$\begin{bmatrix} T_{\theta_r} \end{bmatrix} \left[\frac{d}{dt} \begin{bmatrix} T_{\theta_r} \end{bmatrix}^{-1} \right] = (\omega_s - \omega_m) \begin{bmatrix} 0 & 1 \\ -1 & 0 \end{bmatrix} \quad (3.63)$$

Then

$$\begin{bmatrix} v_{qr} \\ v_{dr} \end{bmatrix} = \begin{bmatrix} R_r & 0 \\ 0 & R_r \end{bmatrix} \begin{bmatrix} i_{qr} \\ i_{dr} \end{bmatrix} + \frac{d}{dt} \begin{bmatrix} \psi_{qr} \\ \psi_{dr} \end{bmatrix} + (\omega_s - \omega_m) \begin{bmatrix} \psi_{dr} \\ -\psi_{qr} \end{bmatrix} \quad (3.64)$$

Then the stator voltage equations in d-q frame is

$$v_{qs} = R_s i_{qs} + \frac{d\psi_{qs}}{dt} + \omega_e \psi_{ds} \quad (3.65)$$

$$v_{ds} = R_s i_{ds} + \frac{d\psi_{ds}}{dt} - \omega_e \psi_{qs} \quad (3.66)$$

Then the rotor voltage equations in d-q frame is

$$v_{qr} = R_r i_{qr} + \frac{d\psi_{qr}}{dt} + (\omega_e - \omega_m) \psi_{dr} \quad (3.67)$$

$$v_{dr} = R_r i_{dr} + \frac{d\psi_{dr}}{dt} - (\omega_e - \omega_m) \psi_{qr} \quad (3.68)$$

Stator winding flux linkage equations

$$\psi_{qs} = L_s i_{qs} + L_m i_{qr} \quad (3.69)$$

$$\psi_{ds} = L_s i_{ds} + L_m i_{dr} \quad (3.70)$$

Rotor winding flux linkage equations

$$\psi_{qr} = L_r i_{qr} + L_m i_{qs} \quad (3.71)$$

$$\psi_{dr} = L_r i_{dr} + L_m i_{ds} \quad (3.72)$$

Active and reactive power equations

$$P_s = \frac{3}{2} (v_{qs} i_{qs} + v_{ds} i_{ds}) \quad (3.73)$$

$$Q_s = \frac{3}{2} (v_{qs} i_{ds} - v_{ds} i_{qs}) \quad (3.74)$$

$$P_r = \frac{3}{2} (v_{qr} i_{qr} + v_{dr} i_{dr}) \quad (3.75)$$

$$Q_r = \frac{3}{2} (v_{qr} i_{dr} - v_{dr} i_{qr}) \quad (3.76)$$

Torque equations

$$T_e = \left(\frac{3}{2} \right) \left(\frac{p}{2} \right) L_m [i_{qs} i_{dr} - i_{ds} i_{qr}] \quad (3.77)$$

$$\omega_m = \int \frac{P}{2J} [T_e - T_l] dt \quad (3.78)$$

Where

$v_{qs}, v_{ds}, v_{qr}, v_{dr}$ are the stator and rotor voltages component respectively (v) .
 $i_{qs}, i_{ds}, i_{qr}, i_{dr}$ are the stator and rotor currents component respectively (A).
 P_s, P_r are the stator and rotor power respectively (W).
 Q_s, Q_r are the stator and rotor reactive power respectively (VAR).
 T_e is the electromagnetic torque developed by the DFIG (N.m).
 p is the number of poles of DFIG.
 J is the rotor inertia (Kg.m²).

Equations (3.65) through (3.72) can be visualized as the equivalent circuit in q-axis and d-axis as shown Figure (3.7).

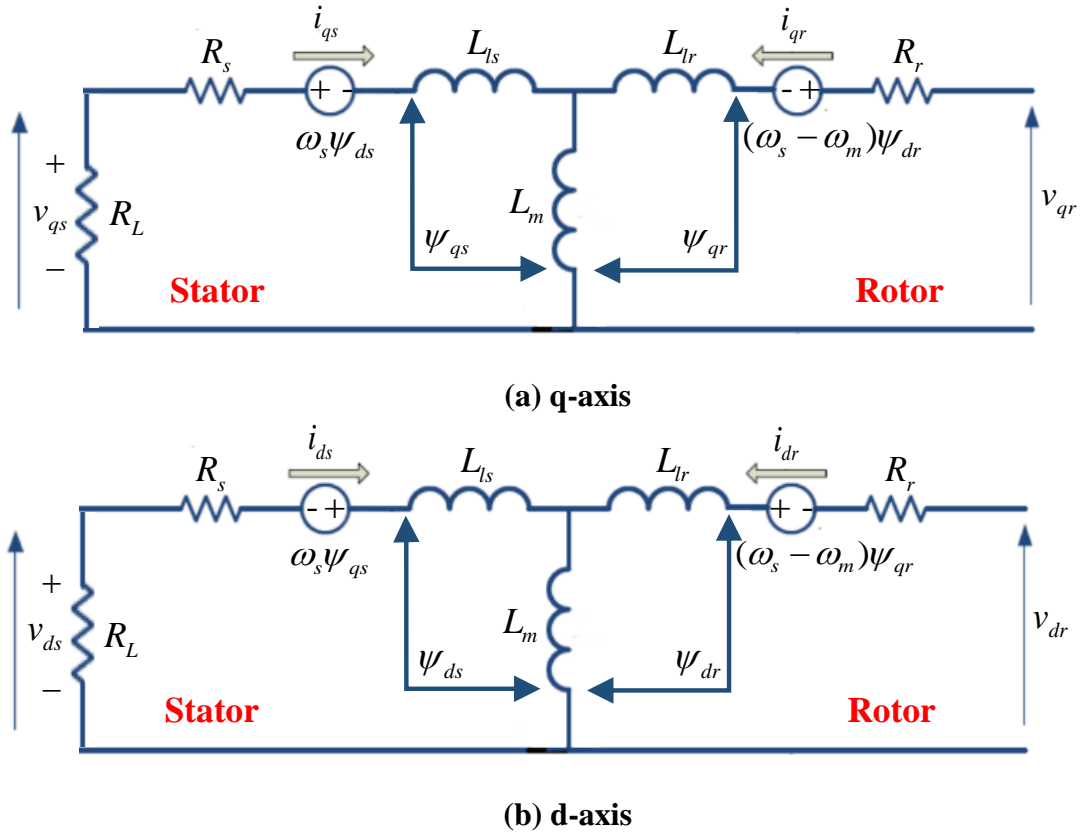


Figure 3.7: Dynamic d – q equivalent circuit of DFIG in synchronously rotating reference frame ((a) q-axis and (b) d-axis)

3.4. MATLAB/ SIMULINK Model for DFIG

The basic data for a 2 MW DFIG used in simulation as follows in table 3.1 [10]:

Table 3.1: DFIG Main Parameters

Parameter	Value
Nominal stator active power	2 MW
Nominal torque	12732 N.m
Stator voltage	690 V
Stator frequency	50 Hz
Nominal speed	1500 rpm
Speed range	900-2000 rpm
Pole pairs	2
Turns ratio	0.34
Magnetizing inductance L_m	2.5×10^{-3} H
Stator leakage inductance L_{ls}	87×10^{-6} H
Rotor leakage inductance L_{lr}	87×10^{-6} H
Stator resistance R_s	0.026 Ω
Rotor resistance R_r	0.026 Ω
inertia J_m	90 Kg.m ²

The operating point is chosen as follows:

Stator output power $P_s = -218$ kW (about 11% from DFIG rated power)

Stator output reactive power $Q_s = 0$ kVAR

Generator speed $N_g = 1220$ rpm

Slip $s = 0.186$

From the Calculation file all needed parameters can be calculated for Simulink/Model using Matlab M-file as shown in Figure (3.8) and the steady state required rotor input voltage, magnitude and frequency, and power is obtained as follows:

Figure 3.8: Matlab M-file calculations for DFIG

Rotor input power $P_r = 43.2$ kW

Rotor input reactive power $Q_r = 118$ kVAR

Rotor input voltage $V_{r_input} = 77.59$ V(rms, phase value)

phase angle of rotor input voltage = 17.81° (elect. degree)

Rotor input frequency $F_r = 9.33$ Hz

For the Simulink/Model shown in Figure (3.9), the turbine firstly free run to steady state at no-load for 15 sec. with the desired rotor input voltage is applied. After that the load is connected for 15 sec.. The Figures (3.10), (3.11), (3.12) and (3.13) show the output stator voltage, frequency, generator speed and electromagnetic torque of DFIG under this condition.

For given wind speed (5.5 m/s) and from the curve $T_m = 1387 \text{ N.m}$, $N_g = 1220 \text{ RPM}$, $P_m = 1.773e5$, $s = 0.1867$, $P_s = 2.18e5 \text{ W}$ from Calculation file all needed parameters can be calculated for simulink using field oriented control method (iqr , idr) then Vabcr required to the rotor is calculated. The turbine first run to steady state after 35 sec then desired rotor voltage applied for 5 sec and then load connected for 15 sec

Turbine model calculation file

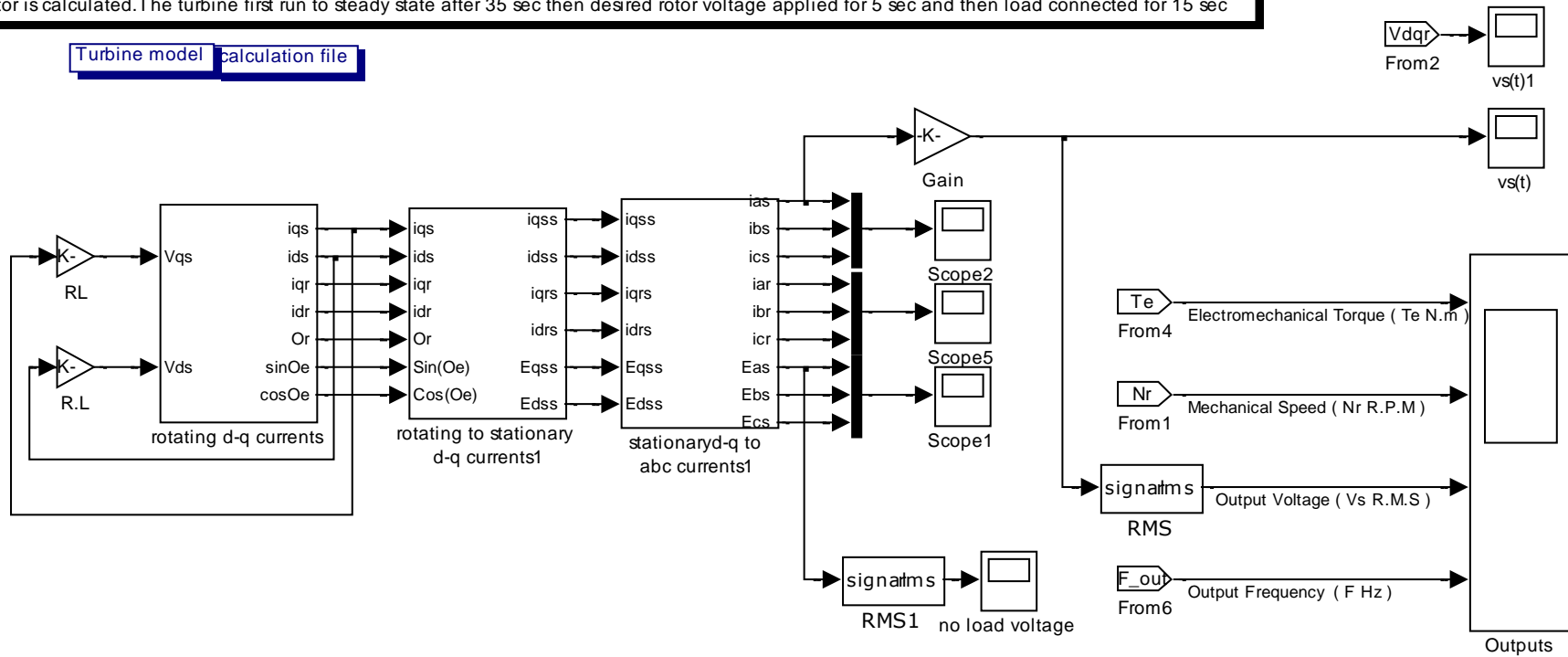


Figure 3.9: Schematic block diagram for the dynamic modelling of DFIG using MATLAB/SIMULINK

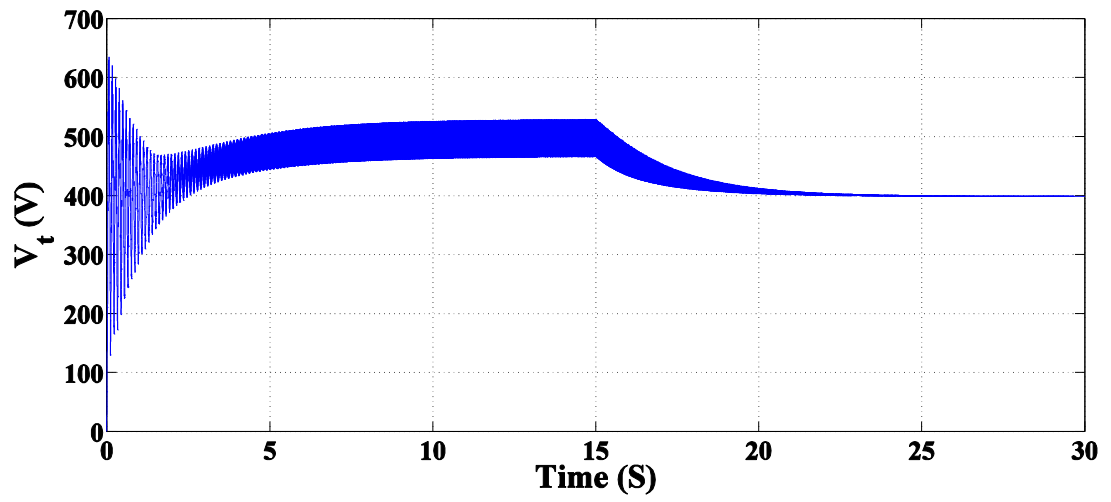


Figure 3.10: Stator rms terminal output voltage V_t (V)

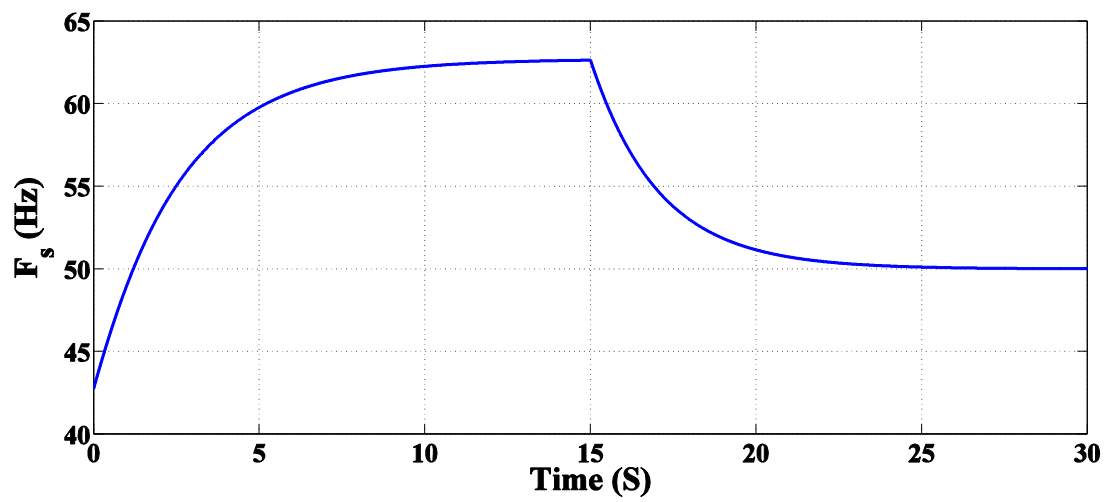


Figure 3.11: Stator output frequency F_s (Hz)

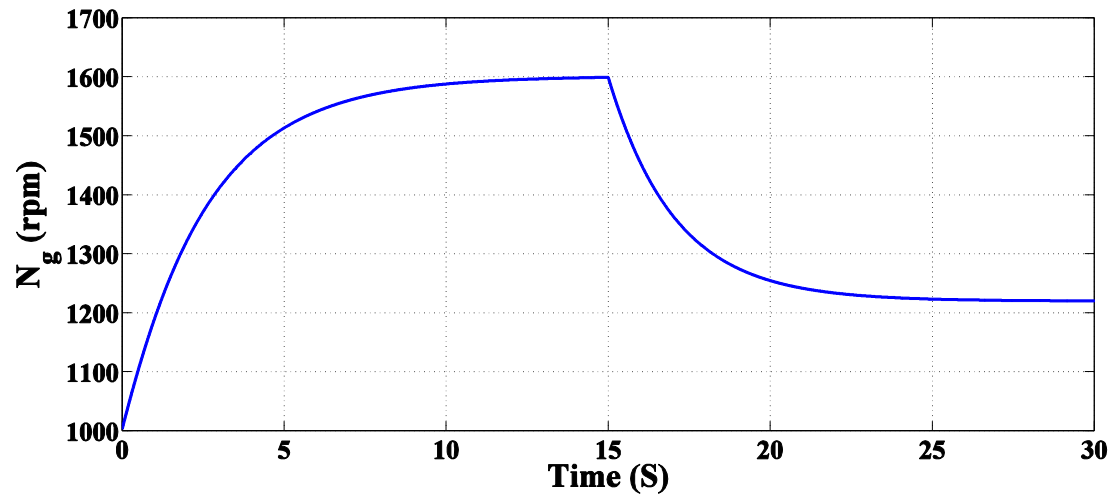


Figure 3.12: Generator rotational speed N_g (rpm)

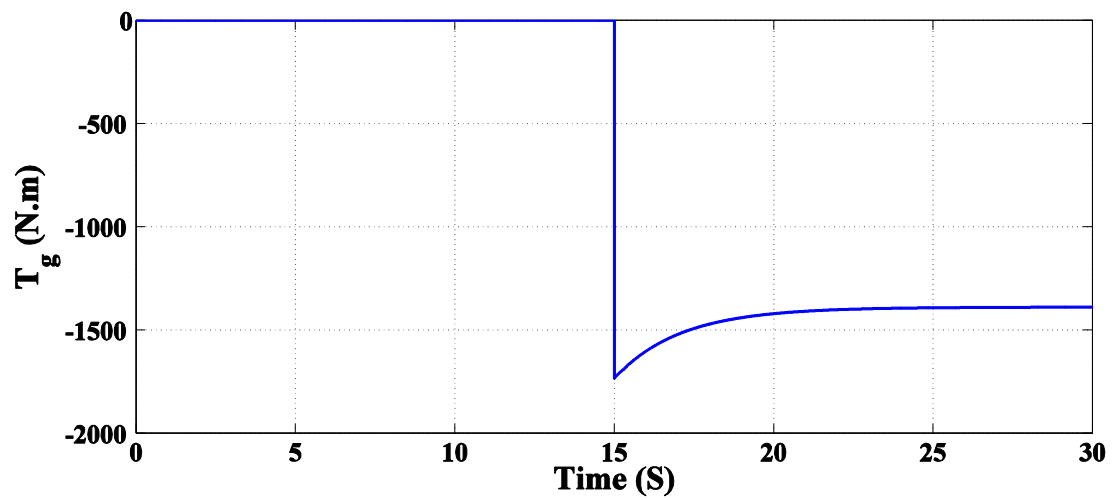


Figure 3.13: Generator electromechanical torque T_g (N.m)

Chapter 4 : Control and MPPT of Stand-Alone DFIG used in WECS

4.1. Introduction

Controlling of the stand-alone DFIG is more complicated than the control of other electrical generators. The main goals to control the magnitude and frequency of DFIG output voltage and power exchanges between the DFIG and the loads. By the help of a power electronic converters the rotor's voltages, currents and frequency can be controlled. There are several control methods applied on DFIG and connected power converters to achieve the required performance from them. The choice of control method must be achieve the required performance from the DFIG without complicated algorithm and large variables dependability. One common way from them used to controlling the DFIG is by means of vector (field-oriented) control. The main advantages of this control method are [29]:

- 1- High efficiency by aligning the stator flux with the rotor current to produce the desired output voltage and frequency from the DFIG.
- 2- No positions sensors are required in this method because speed and position of the DFIG are estimated based on currents and voltages.
- 3- Improves dynamic response by adjusting both amplitude and phase of the control signals fed back to the DFIG.
- 4- Allow decoupled or independent control of both active and reactive power.

There are several vector control schemes for the DFIG have been proposed such as direct and indirect vector control. Indirect vector control method is chosen to perform required DFIG control. This control can be achieved by the help of stator-flux orientation method [30-33].

Also as the wind speed always swinging in WECS, the wind energy is continuously varying over the day. To achieve high efficiency in WECS, the maximum power point tracking (MPPT) must be applied on the system for each wind speed value. In this chapter the third methods will be explained in details and then one of them will be chosen for the proposed system of stand-alone DFIG.

4.2. Effects of Rotor Input Voltage of DFIG

To control both the magnitude and frequency of stator voltage, the rotor input voltage is controlled [17, 18, 34]. Controlling the magnitude, frequency, phase shift and phase sequence of the rotor voltage is achieved by using a three-phase RSC connected to the rotor terminals of DFIG. Also for active, reactive power control, the amplitude of three phase rotor input voltages parameters must be modified according to the rotational speed of the rotor for the wide range of operation.

The proposed system of a stand-alone DFIG can be operated in two modes of operation according to the power captured by the wind and the output power from the generator. At sub-synchronous mode the rotational speed of the rotor is less than the synchronous speed of the generator and the RSC transfer power from the battery to the generator. At super-synchronous mode, the rotational speed of the rotor is higher than the synchronous speed of the generator and RSC transfer the power from the generator to the battery. Also the battery can support the load through the LSC in case of low power captured from the wind. This chapter investigates the DFIG in sub-synchronous and super-synchronous modes of operation.

4.2.1. Sub-Synchronous Speed Mode of Operation

Consider that the power which is captured from the wind requires that the DFIG generator rotates at speed less than synchronous speed of the generator. Then, the rotor frequency is adjusted to maintain the stator frequency at the nominal value as follows:

$$\omega_r = \omega_s - \omega_m \quad (4.1)$$

Where

ω_r is angular frequency of the voltages and currents of the rotor windings (elec. rad/s).

The equations of the rotor input voltage can be expressed in **abc** frame as follows:

$$v_{ar} = V_m \cos(\omega_r t + \phi) \quad (4.2)$$

$$v_{br} = V_m \cos(\omega_r t + \phi - 120^\circ) \quad (4.3)$$

$$v_{cr} = V_m \cos(\omega_r t + \phi + 120^\circ) \quad (4.4)$$

Where

v_{ar}, v_{br}, v_{cr} is the instantaneous value of the rotor input voltages per phase (V).
 V_m is the amplitude of the rotor input voltage per phase (V).
 ϕ is the phase shift angle (in degrees).

Variables in Eq. (4.2) to Eq. (4.4) can be expressed in d_r^s - q_r^s reference frame fixed on the rotor, as shown in Figure (4.1), by using Clark's transformation, indicated in Eq. (3.32), as follows [25]:

$$v_{qr}^s = V_m \cos(\omega_r t + \phi) \quad (4.5)$$

$$v_{dr}^s = -V_m \sin(\omega_r t + \phi) \quad (4.6)$$

The equations of the rotor input voltage can be expressed in **acb** frame as follows:

$$v_{ar} = V_m \cos(\omega_r t + \phi) \quad (4.11)$$

$$v_{br} = V_m \cos(\omega_r t + \phi + 120^\circ) \quad (4.12)$$

$$v_{cr} = V_m \cos(\omega_r t + \phi - 120^\circ) \quad (4.13)$$

Variables in Equations (4.11), (4.12) and (4.13) can be expressed in d_r^s - q_r^s reference frame fixed on the rotor, as shown in Figure (4.2), by using Clark's transformation as follows:

$$v_{qr}^s = V_m \cos(\omega_r t + \phi) \quad (4.14)$$

$$v_{dr}^s = V_m \sin(\omega_r t + \phi) \quad (4.15)$$

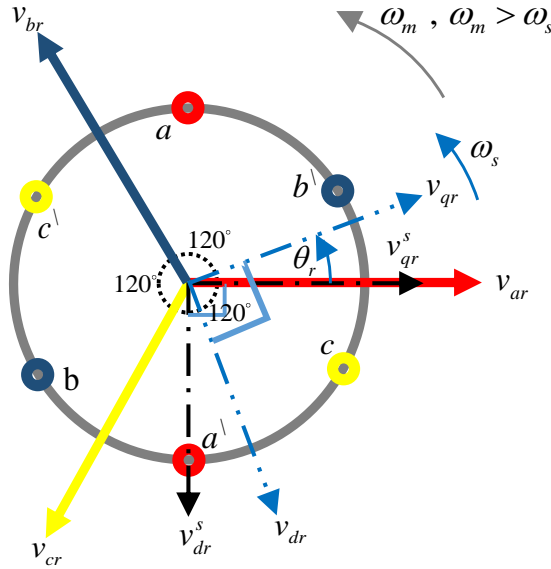


Figure 4.2: Transformation of rotor acb reference frame to d_r - q_r synchronously rotating reference frame at super-synchronous speed

Then the variables in Equations (4.14) and (4.15) are expressed in d_r - q_r synchronously rotating reference frame by using Park's transformation and are obtained as follows:

$$v_{qr} = V_m \cos(\phi) \quad (4.16)$$

$$v_{dr} = V_m \sin(\phi) \quad (4.17)$$

Where the angle between two reference frames d_r-q_r and $d_r^s-q_r^s$ is in this case as the same in first case.

4.3. Fundamentals of Vector Control of Induction Machines

When the vector control strategy is applied to an induction machine its operation similarly likes the operation of a separately excited DC machine where the controlling of the machine torque and flux can be achieved independently by controlling the currents of the armature and the field respectively. From the characteristics of a separately excited DC machine the electro-magnetic torque equation as function of armature and field currents is expressed as follows [25]:

$$T = K I_f I_a \quad (4.18)$$

Where

T is the electro-magnetic torque (N.m),
 K is the machine constant (N.m/A.Wb),
 I_a is the armature current (A), and
 I_f is the field current (A).

The flux ψ_a produced by the armature current I_a (current and flux in phase) is perpendicular to the field flux ψ_f produced by the field current I_f . Because of that the field flux and armature flux are naturally decoupled as illustrated in Figure (4.3) [25].

This decoupling causes the armature torque not affected during controlling the field flux through the field current I_f and similarly the field flux not affected during controlling the armature torque through the armature current I_a [25].

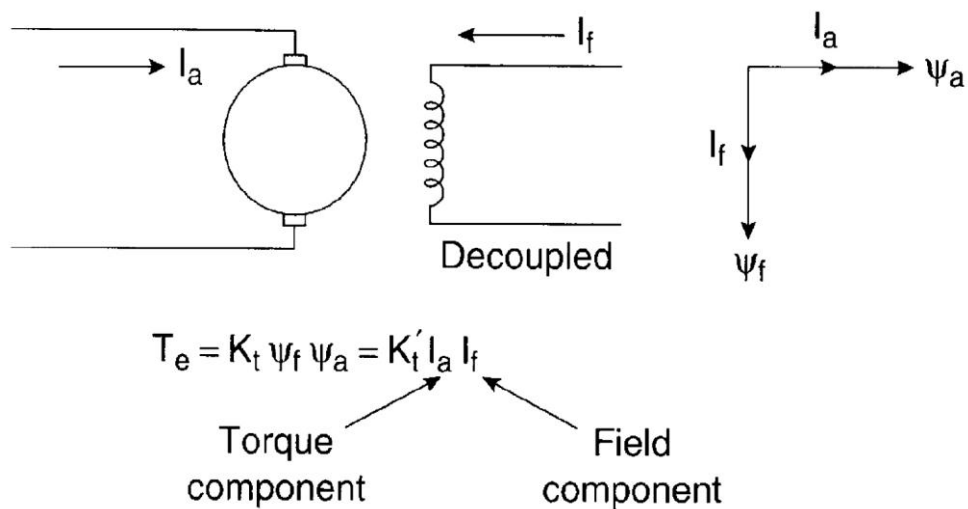


Figure 4.3: Separately excited DC motor control

The decoupling characteristic in the separately excited DC machine can be extended to a vector-controlled induction machine. The vector control uses unit vectors to obtain the suitable control action. The main function of unit vector is to transform the 3-phase **abc** reference frame model into 2-phase d-q synchronously rotating reference frame model and vice versa. The control signals which will be fed to the controlled machine or converters should be in **abc** reference frame, so the process requires repeated transformation from three-phase to two-phase parameter or vice versa following the necessary action being taken for the system [35].

There are basically two general methods of vector control [25]:

- 1- Direct vector control method.
- 2- Indirect vector control method.

The two methods are different from each other by the process of generating unit vector ($\cos(\theta_e)$, $\sin(\theta_e)$) for control. The unit vector are generally generated by either using the flux vectors or using voltage vectors. The name of the orientation of unit vector is given according to the vector taken for generation of θ_e .

The names of the orientations used are given below [36]:

- 1- Rotor flux orientation.
- 2- Stator flux orientation.
- 3- Air gap flux orientation.

After creating of 2-phase d-q synchronously rotating frame model, the current component i_d on the d- axis corresponds to the field current as in separately excited DC machine, and the current component i_q on the q-axis corresponds to the armature current. This means, for a vector controlled machine, both i_d and i_q are mutually orthogonal (hence, decoupled) where the torque component i_q is aligned with q-axis, and the flux component i_d is aligned with the d-axis. The principles implementation of vector control technique can be illustrated as shown in Figure (4.4) [25].

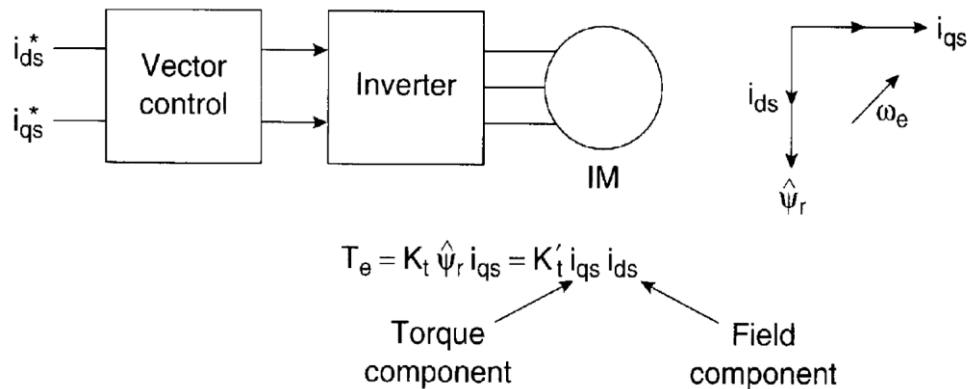


Figure 4.4: Vector-controlled induction machine

The electromagnetic torque of a vector-controlled induction machine can be expressed as a function of both i_d and i_q as follows [25]:

$$T = K i_q i_d \quad (4.19)$$

The implementation of vector control strategy is illustrated in Figure (4.5) [36]. By using the vector control strategy the components of **a**, **b**, **c** are obtained from the reference components **a***, **b***, **c***. The parameters of the machine (currents or voltages) are transferred to ds-qs stationary frame by using Clark's transformation (3-phase to 2-phase transformation). Then they are transformed to synchronously rotating reference frame d-q by using Park's transformation by the help of unit vectors ($\cos(\theta_e)$, $\sin(\theta_e)$). The controller makes two stage of inverse transformation as shown, so that the control components d^* and q^* corresponds to the machine parameters d and q respectively [36].

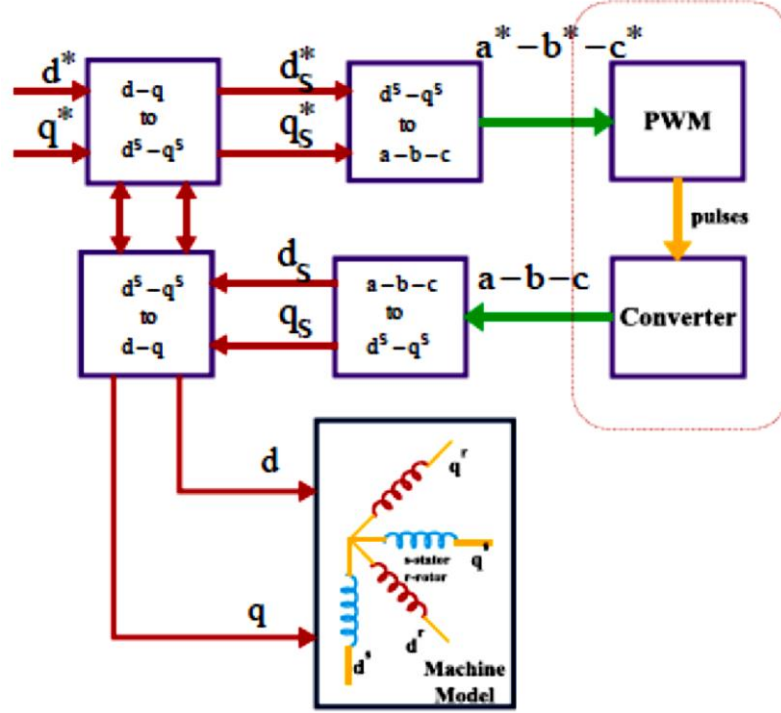


Figure 4.5: Implementation of vector control principle

In this chapter indirect vector control with stator flux orientation method are discussed in details.

4.4. Vector Control Implementation of DFIG

In vector control of a DFIG, the components of the d-q axes of the rotor current are controlled using indirect vector control method. The d-q reference frame is oriented with the stator flux. Hence the output voltage, magnitude and frequency, and power flows of the DFIG can be controlled independently by means of the quadrature and the direct current, respectively as shown in Figure (4.6) [10].

Indirect vector control method is applied to the DFIG to control the stator output power and voltage. This method can be achieved by the orientation of the d-axis in the direction of stator flux [18, 19, 34] as shown in Figure (4.7) [10]. The control equations can be obtained by setting the following condition [32]:

$$\psi_{qs} = 0, \quad \psi_{ds} = \psi_s = \text{const} \quad (4.20)$$

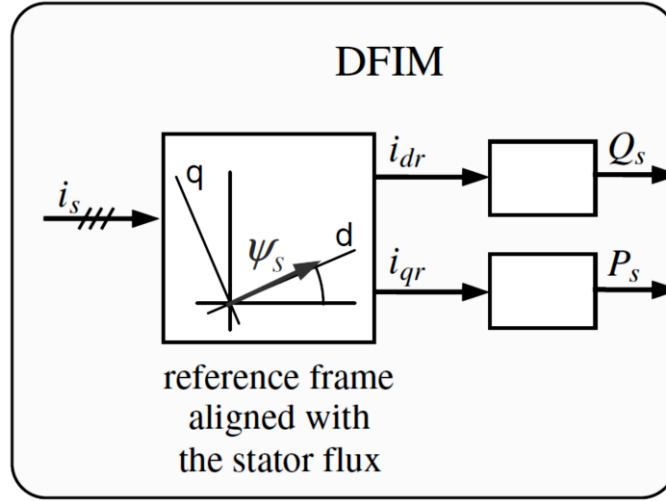


Figure 4.6: Vector control of DFIG

Then the machine Equations (3.65) to (3.77) of the DFIG in the synchronously rotating d-q reference frame will be modified. By substitute Eq. (4.20) in stator and rotor flux linkage Equations (3.69) to (3.72) then [18, 37]:

$$i_{qs} = -\frac{L_m}{L_s} i_{qr} \quad (4.21)$$

$$i_{ds} = \frac{\psi_{ds}}{L_s} - \frac{L_m}{L_s} i_{dr} \quad (4.22)$$

The voltage drop of the stator resistance is very small in comparison with the load voltage of DFIG, therefore the stator resistance influence can be neglected. Assume three phase resistive load is connected across the terminals of DFIG with value of R_L (Ω) per phase then:

$$v_{qs} = -R_L i_{qs} \quad (4.23)$$

$$v_{ds} = -R_L i_{ds} \quad (4.24)$$

Substitute (4.20) in (3.65) and (3.66) and neglect R_s then:

$$v_{qs} = \omega_s \psi_{ds} \quad (4.25)$$

$$v_{ds} = 0 \quad (4.26)$$

Substitute Equations (4.21) and (4.23) in Eq. (4.25). Also substitute Equations (4.22) and (4.24) in Eq. (4.26) then:

$$\omega_s = \frac{R_L L_m}{\psi_{ds} L_s} i_{qr} \quad (4.27)$$

$$\psi_{ds} = L_m i_{dr} \quad (4.28)$$

Substitute Eq. (4.28) in Eq. (4.22) then:

$$i_{ds} = 0 \quad (4.29)$$

Substitute Equations (4.21), (4.28) and (4.29) in Eq. (3.77) then:

$$T_e = \left(\frac{3}{2}\right) \left(\frac{p}{2}\right) \left(-\frac{L_m}{L_s}\right) \psi_{ds} i_{qr} \quad (4.30)$$

Substitute Equations (4.21), (4.25) and (4.29) in Eq. (3.73) then:

$$P_s = \left(\frac{3}{2}\right) \left(-\frac{L_m}{L_s}\right) \omega_s \psi_{ds} i_{qr} \quad (4.31)$$

Substitute Equations (4.26) and (4.29) in Eq. (3.74) then:

$$Q_s = 0 \quad (4.32)$$

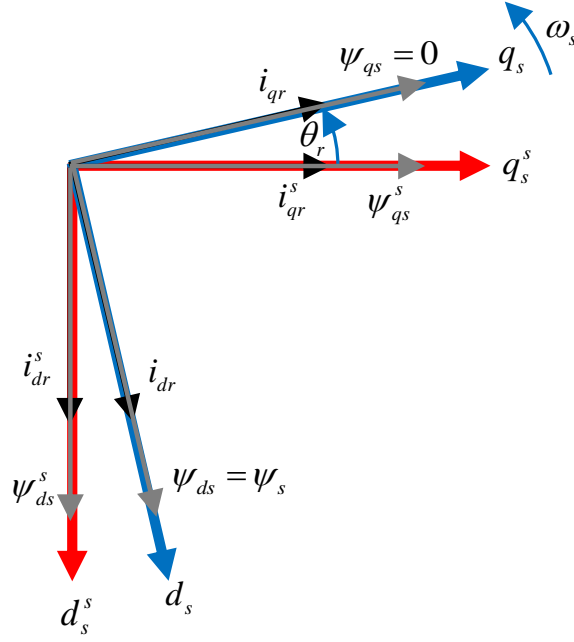


Figure 4.7: Phasor diagram for stator flux oriented vector control

Equations (4.25), (4.28), and (4.31) show that the terminal voltage and stator active power can be controlled by controlling the values of input rotor currents i_{qr} and i_{dr} . This can be achieved by using a voltage-fed current-regulated inverter in the rotor circuit. The values of rotor input voltage can be obtained as follows:

$$v_{qr} = R_r i_{qr} + \frac{d}{dt} \left[\left(L_r - \frac{L_m^2}{L_s} \right) i_{qr} \right] + (\omega_s - \omega_m) (L_r i_{dr}) \quad (4.33)$$

$$v_{dr} = R_r i_{dr} + \frac{d}{dt} (L_r i_{dr}) - (\omega_s - \omega_m) \left[\left(L_r - \frac{L_m^2}{L_s} \right) i_{qr} \right] \quad (4.34)$$

Also to control the DFIG stator voltage frequency ω_s the angular frequency ω_r of the rotor currents must be regulated according to the variable mechanical speed of the DFIG ω_m from the relations in Equations (4.1) and (4.10) [18, 19].

In the next chapter a MATLAB/SIMULINK model for proposed system of stand-alone DFIG is generated and the vector control method is applied in sub-synchronous and super-synchronous speed mode of operation.

4.5. Maximum Power Point Tracking for DFIG Used in WECS

Irrespective of the type of generator used in WECS, the amount of output power depends on the accuracy with which the peak power points are tracked by the help of MPPT controller of the WECS control system [38]. To applying MPPT control on the WECS the characteristics of wind turbine firstly must be analyzed according to the variation of wind speed and associated mechanical power and speed curves. Secondly, the versus types of MPPT Algorithms applied in WECS application must be studied so that the suitable one of them could be chosen for the proposed system of stand-alone DFIG.

4.5.1. Characteristics of Wind Turbines for MPPT

The wind turbine characteristics is explained in details before in chapter (2). From Eq. (2.2) the extracted mechanical power from the turbine at any wind speed is:

$$P_t = \frac{1}{2} \rho \pi R^2 V_w^3 C_p \quad (4.35)$$

The C_p coefficient is given as a function of tip-speed ratio (λ). From Eq. (2.3) the tip speed ratio is

$$\lambda = \frac{\omega_t R}{V_w} \quad (4.36)$$

In this thesis, a fixed pitch angle of the rotor blades equal zero is used and the characteristics of C_p mainly depend on λ as illustrated in chapter (2) in Figure (2.7).

The mechanical power can be plotted against the turbine rotor speed at different wind speed for blades angle equal zero as shown in Figure (4.8) [39]. The Figure shows that the maximum power occur at a certain value of the turbine rotor speed called optimum rotor speed ω_{opt} which changes with changing the wind speed. The corresponding tip speed ratio at this speed is called optimum tip speed ratio λ_{opt} . The maximum possible output power can be obtained only when the turbine operate at λ_{opt} . This is achieved by controlling the turbine rotational speed by using one of the MPPT algorithms so that it always has the optimum speed of rotation and maximum output power at certain wind speed [38].

Then from Equations (4.35) and (4.36) the optimum or maximum power extracted from a wind turbine can be expressed as follows [38]:

$$P_{\max} = K_{opt} \omega_{opt} \quad (4.37)$$

Where,

$$K_{opt} = \frac{0.5 \pi \rho R^5 C_{p \max}}{\lambda_{opt}^3} \quad (4.38)$$

And

$$\omega_{opt} = \lambda_{opt} \frac{V_w}{R} \quad (4.39)$$

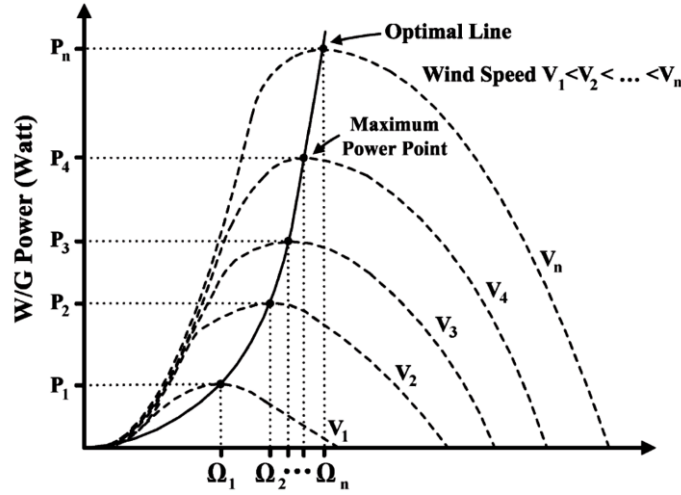


Figure 4.8: Mechanical power against rotor speed for different wind speeds

Wind turbines are controlled to operate in a specified range of wind speeds [10, 40]. This variation is limited between the cut-in speed (V_{cut-in}) and cut-out speed ($V_{cut-out}$). Otherwise these limits, the turbine must be stopped from operation in order to protect the turbine and generator from low and high speeds of operations. From the wind turbine typical power curve shown in Figure (4.9), it has three different regions of operation [40].

4.5.1.1. Low-Speed Region

That is the region under cut-in speed which the turbine must be stopped in order to prevent the turbine to operate with rotational speeds corresponding to the tower resonant frequency. This resonance frequency is about 0.5 Hz and a rotational speed too small can excite it [10].

4.5.1.2. Moderate-Speed Region

That is the region between the cut-in speed at which the turbine starts working, and the rated speed (V_{rated}), at which the turbine produces its rated power. The turbine produces maximum power in this region, as it is controlled to follow the path of maximum power extraction available from the wind [10, 40].

4.5.1.3. High-Speed Region

That is the region between rated speed and cut-out speed. The power extracted from the turbine is limited by using pitch angle control to do not cause over-load on the turbine and generator and avoid the mechanical failure caused by dynamic loads. Hence

to achieve the protection for the turbine from structural overload, it must be shut down above the cut-out speed [40].

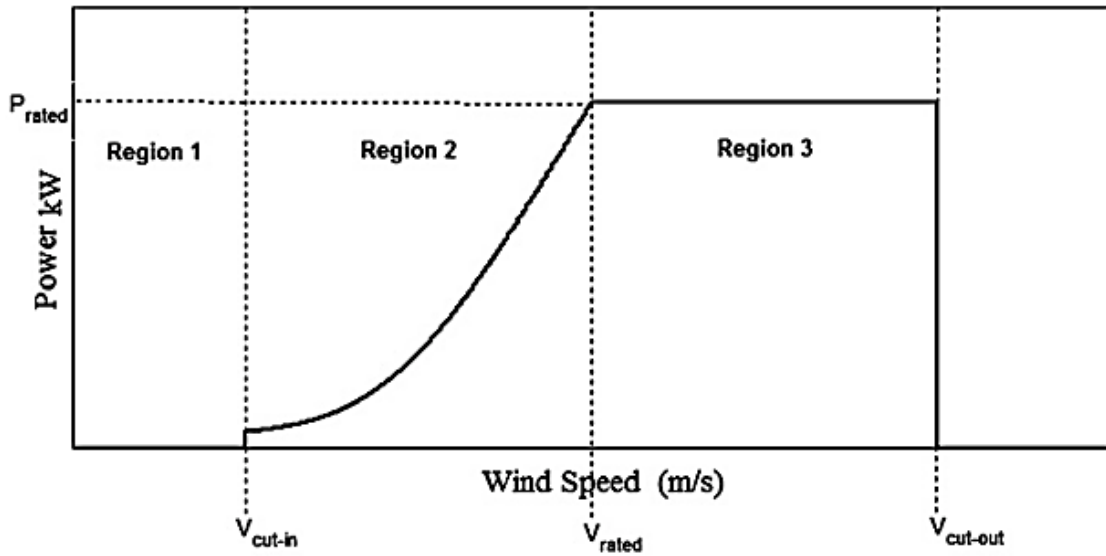


Figure 4.9: Ideal power curve of wind turbine

The speed of the wind turbine could be fixed or variable. Hence the maximization of the extracted power can be obtained only with variable speed wind turbines. Since these turbines are able to change their rotational speed in order that it can follow the instantaneous changes in wind speed, they are capable of operating at constant rotational speed to wind speed ratio.

4.5.2. Maximum Power Point Tracking Control Algorithms

The studied algorithms in MPPT mainly have three algorithms, namely [38]:

- 1- Algorithms based on wind speed and turbine speed,
- 2- Algorithms based on the output power measurement and calculation, and
- 3- Algorithms based on power characteristic curve.

These different control techniques are explained below as follows:

4.5.2.1. Algorithms Based on Wind Speed and Turbine Speed

This method is called tip speed ratio (TSR) control. In TSR control method the rotational speed of the generator is regulated so that the TSR is maintained at optimum value at which the power extracted from the wind is maximum [38]. Both the wind speed and the turbine rotational speed are required to be measured or estimated. Also the knowledge of optimum TSR of the used turbine is required so that the system be able to extract maximum possible power. Figure (4.10) shows the block diagram of a WECS with TSR control [38].

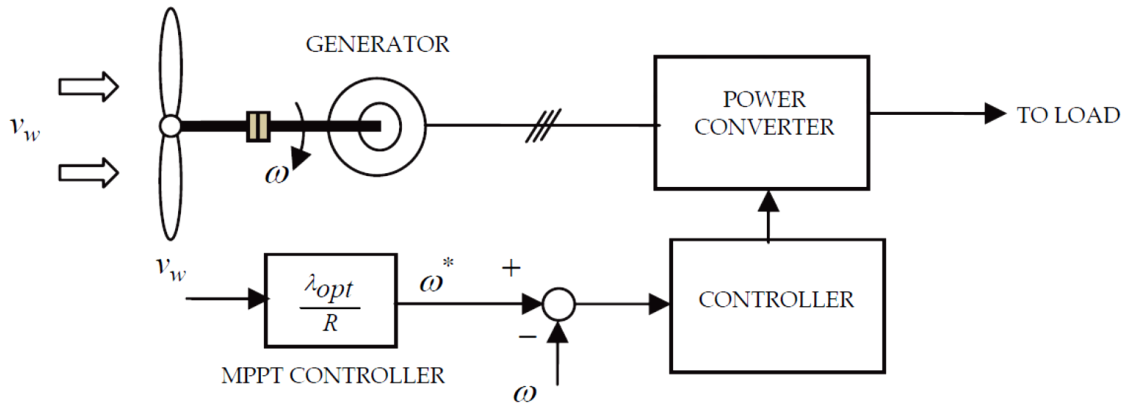


Figure 4.10: Tip speed ratio control of WECS

4.5.2.2. Algorithms Based on The Output Power Measurement and Calculation

This method is called hill-climb search (HCS) control. In HCS control method the algorithm continuously searches for the peak power of the used wind turbine [38]. Depending on the location of the operating point and relation between the changes in power and speed, the tracking algorithm calculates the desired optimum signal to reach the system to the maximum power point. Figure (4.11) shows the principle of HCS control while Figure (4.12) depicts a WECS with HCS controller for tracking maximum power points [38].

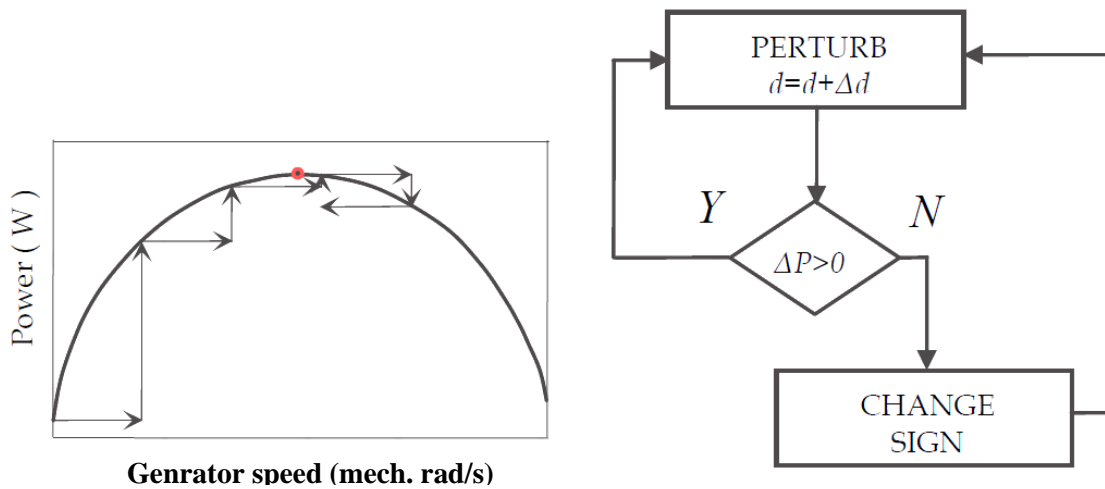


Figure 4.11: HCS Control Principle

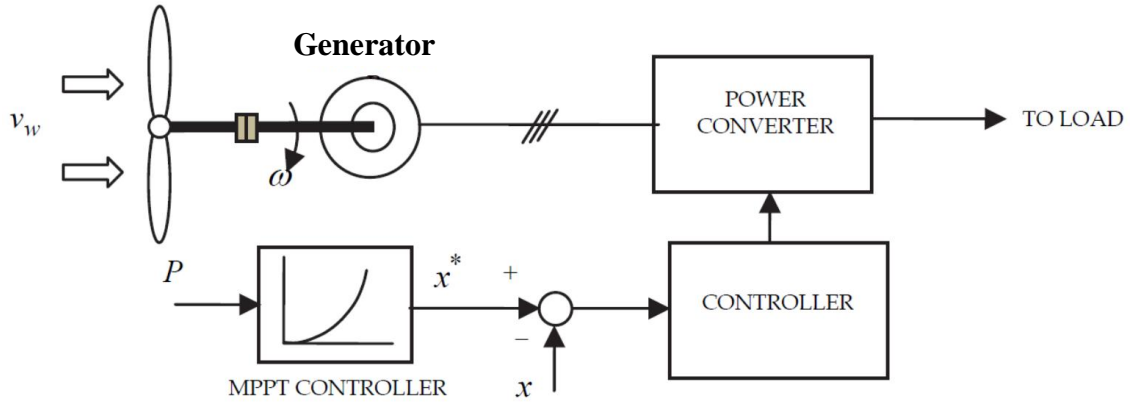


Figure 4.12: WECS with hill climb search control

4.5.2.3. Algorithms Based on Power Characteristic Curve

This method is called power signal feedback (PSF) control. In PSF control method the knowledge of the used wind turbine's maximum power curve is required to have and then by using the control mechanisms of this method to track this curve [38]. By using off-line experiment or simulations on the used wind turbine the maximum power curve can be obtained. Reference power is generated, where the wind speed or the rotor speed is used as the input, in this method instead of using the mechanical power equation or using a recorded maximum power curve of the used wind turbine. Figure (4.13) shows the block diagram of a WECS with PSF controller for maximum power extraction [38].

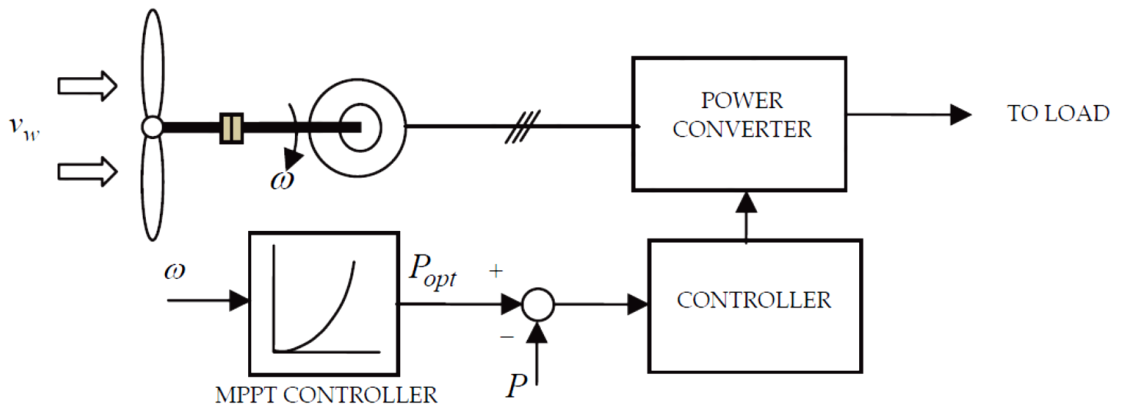


Figure 4.13: Power signal feedback control

After the three algorithms are explained, the PSF control method is chosen in this thesis due to the simplicity of this method and does not has any additional wind speed measurement costs. In the next chapter the performance of the proposed system can be analyzed in a closed loop control and verified by the help of MATLAB/SIMULINK package.

Chapter 5 : MATLAB/SIMULINK and Simulation Results

5.1. Introduction

The proposed system of stand-alone DFIG as mention before in previous chapters consists of multiple systems such as wind, wind turbine mechanism, DFIG, power converters, loads and finally control system. Each of them has been studied separately in details. Now all this systems must be connected together to produce the final system as proposed in Figure (1.12) in chapter (1). The performance of the proposed system can be analysis and verified by the help of MATLAB/SIMULINK package.

In this chapter a MATLAB/Simulink models of stand-alone DFIG are generated which consist of:

- 1- Model of aerodynamic system for wind turbine (mention in chapter 2).
- 2- Model of DFIG (mentioned in chapter 3).
- 3- Model of Loads (mentioned in chapter 4).
- 4- Model of control algorithm (mentioned in chapter 4).
- 5- Model of MPPT technique applied on DFIG (mentioned in chapter 4).

Firstly, the control method is chosen for open loop control on DFIG at certain value of wind speed in sub-synchronous and super-synchronous speed mode of operations. The loads have different values in each case. Finally, applying MPPT algorism with the variation of wind speed for sub-synchronous and super-synchronous speed mode of operations in a closed loop control system.

5.2. DFIG Power Flow

As mentioned before in Eq. (4.25) and Eq. (4.28), the output voltage of DFIG is controlled at desired value by controlling the direct component of the rotor current (i_{dr}). Also in Eq. (4.31), the stator output power is controlled at required value, for certain mechanical input power, by controlling the quadrature component of the rotor current (i_{qr}). So firstly at any operating point of DFIG the operating values of the voltage, output power and frequency must be determined to obtain the right values of required i_{dr} and i_{qr} and then required rotor input voltage and frequency through the rotor side converter. The output frequency can be controlled as mentioned in Eq. (4.1). The next analysis illustrates the controlling of DFIG by the help of open loop vector control method.

From the steady state equivalent circuit and relations of the DFIG the power relations of DFIG shown in Figure (5.1) [16] is expressed as follows [10, 16]:

$$P_s + P_r = P_{cus} + P_{cur} + P_m \quad (5.1)$$

Where

- P_s is the stator electrical output power (W),
- P_r is the rotor electrical (in/out) power (W),
- P_{cus} is the stator copper losses (W),
- P_{cur} is the rotor copper losses (W),
- P_m is the mechanical input power (W).

By neglecting the copper power losses in the rotor and stator resistances, then the relation between the rotor and the stator power is given by [10, 16]:

$$P_r = -sP_s \quad (5.2)$$

Where

s is the slip

Also if the mechanical power losses in the DFIG and wind turbine is neglected then:

$$P_m = P_t \quad (5.3)$$

Where

P_t is the effective mechanical power extracted from wind turbine.

Then the stator output power can be expressed as function of input mechanical power as follows [10, 16]:

$$P_s = P_t / (1-s) \quad (5.4)$$

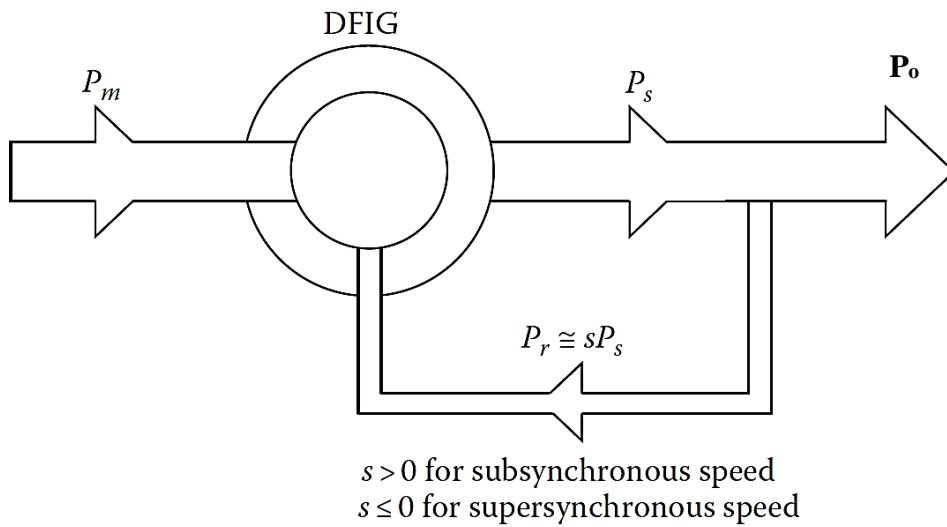


Figure 5.1: Power flow diagram of DFIG

Now for a given wind speed the relations of the mechanical input power P_t to the generator rotational speed N_g and mechanical torque T_g to the generator rotational speed N_g are obtained. Then from the curve the operating point Q is chosen at two different wind speed to apply the control method on the DFIG and analysis it's performance in sub-synchronous and super-synchronous speed modes of operation.

5.3. Sub-Synchronous Speed Mode of Operation

5.3.1. Mechanical Calculations

Assume the wind speed is 5.5 m/s and the relations of P_t and T_g with N_g is shown in Figures (5.2) and (5.3). The operating point Q_1 is chosen on the curve so that the mechanical speed of the generator causes it to operate under sub-synchronous speed (below 1500 rpm).

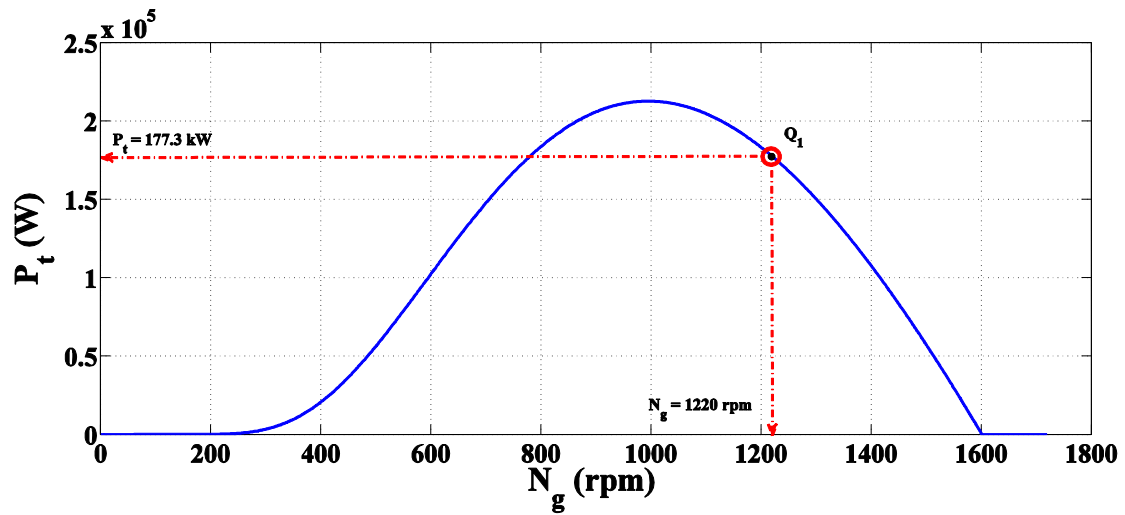


Figure 5.2: Turbine power with generator rotational speed at wind speed 5.5 m/s

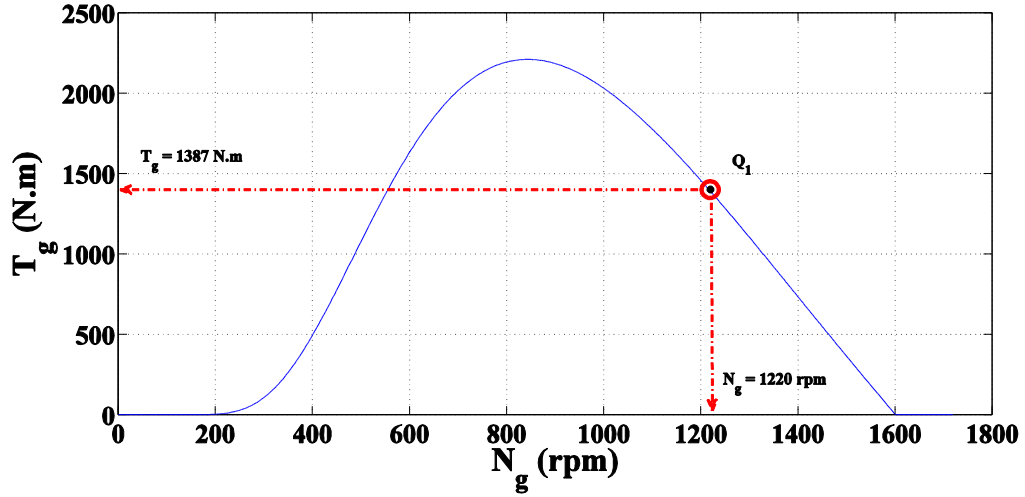


Figure 5.3: Generator mechanical torque with rotational speed at wind speed 5.5 m/s

From the curves in Figures (5.2) and (5.3) the mechanical values of the generator at the operating point are:

Generator speed	$N_g = 1220$ rpm,
Generator torque	$T_g = 1387$ N.m,
Turbine extracted power	$P_t = 177.3$ kW,
Slip	$s = 0.1867$.

Now all the required electrical parameters are calculated from the generator relations to determine the controlled values of i_{dr} , i_{qr} and F_r .

5.3.2. Electrical Calculations

By substituting the values of the extracted turbine power P_t and slip s in Equations (5.2) to (5.4) then the stator of the DFIG can develop power as follows:

$$P_s = - 218 \text{ kW.}$$

Also the rotor power is:

$$P_r = 40.7 \text{ kW.}$$

The positive sign indicates to input power and negative sign indicates to output power from the DFIG. in sub-synchronous speed mode of operation the rotor circuit consumes power to develop the stator output power.

From the generator main parameters the rated stator output voltage per phase (rms) and frequency of DFIG is:

$V_s = 398.3717$ V, $F_s = 50$ Hz, and [25]:

$$V_m = \sqrt{V_{qs}^2 + V_{ds}^2} \quad (5.5)$$

Where

V_m is the maximum value of stator output voltage = 563.3826 V.

Substitute Equations (4.25) and (4.26) in Eq. (5.5) then

$$V_{qs} = V_m = \omega_s \psi_{ds} \quad (5.6)$$

Where

$$\omega_s = 2\pi F_s = 314.159 \text{ elec. rad/sec.}$$

From Eq. (5.6) the value of stator flux linkage can be determine which equal to:

$$\psi_{ds} = 1.7933 \text{ Wb.turn.}$$

By substitute the values of ψ_{ds} , ω_s and P_s in Equations (4.28) and (4.31) the required reference values of the rotor input currents by using vector control are:

$$\begin{aligned} i_{qr} &= 266.9432 \text{ A.} \\ i_{dr} &= 717.3211 \text{ A.} \end{aligned}$$

This reference values are used to generating the required reference values of rotor input voltage v_a , v_b , v_c for this operating point. The frequency of the rotor input voltage is regulated from the relation in Eq. (4.1). Figure (5.4) illustrates the control scheme for the stand-alone DFIG. After applying the rotor voltage the results must show that the generator goes to the steady state operating point at the desired setting of output power, torque, speed, output terminal voltage and frequency for this controlling method.

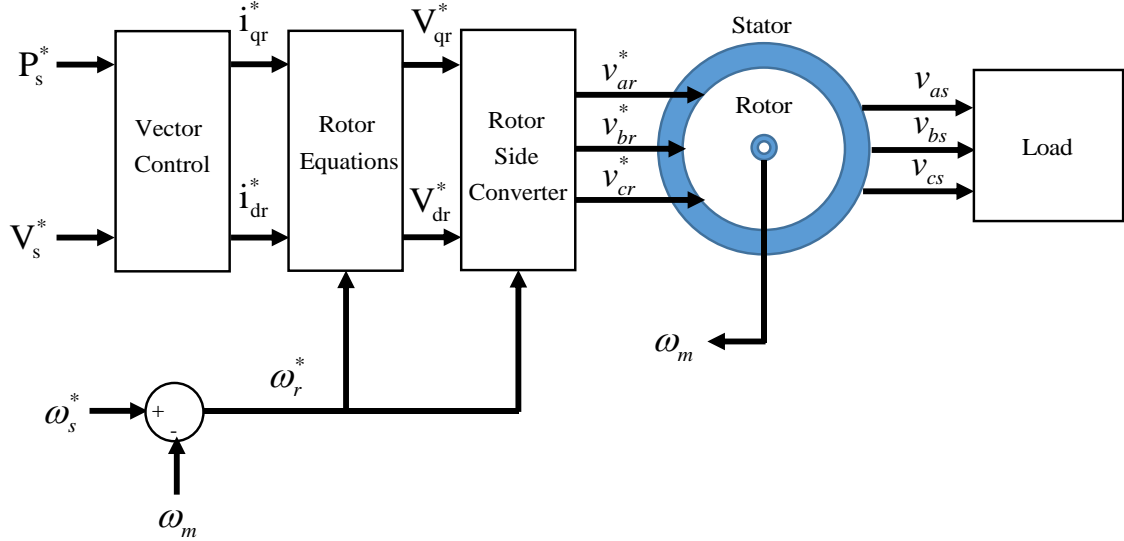


Figure 5.4: Control scheme for the stand-alone DFIG

5.3.3. Simulation and Results

Finally from the Calculations M-file which contains the DFIG and wind turbine parameters all needed parameters can be calculated for Simulink. The Simulink/Model is shown in Figure (5.5) consists of

- 1- The DFIG and loads modelling.
- 2- Wind turbine modelling.
- 3- Vector control algorithm.

The Simulink/model has a simulation time of 40 second which is divided into three periods explained as follows:

- 1- The first period (from 0 to 15 second) the wind turbine runs to steady state without connecting the rotor voltage and the loads to the DFIG terminals.
- 2- The second period (from 15 to 25 second) the desired rotor input voltage is applied according to the present value of wind speed and no-loading condition of the DFIG by using vector control algorithm until the system reaches to the steady state.
- 3- The final period (from 25 to 40 second) the load is connected and the model regenerate the required rotor input voltage according to the load condition. There is no change in wind speed and load condition in this model.

The results of the DFIG system under study are shown in Figures (5.6) to (5.17). Figures (5.6) and (5.7) show the actual values of q- and d-axes rotor currents (i_{qr} and i_{dr} , respectively), and their respective reference currents. The variations in the reference values of the rotor currents are controlled such that the transient in the stator outputs are small. As shown in Figures (5.6) and (5.7), the transients in i_{qr} and i_{dr} almost die out in 5 seconds from the point at which the load is applied. The maximum over shooting is about 6 % in i_{qr} and 4 % in i_{dr} . The steady-state error never exceed 0.13 % in both currents.

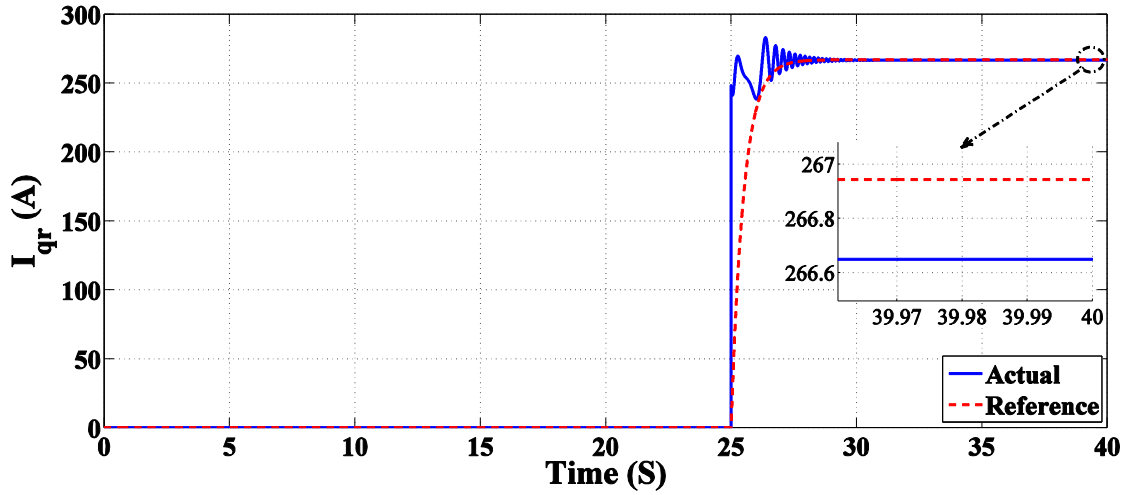


Figure 5.6: Quadrature axis of the rotor input current I_{qr} (A)

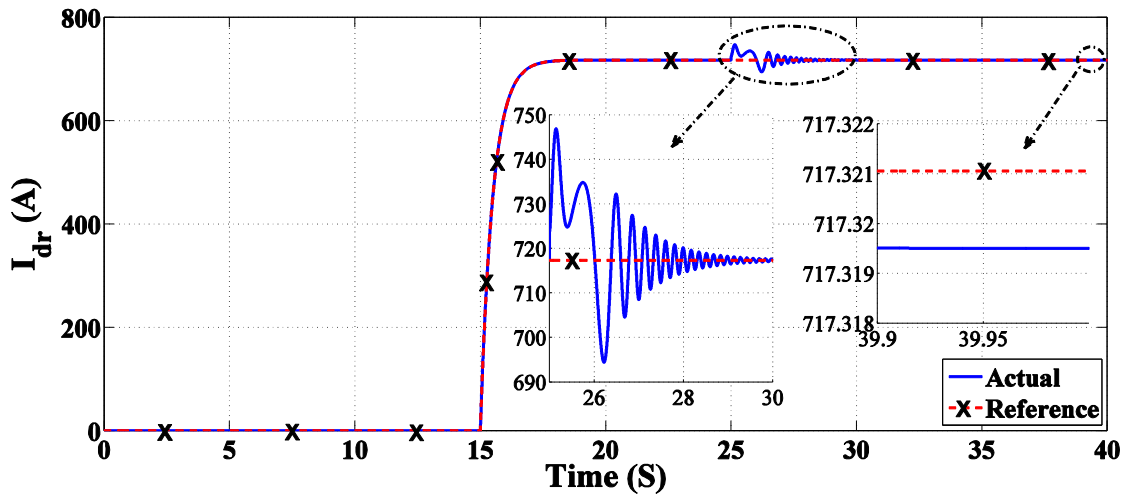


Figure 5.7: Direct axis of the rotor input current I_{dr} (A)

Figure (5.8) shows the instantaneous rotor input voltages waveforms v_{abcr} (V). As shown in the figure, from 0 to 15 seconds the rotor terminals are disconnected from its power supply. This is to allow the rotating parts of DFIG to easily reach its steady-state speed. At $t = 15$ second, the rotor supply voltages is connected. A zoom view of the

rotor input voltage is displayed in Figure (5.9). From 15 to 25 second, the DFIG is running with no-load. At $t=25$ second, the full-load is applied to the stator terminals and the rotor voltages waveforms are depicted in the period from $t=24.5$ second to $t=27$ second. It should be noted that, the rotor voltages phase sequence are reversed after the full-load is applied. This is explained by the fact that the DFIG changes its mode of operation from super-synchronous speed (for time less than $t= 25.77$ second) to sub-synchronous speed after this time.

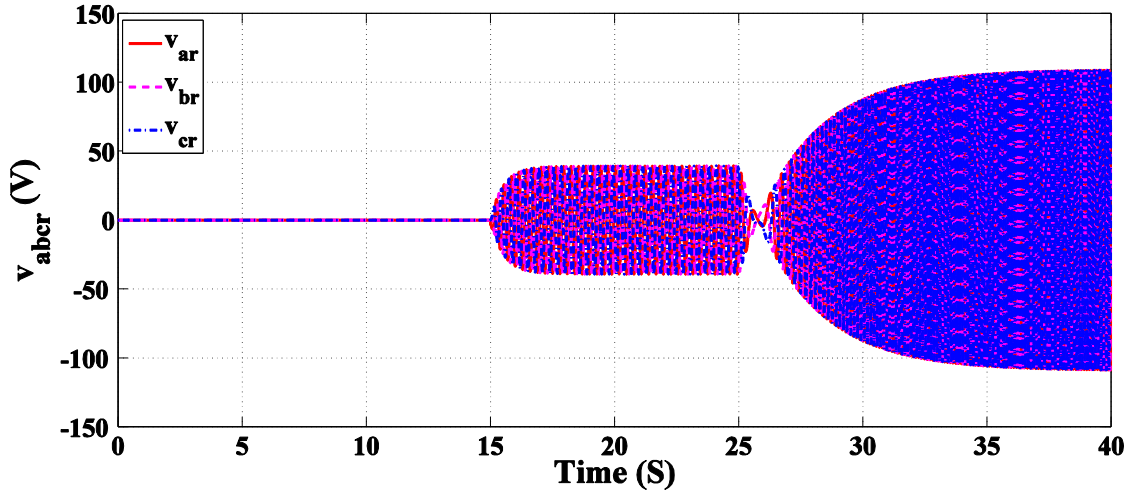


Figure 5.8: Instantaneous value of the rotor input voltage v_{abcr} (V)

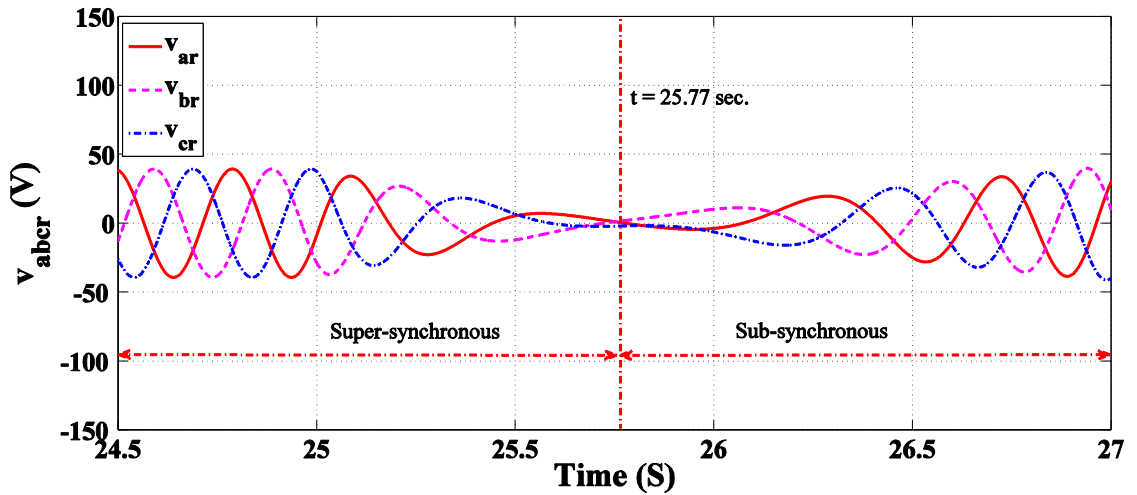


Figure 5.9: Zoom view of Figure 5.8 between 24.5 and 27 second

Figure (5.10) shows the change in the rotor frequency due to change of the speed of DFIG. The negative values of the rotor frequency indicated in the figure imply phase reversal of the rotor voltage.

Figure (5.11) shows the DFIG rotational speed N_g in rpm. From 0 to 15 second the DFIG is freely running until the speed reaches its steady-state final value (1601 rpm). At the instant of $t=15$ seconds, the rotor terminals are connected with its supply and there is still no-load connected to the stator terminals for a period of 10 seconds. At $t=25$ seconds, the full load is applied and the DFIG speed starts to decrease until it reaches final value of 1222 rpm with a steady-state error of approximately equal to 0.18 %.

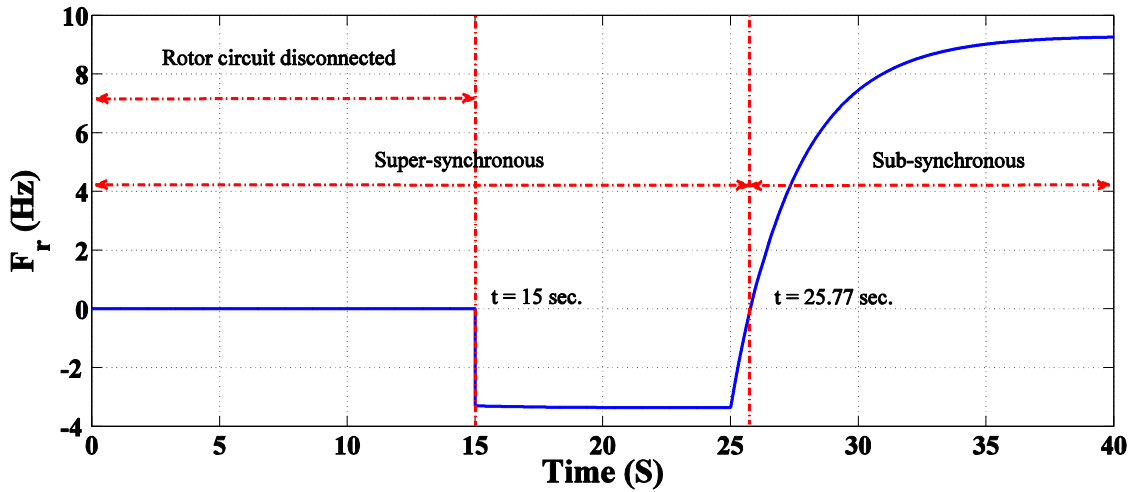


Figure 5.10: Frequency of the rotor input voltage F_r (Hz)

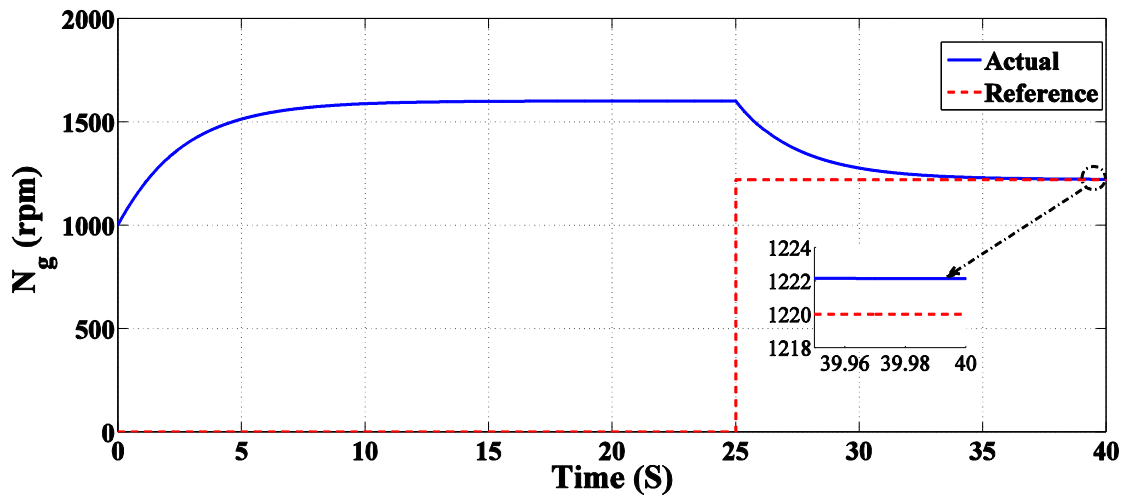


Figure 5.11: Generator rotational speed N_g (rpm)

Figure (5.12) shows the actual and reference values of the rotor power, P_r . The negative actual power from 25 to 25.77 second is due to the fact that the loading of DFIG starts when its speed is above synchronous speed. After this point, the rotor speed slowly decrease until it reaches its steady-state value of 1222 rpm (rotor slip=0.185). The figure also shows that from 15 to 25 second (the load is not connected

yet) power is injected into the rotor circuit to supply the rotor copper and machine iron losses. The figure also shows the steady-state error between the actual rotor power and its reference value is approximately 5.36 %.

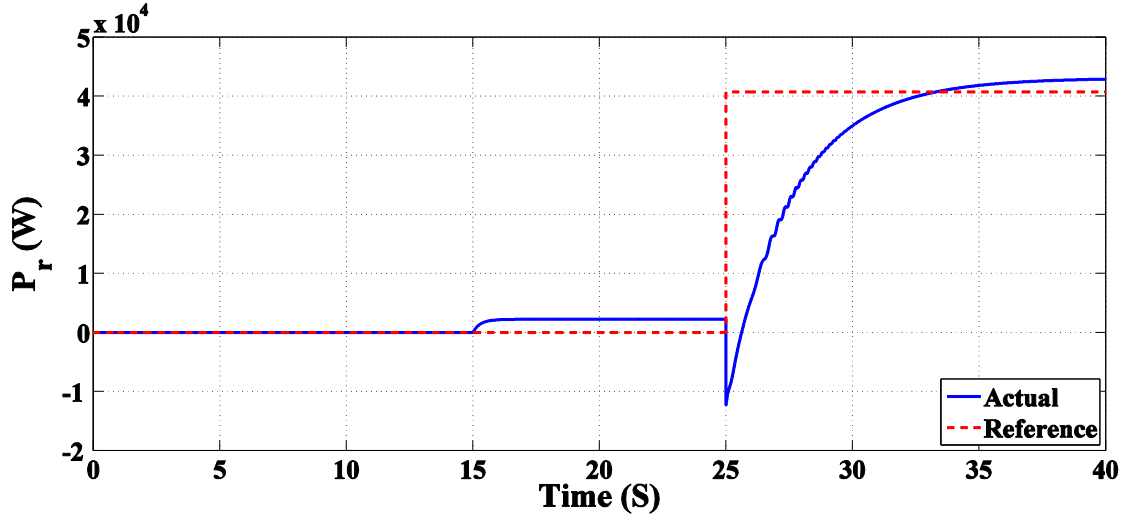


Figure 5.12: Rotor power P_r (W)

Figure (5.13) depicts the steady-state waveform of the stator output phase voltage. The figure shows that the stator voltages are pure sinusoidal waveforms. Figure (5.14) shows the time variation of the magnitude of the stator phase voltage. The figure shows that the load voltage magnitude has a maximum excursion from its reference wave by 3.2 % for 4 seconds. The magnitude of the stator voltage has a steady-state error of 0.15 %. Figure (5.15) shows that the frequency of the stator voltage is kept fixed at 50 Hz through the whole range of operation.

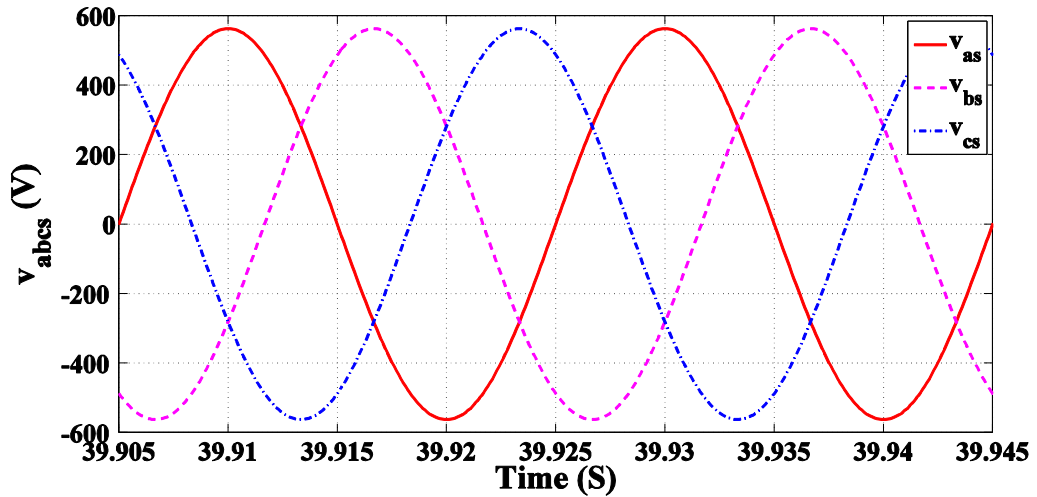


Figure 5.13: Instantaneous stator output voltage v_{abc} (V) of DFIG

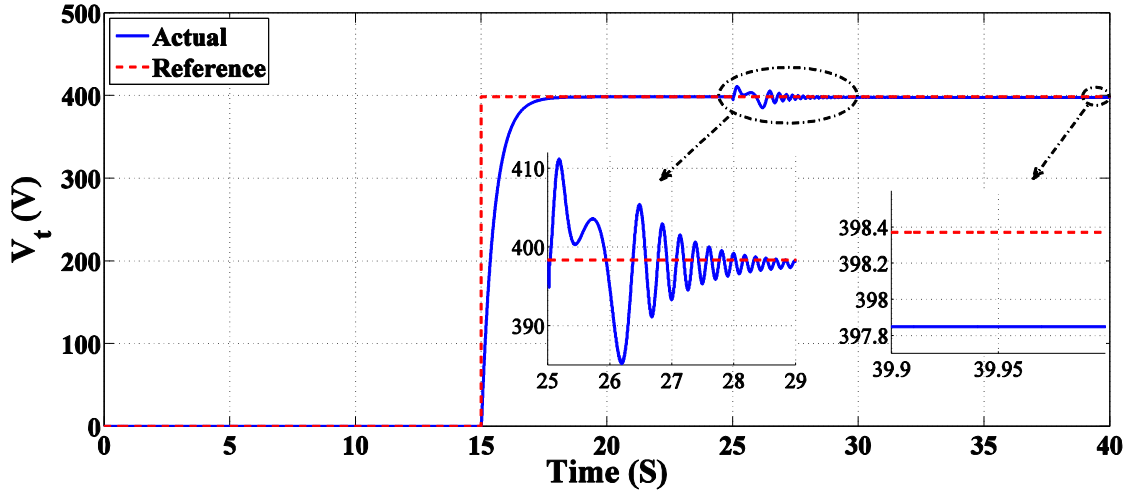


Figure 5.14: Stator rms terminal output voltage V_t (V)

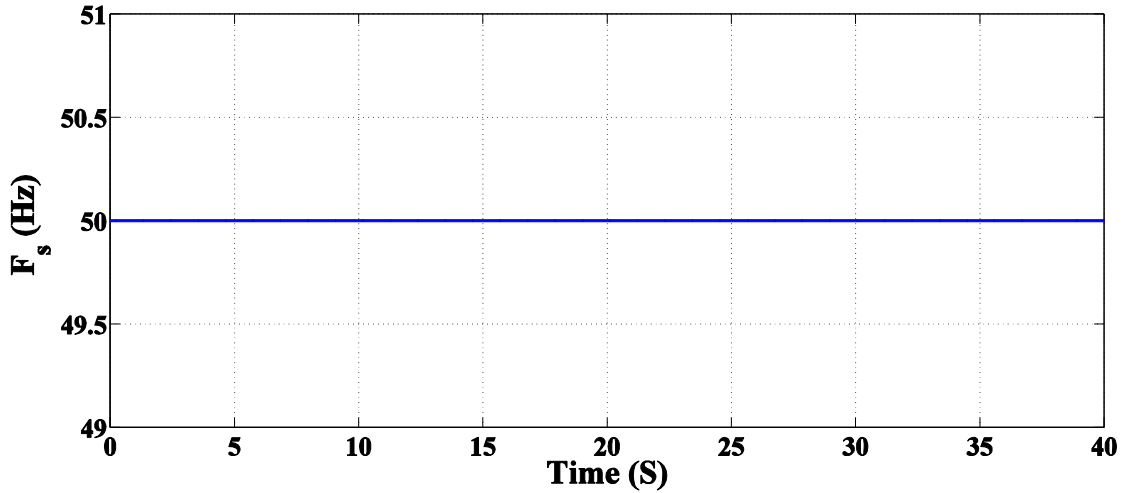


Figure 5.15: Stator output frequency F_s (Hz)

Figure (5.16) shows the stator output power and its reference power P_s (W). Note that the difference between the actual and reference value of the steady-state power is due to the fact that losses in the stator circuit. The oscillations of the power at the instant of applying the load on the DFIG has maximum overshoot about 6.4%. Finally, the generator reference and actual torque, T_g (N.m), are shown in Figure (5.17). The difference between the actual and reference values is due to DFIG power losses as mentioned before. Also the final values have small error.

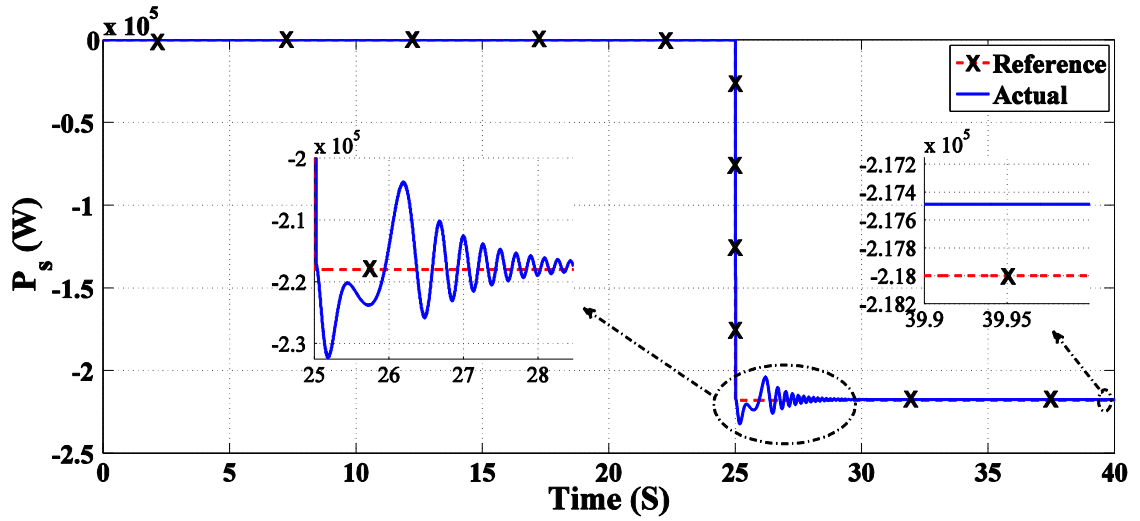


Figure 5.16: Stator output and reference power (W)

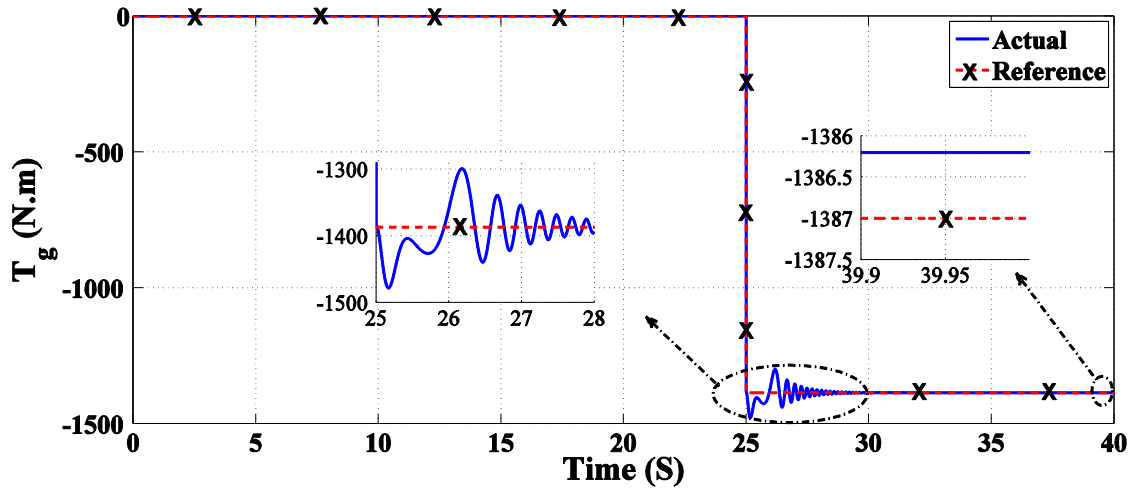


Figure 5.17: Generator electromechanical torque T_g (N.m)

5.4. Super-Synchronous Speed Mode of Operation

5.4.1. Mechanical Calculations

Assume the wind speed is 7.5 m/s and the relations of P_t and T_g with N_g is shown in Figures (5.18) and (5.19). The operating point Q_2 is chosen on the curve so that the mechanical speed of the generator causes it to operate under super-synchronous speed (above 1500 rpm).

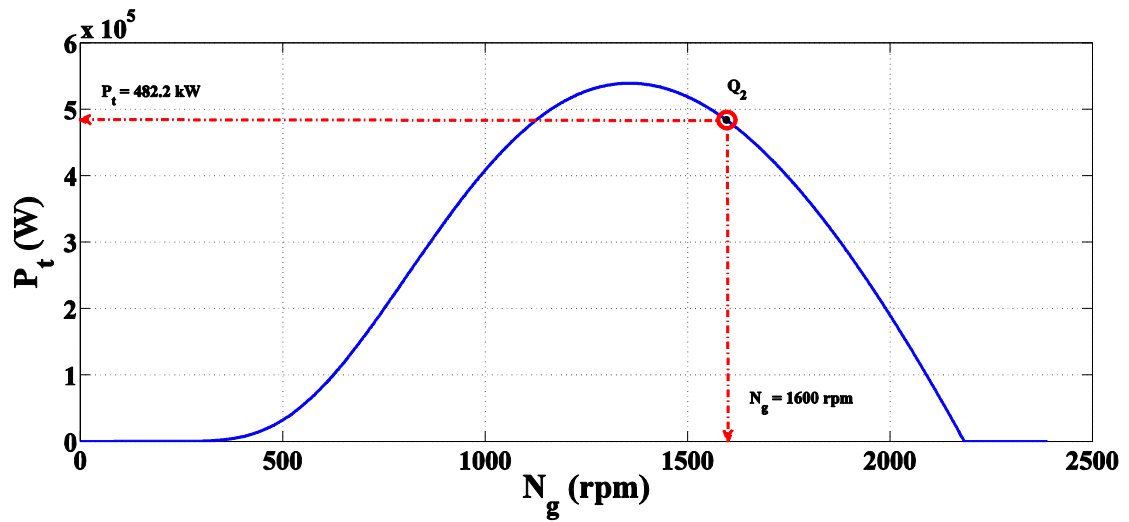


Figure 5.18: Turbine power with generator rotational speed at wind speed 7.5 m/s

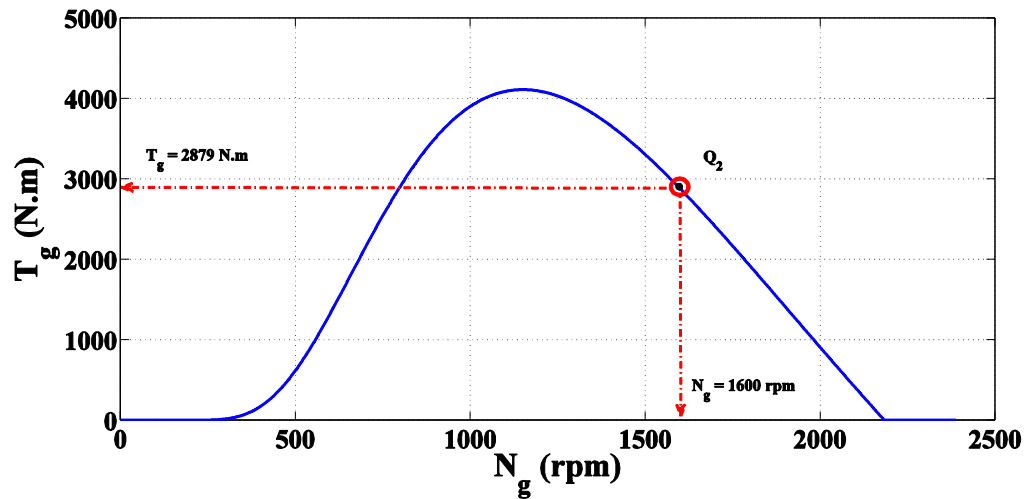


Figure 5.19: Generator mechanical torque with rotational speed at wind speed 7.5 m/s

From the curves in Figures (5.18) and (5.19) the mechanical values of the generator at the operating point are:

Generator speed	$N_g = 1600 \text{ rpm}$,
Generator torque	$T_g = 2879 \text{ N.m}$,
Turbine extracted power	$P_t = 482.2 \text{ kW}$,
Slip	$s = -0.06633$.

Now all the required electrical parameters are calculated from the generator relations to determine the controlled values of i_{dr} , i_{qr} and F_r .

5.4.2. Electrical Calculations

By substitute the values of the extracted turbine power P_t and slip s in Equations (5.2) to (5.4) then the stator of the DFIG can develop power as follows:

$$P_s = -452.2 \text{ kW, and}$$

The rotor input power is:

$$P_r = -29.99 \text{ kW}$$

From the generator main parameters the rated stator output voltage per phase (rms) and frequency of DFIG is:

$$V_s = 398.3717 \text{ V, } F_s = 50 \text{ Hz, and [25]:}$$

$$V_m = \sqrt{V_{qs}^2 + V_{ds}^2} \quad (5.7)$$

Where

V_m is the maximum value of stator output voltage = 563.3826 V.

Substitute Equations (4.25) and (4.26) in Eq. (5.7) then

$$V_{qs} = V_m = \omega_s \psi_{ds} \quad (5.8)$$

Where

$$\omega_s = 2\pi F_s = 314.159 \text{ elec. rad/sec.}$$

From Eq. (4.40) the value of stator flux linkage can be determine and equal to:

$$\psi_{ds} = 1.7933 \text{ Wb.turn (Constant for two modes).}$$

By substitute the values of ψ_{ds} , ω_s and P_s in Equations (4.28) and (4.31) the required reference values of the rotor input currents by using vector control are:

$$i_{qr} = 553.72 \text{ A.}$$

$$i_{dr} = 717.3211 \text{ A.}$$

This reference values are used to generating the required reference values of rotor input voltage v_a , v_b , v_c for this operating point. The frequency of the rotor input voltage is regulated from the relation in Eq. (4.1). Figure (4.12) illustrates, as in sub-synchronous mode of operation, the control scheme for the stand-alone DFIG. After applying the rotor voltage the results must show that the generator goes to the steady

state operating point at the desired setting of output power, torque, speed, output terminal voltage and frequency for this controlling method.

5.4.3. Simulation and Results

This model is the same as in sub-synchronous speed mode of operation shown in Figure (5.5) just the wind speed is changed in this case to 7.5 m/s.

The results of the DFIG system under study are shown in the Figures (5.20) to (5.31). Figures (5.20) and (5.21) show the actual values of q and d axes rotor currents (i_{qr} and i_{dr}), respectively, and their respective reference currents. The changes in the reference values of the rotor currents are controlled such that the transients in the stator outputs are small. As shown in Figures (5.20) and (5.21) the transients in i_{qr} and i_{dr} almost die out in 3 seconds from the point at which the load is applied to steady-state. The maximum overshoot about 5 % in i_{dr} . The steady-state error never exceed 0.2 % in both currents.

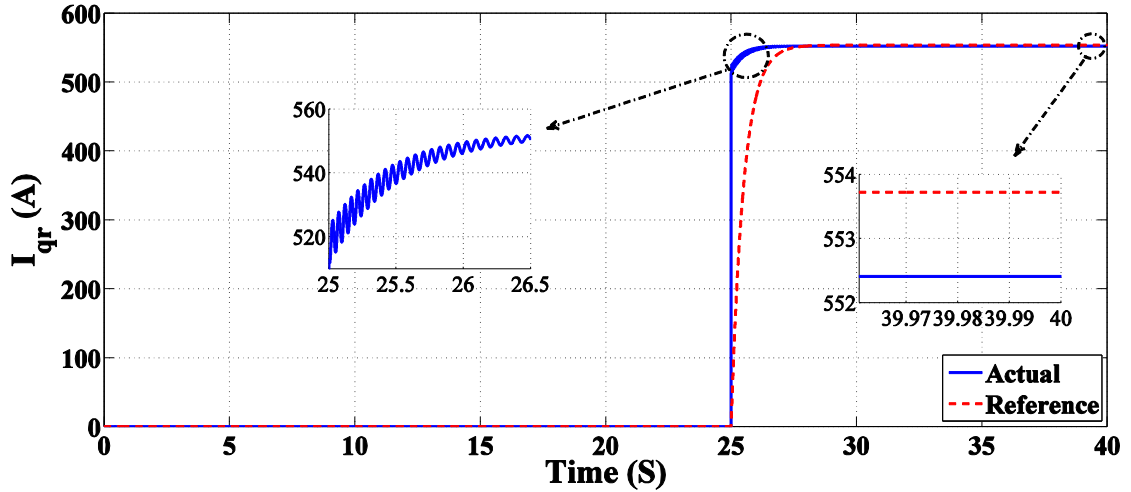


Figure 5.20: Quadrature axis of the rotor input current I_{qr} (A)

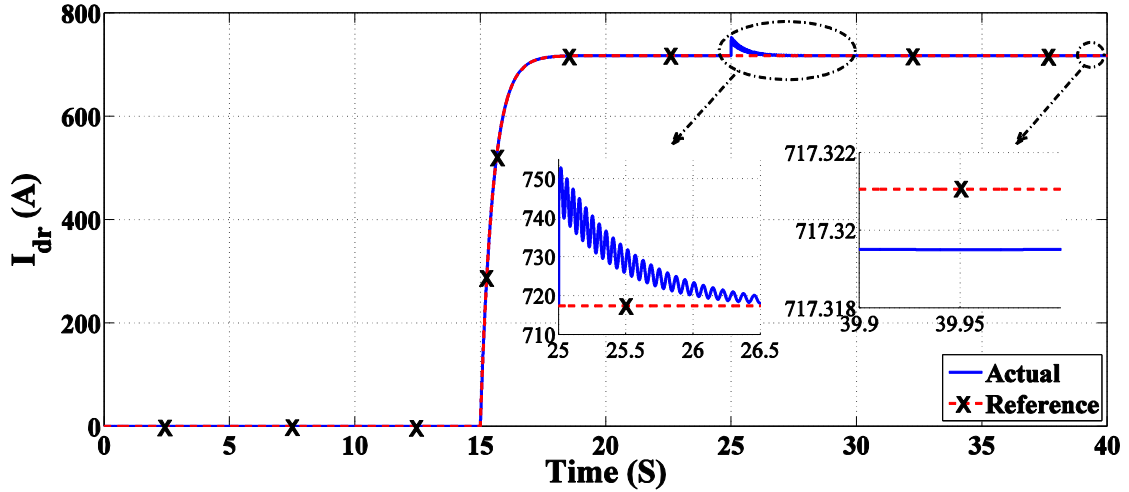


Figure 5.21: Direct axis of the rotor input current I_{dr} (A)

Figure (5.22) shows the instantaneous rotor input voltages waveforms v_{abcr} (V). As shown in the figure from 0 to 15 seconds the rotor terminals are disconnected from its supply. This is to allow the rotating parts of DFIG to easily reach its steady-state speed. At $t = 15$ second, the rotor supply voltage is connected. A zoom view of the rotor input voltage is displayed in Figure (5.23). From 15 to 25 second, the DFIG is running with no-load. At $t = 25$ second, the full-load is applied to the stator terminals and the rotor voltages waveforms are depicted in the period from $t = 25$ second to $t = 30$ second. It should be noted that, the rotor voltage phase sequence is not reversed after the full-load is applied as in sub-synchronous speed mode of operation. This explained by the fact that the super-synchronous speed mode of operation of DFIG is not changed during the whole rang.

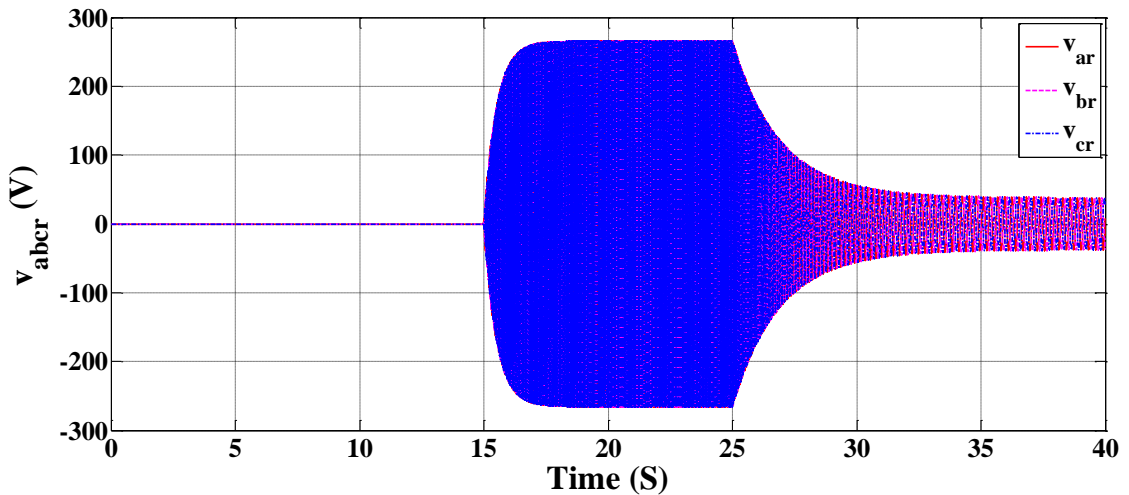


Figure 5.22: Instantaneous value of the rotor input voltage v_{abcr} (V)

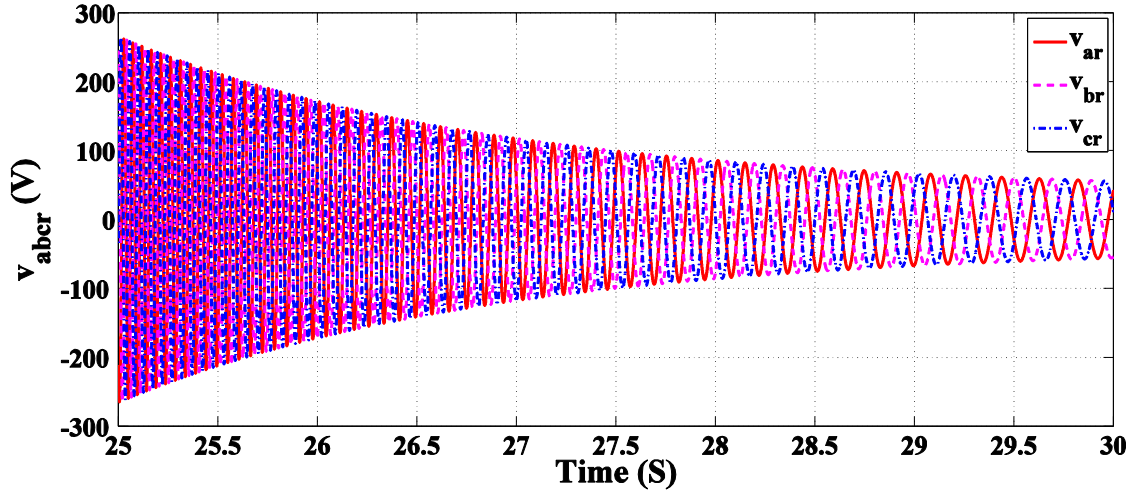


Figure 5.23: Zoom view of Figure 5.22 between 25 and 30 second

Figure (5.24) shows the change in the rotor frequency due to change of the speed of DFIG. The negative values of the rotor frequency indicated in the figure implies phase reversal of the rotor voltage in super-synchronous speed mode of operation.

Figure (5.25) shows the DFIG rotational speed N_g (rpm). From 0 to 15 second the DFIG is freely running until the speed reaches its steady-state final value (2183 rpm). At the instant of $t = 15$ seconds, the rotor terminals are connected with its supply and there is no-load connected to the stator terminals for a period of 10 seconds. At $t = 25$ seconds, the full load is applied and the DFIG speed starts to decrease until it reaches final value of 1602 rpm with a steady-state error of approximately equal to 0.12 %.

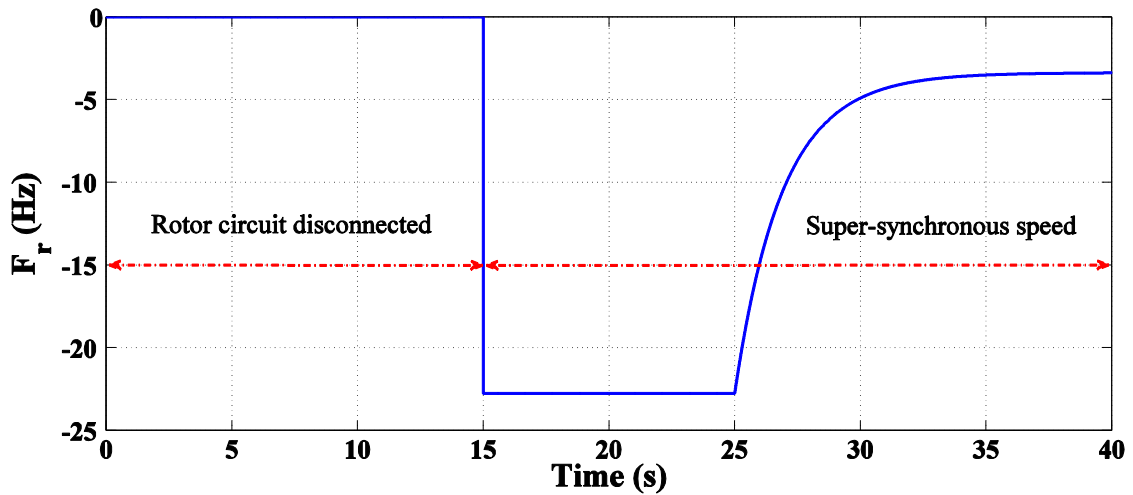


Figure 5.24: Frequency of the rotor input voltage F_r (Hz)

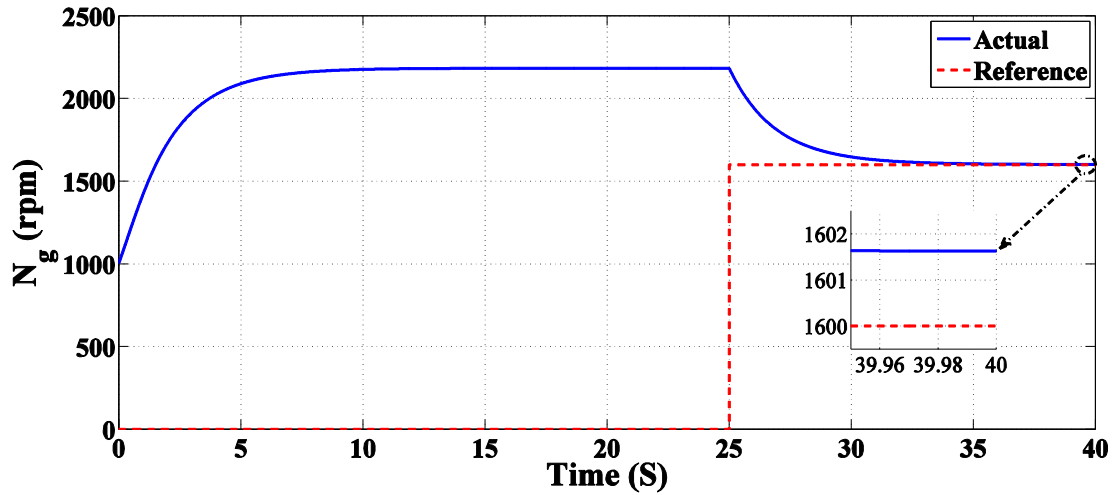


Figure 5.25: Generator rotational speed N_g (rpm)

Figure (5.26) shows the actual and reference values of the rotor power P_r (W). The figure shows that from 15 to 25 second (the load is not connected yet) power is injected into the rotor circuit to supply the rotor copper and machine iron losses. The negative actual power from 25 to 40 second is due to the fact that the loading of DFIG starts when its speed is above synchronous speed. After this point, the rotor speed slowly decrease until it reaches its steady-state value of 1602 rpm ($s = -0.068$). As the DFIG rotational speed is above synchronous speed the rotor extract power from its circuit. The figure also shows the steady-state error between the actual rotor power and its reference value is approximately 10 %.

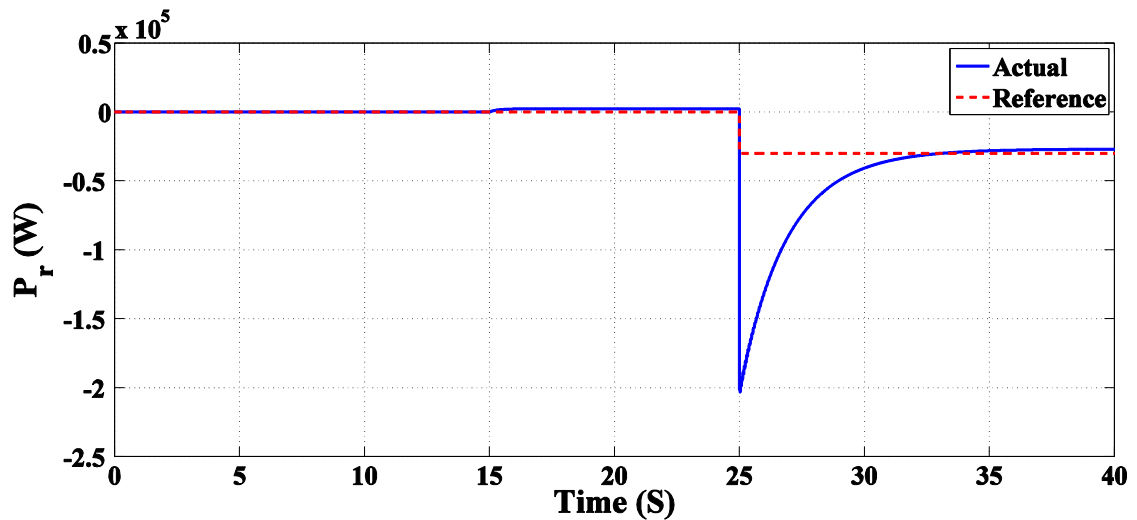


Figure 5.26: Rotor power P_r (W)

Figure (5.27) shows the steady-state waveform of the stator output phase voltage. The figure shows that the stator voltages are pure sinusoidal waveforms. Figure (5.28) shows the time variation of the magnitude of the stator phase voltage. The figure shows

that the load voltage magnitude has a maximum excursion from its reference wave by 0.82 % for 3 seconds. The magnitude of the stator voltage has a steady-state error of 0.25 %. Figure (5.29) shows that the frequency of the stator voltage is kept fixed at 50 Hz through the whole range of operation.

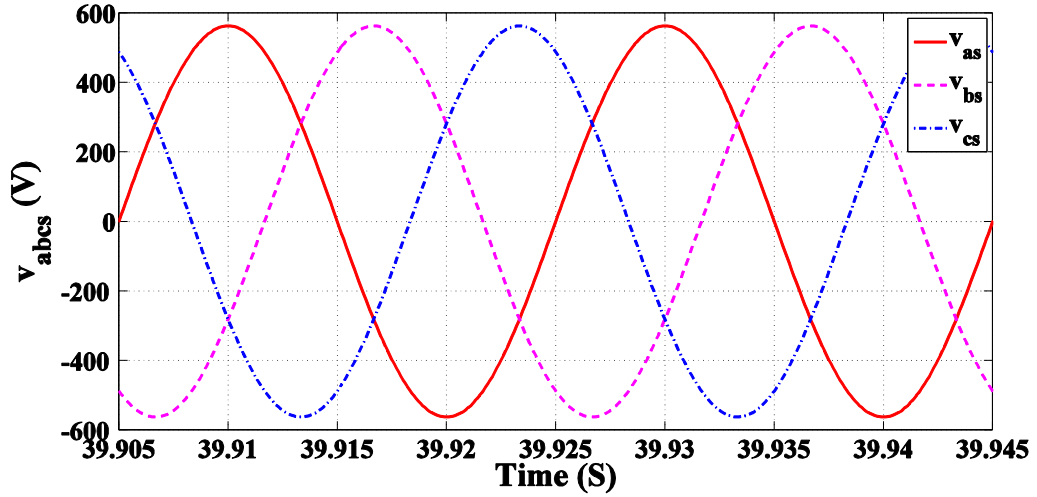


Figure 5.27: Instantaneous stator output voltage v_{abc} (V) of DFIG

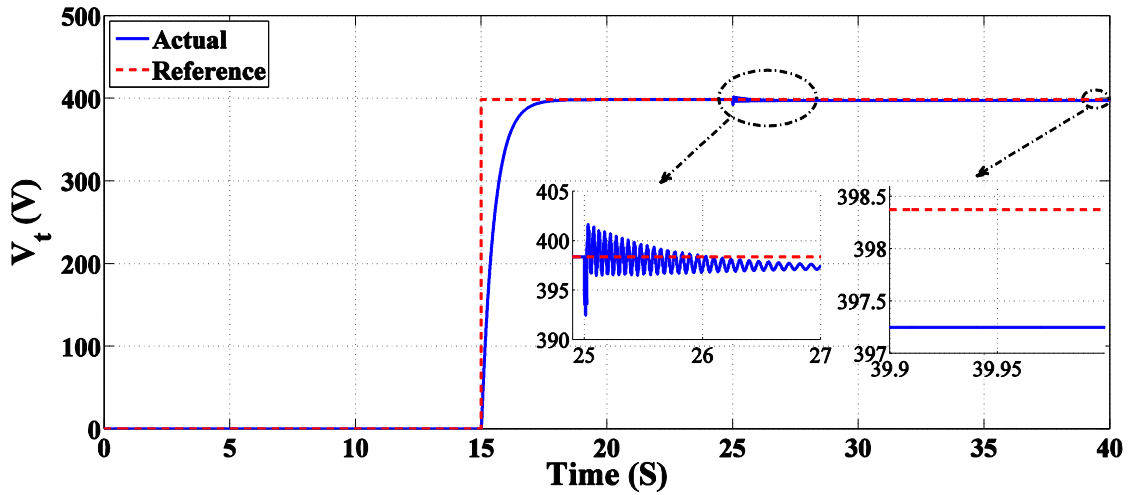


Figure 5.28: Stator rms terminal output voltage V_t (V)

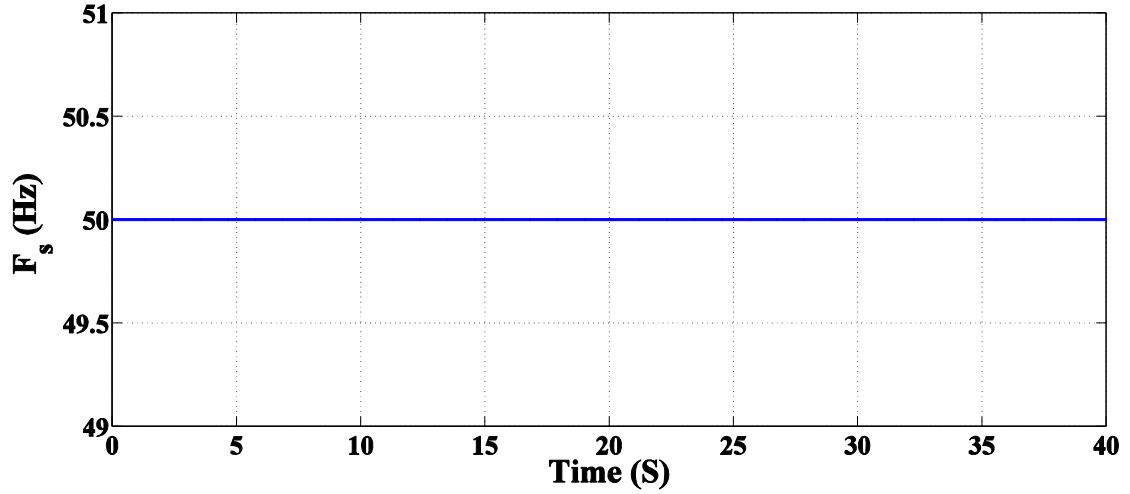


Figure 5.29: Stator output frequency F_s (Hz)

Figure (5.30) shows the stator output power and its reference power P_s (W). Note that the difference between the actual and reference value of the steady-state power is due to the losses in the stator circuit. The oscillations of the power at the instant of applying the load on the DFIG has maximum overshooting about 1.73 %. Finally, the generator reference and actual torque, T_g (N.m), are shown in Figure (5.31). The difference between the actual and reference values is due to DFIG power losses as mention before. Also the final values have a small error percentage.

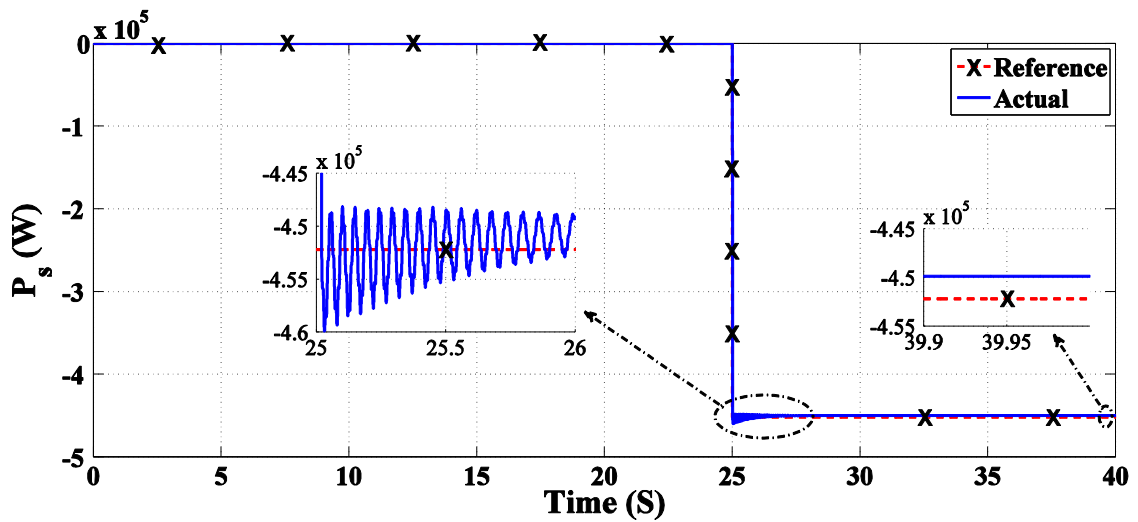


Figure 5.30: Stator output and reference power (W)

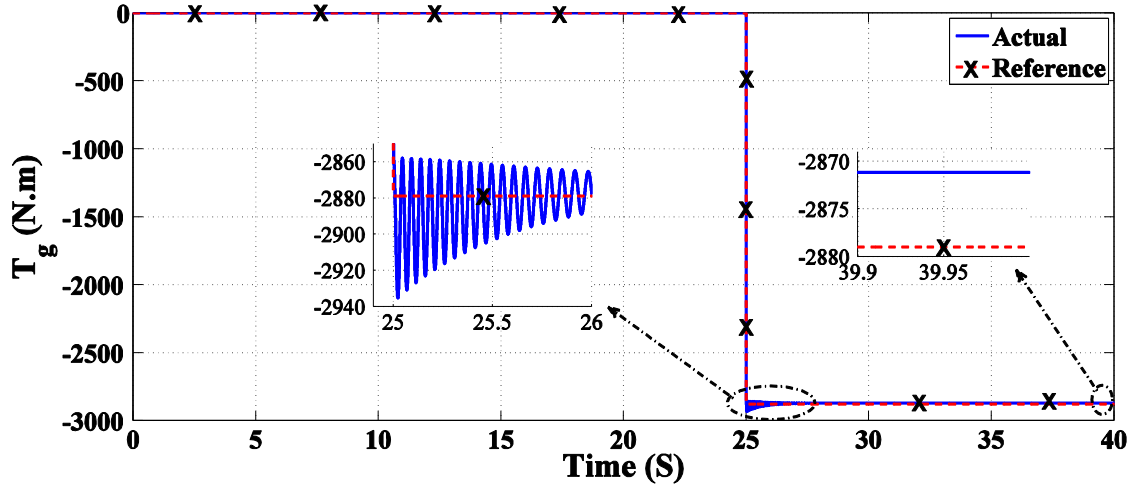


Figure 5.31: Generator electromechanical torque T_g (N.m)

5.5. MPPT for DFIG Based on Power Characteristic Curve Control Strategy

In order to apply the PSF control strategy as mentioned in chapter 4, three important parameters from all the wind turbine parameters mentioned in chapter (2) must be kept in mind [10]:

- 1- The optimum tip speed ratio,
- 2- The radius of wind turbine rotor, and
- 3- The range of the operating speed for the turbine.

The turbine mechanical power versus generator rotational speed curves is obtained as mentioned in chapter (2) at different wind speed by the help of the MATLAB/Simulink and the maximum power curve is generated as shown in Figure (5.32).

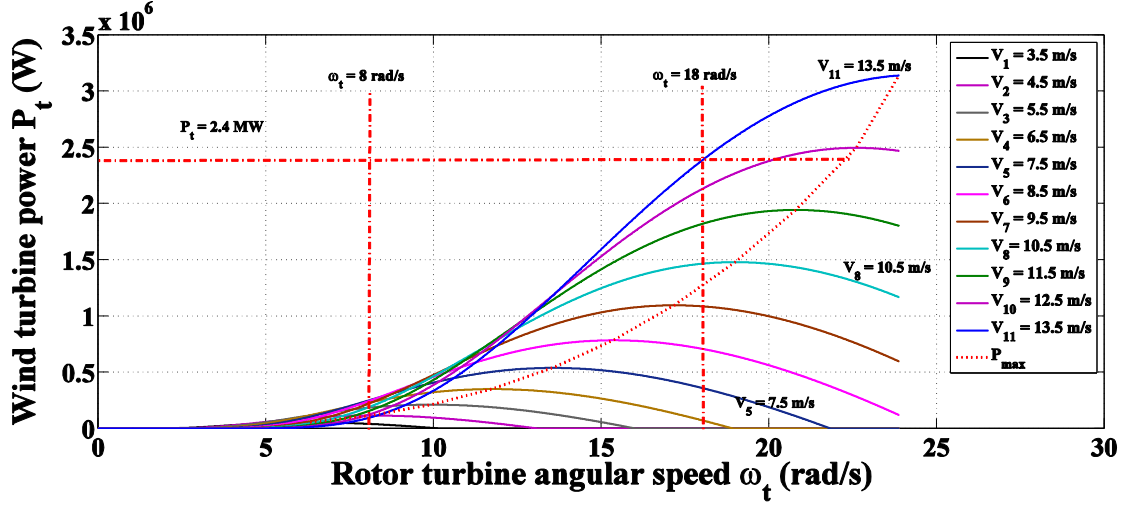


Figure 5.32: The wind turbine power P_t with the rotor angular speed ω_t

The maximum power point with associated generator rotational speed at each wind speed is recorded and are used as a look-up table. Firstly the wind speed is measured and used as an input to lookup table to obtain the maximum mechanical power and associated speed at this wind speed. Secondly the stator power reference is computed from the power relations which is mentioned before in this chapter. Then vector control algorithm is applied on the rotor input parameters to control the stator outputs at each maximum power point. The algorithm diagram is shown in Figure (5.33).

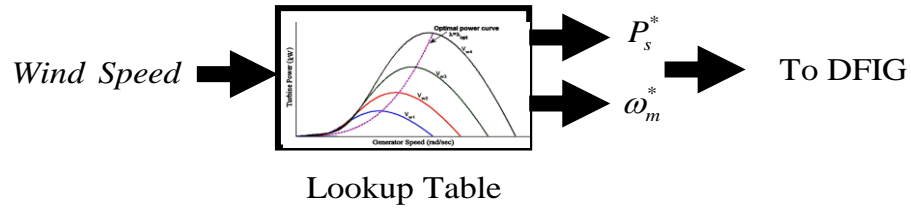


Figure 5.33: MPPT based on Power characteristic curve (Regulation of power)

The transient response of power mode control is relatively slow from other used modes, but the output power is becoming smooth and more accurate [41].

5.5.1. MATLAB/SIMULINK Model Implementation Using MPPT Algorithm

A DFIG wind power system for MPPT is represented and simulated by using MATLAB/Simulink, based on the PSF control strategy. The control method is applied to the DFIG at different wind speed, generator speed, sub-synchronous and super-synchronous speed. Also as the wind speed varies at each time so the generated model must observe this continuous variation and control the DFIG to maintain the output

voltage, magnitude and frequency at desired values and tracking the maximum power point.

The Simulink/model has a simulation time of 100 second which is divided into three periods explained as follows:

- 4- The first period (from 0 to 15 second) the wind turbine runs to steady state without connecting the rotor voltage and the loads to the DFIG terminals with variable wind speed applied on the DFIG.
- 5- The second period (from 15 to 25 second) the desired rotor input voltage is applied according to the present value of wind speed and no-loading condition of the DFIG by using vector control algorism until the system reaches to the steady state.
- 6- The final period (from 25 to 100 second) the load is connected and the model regenerate the required rotor input voltage for maximum power point tracking at each value of wind speed.

The Simulink/model for MPPT is the same as in Figure (5.5) with addition of MPPT based on the PSF control strategy and lookup table as shown in Figure (5.34).

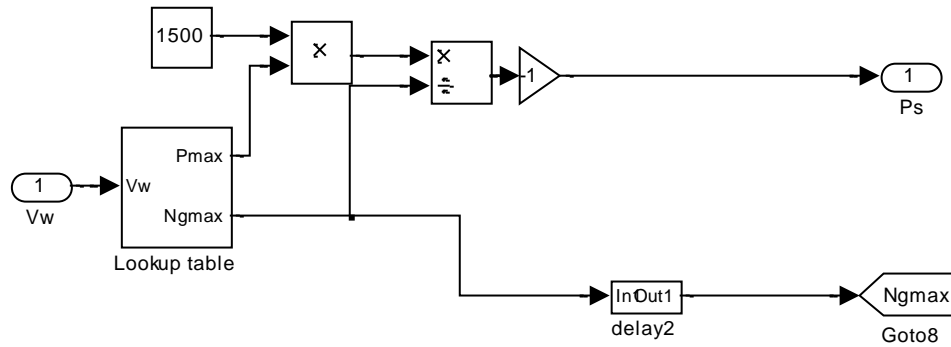


Figure 5.34: PSF control strategy and lookup table

Figure (5.35) represents the instantaneous wind speed for 100 seconds which has an average wind speed equal to 8.7 m/s.

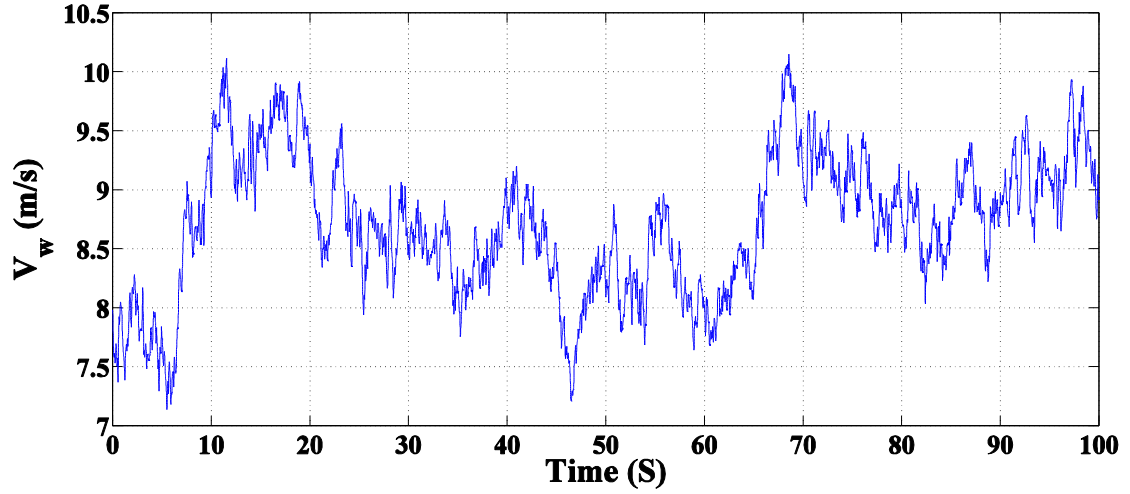


Figure 5.35: Wind speed profile

The simulation results of the DFIG Model with MPPT are shown in Figures (5.36) to (5.46). Figures (5.36) and (5.37) show the actual and reference values of the q- and d-axes rotor currents (i_{qr} and i_{dr}), respectively. From the figures, the value of i_{dr} has a nearly constant value during the simulation time. Also the i_{qr} component changes as the wind speed is changed and MPPT is applied.

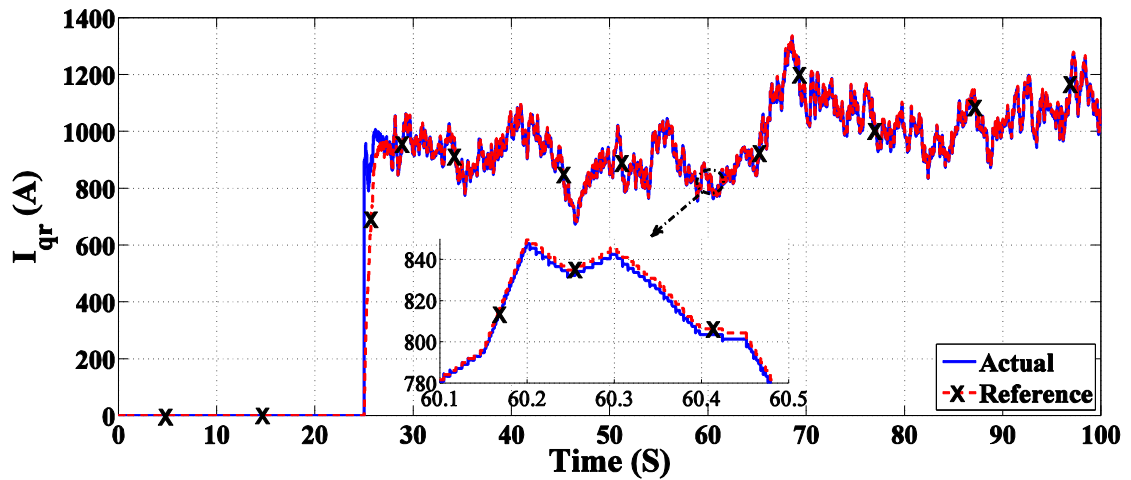


Figure 5.36: Quadrature axis of the rotor input current I_{qr} (A)

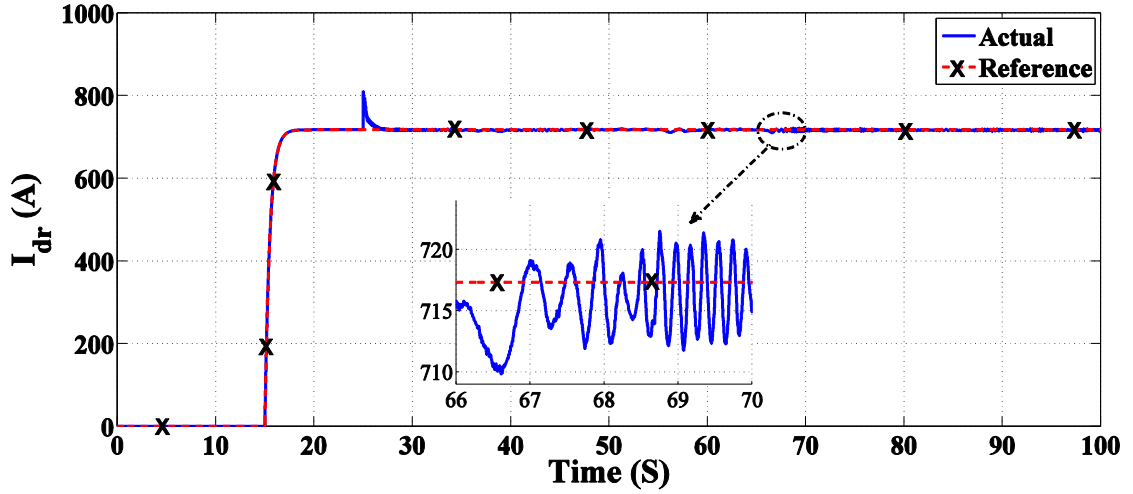


Figure 5.37: Direct axis of the rotor input current I_{dr} (A)

Figure (5.38) shows the instantaneous rotor input voltage waveforms, v_{abcr} (V). As shown in the figure, the rotor voltages continuously varies in magnitude and phase sequence in order to obtain the required rotor currents to achieve the MPPT requirements. A zoom view of the rotor input voltage is displayed in Figure (5.39).

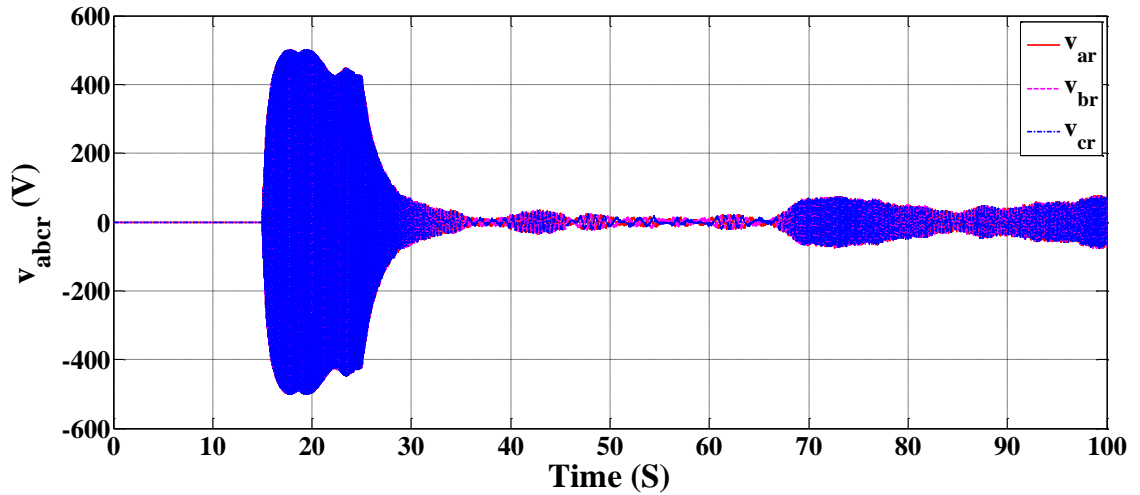


Figure 5.38: Instantaneous value of the rotor input voltage v_{abcr} (V)

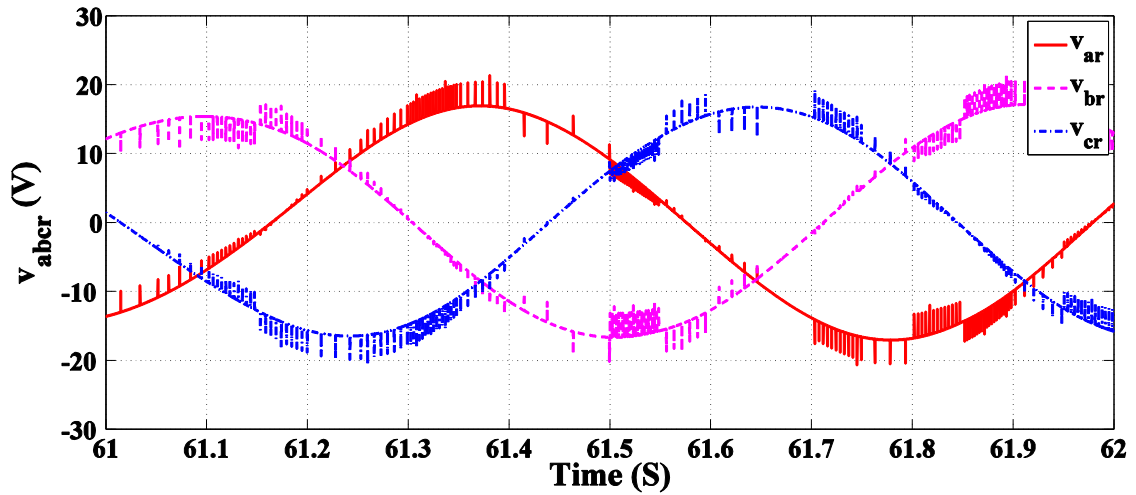


Figure 5.39: Zoom view of Figure 5.38 between 61 and 62 second

Figure (5.40) shows the change in the rotor frequency due to change of the speed of DFIG. The negative values of the rotor frequency indicated in the figure imply phase reversal of the rotor voltage.

Figure (5.41) shows the DFIG rotational speed N_g (rpm). From 0 to 15 second the DFIG is freely running and varying due to the variation of wind speed. At the instant of $t=15$ seconds, the rotor terminals are connected with its supply and there is no-load connected to the stator terminals for a period of 10 seconds. At $t=25$ seconds, the maximum power from the DFIG is applied and the DFIG speed change as the wind speed and the load change during the whole range of operation.

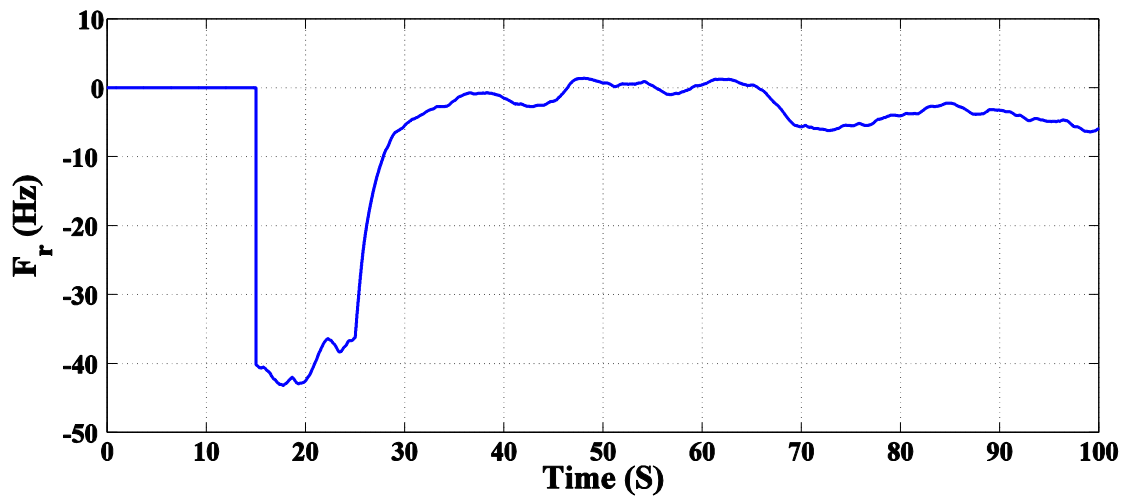


Figure 5.40: Frequency of the rotor input voltage F_r (Hz)

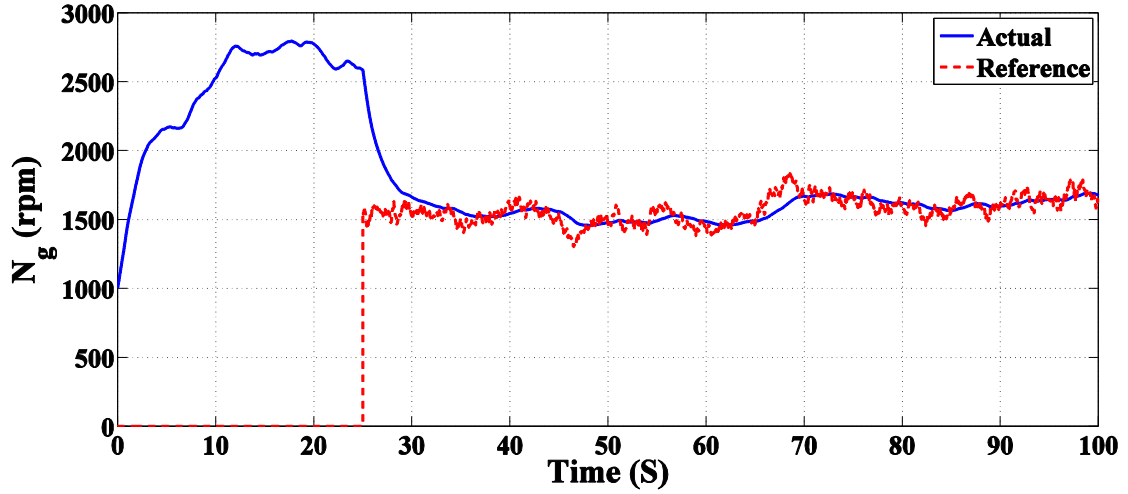


Figure 5.41: Generator rotational speed N_g (rpm)

Figure (5.42) shows the actual and reference values of the rotor power P_r (W). The rotor power can be negative or positive value according to speed mode of operation.

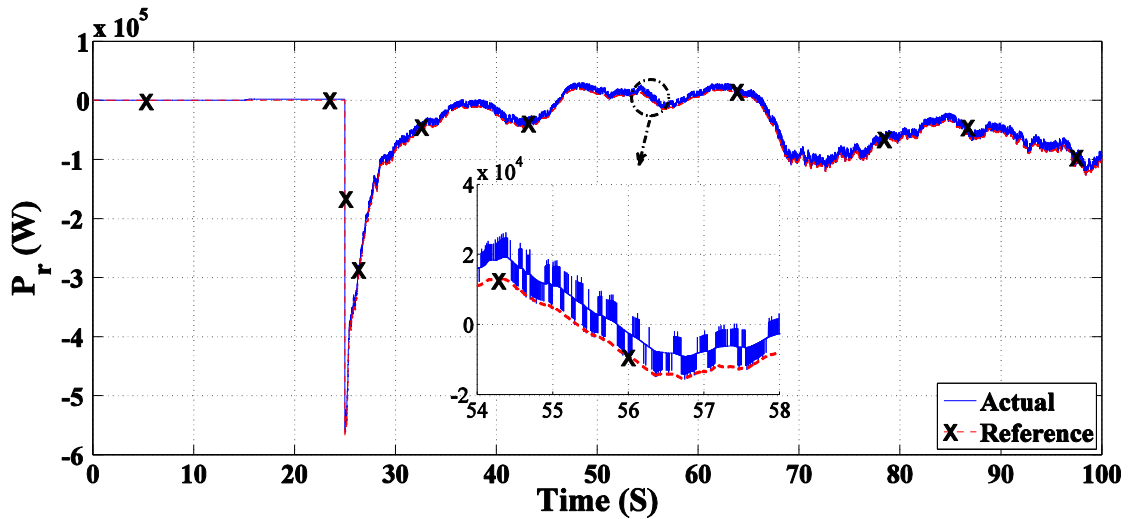


Figure 5.42: Rotor power P_r (W)

Figure (5.43) shows the steady-state waveform of the stator output phase voltage. The figure shows that the stator voltages are pure sinusoidal waveforms. Figure (5.44) shows the time variation of the magnitude of the stator phase voltage. The figure shows that the load voltage magnitude has a maximum excursion from its reference wave by 3.2 % for 4 seconds. The magnitude of the stator voltage slightly changes due to the continuous changes in the rotor currents for MPPT. Figure (5.45) shows that the frequency of the stator voltage is kept fixed at 50 Hz through the whole range of operation.

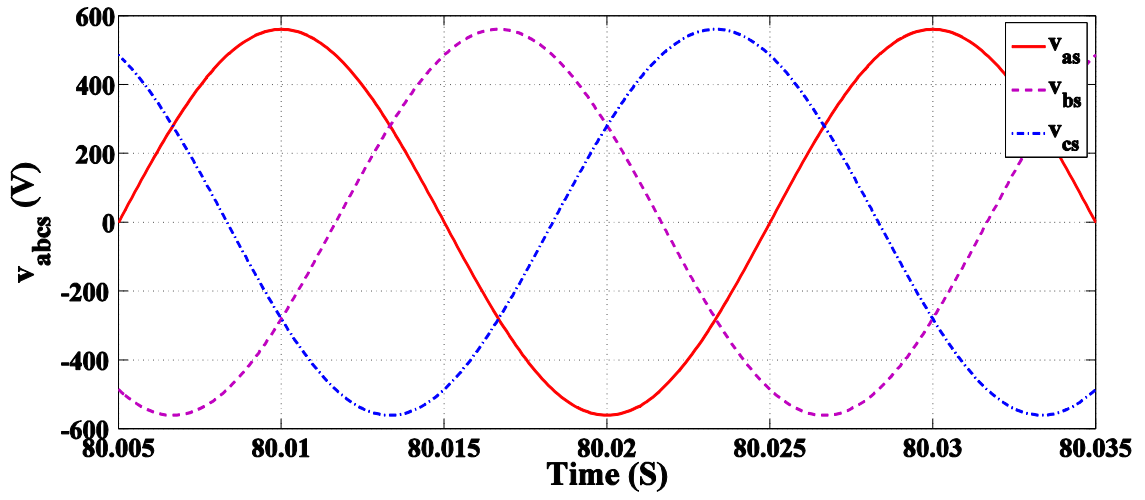


Figure 5.43: Instantaneous stator output voltage v_{abcS} (V) of DFIG

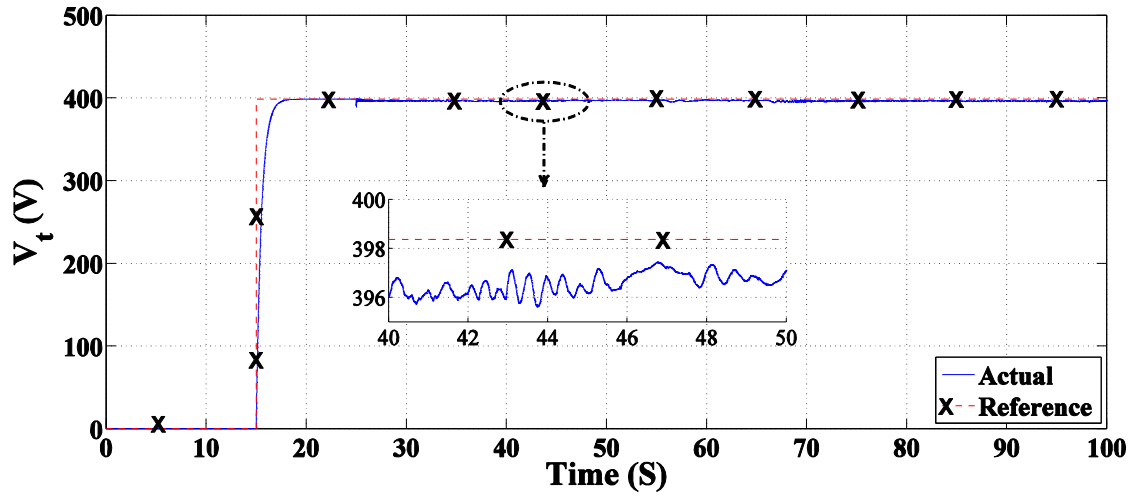


Figure 5.44: Stator rms terminal output voltage V_t (V)

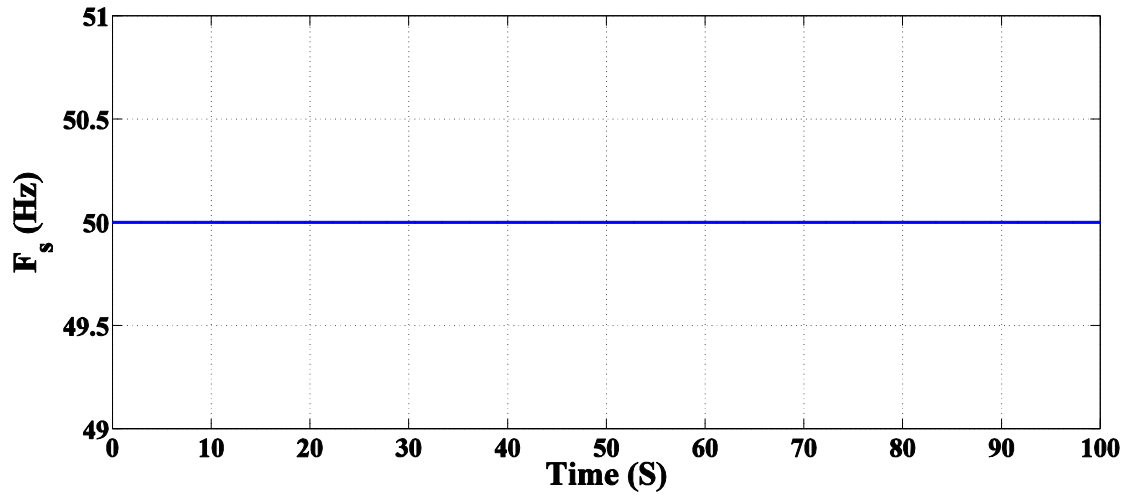


Figure 5.45: Stator output frequency F_s (Hz)

Figure (5.46) shows the stator output power and its reference power P_s (W). The oscillations of the power is due to applying MPPT on DFIG for the whole range of operation.

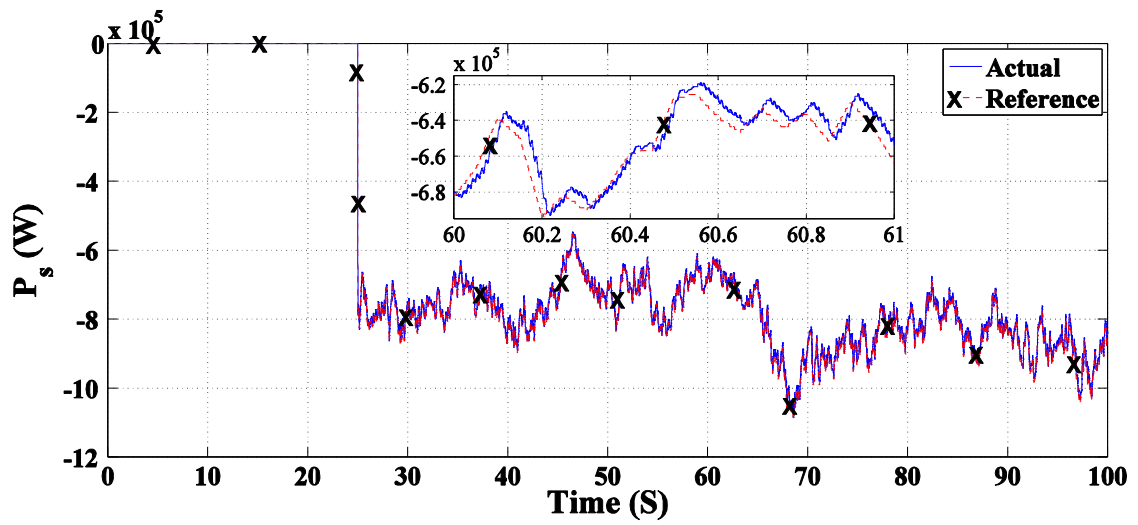


Figure 5.46: Stator output and reference power (W)

Chapter 6 : Conclusions and Future Works

6.1. Summary

Self-excited induction generators are not commonly used in autonomous wind energy sites because their output voltage and frequency change with the load variations. This problem is resolved in this thesis by using doubly fed induction generator (DFIG). It was shown that the DFIG has the advantage of producing constant load frequency and regulated load voltage irrespective of load variation and/or wind speed variation.

A wind energy conversion system consisting of the wind turbine, mechanical parts, DFIG and control system was presented as follows:

- 1- Wind turbine characteristics and modeling are presented then simulated by the help of MATLAB/SIMULINK. The required parameters are obtained at different wind speeds.
- 2- Dynamic modelling of DFIG is studied in abc reference frame and then in d-q synchronously rotating reference frame. The equivalent circuit is presented and all equations of DFIG are illustrated. By using MATLAB/SIMULINK the DFIG is modelled.
- 3- Vector control method is studied in indirect vector control and chosen to control the stand-alone DFIG. The control method is applied on DFIG in two modes of operation sub-synchronous and super-synchronous speed. The results are obtained by the help of MATLAB/SIMULINK.
- 4- MPPT technique is applied on DFIG at different wind speeds by using power characteristic curves control strategy. The results are obtained by the help of MATLAB/SIMULINK.

From the results it is shown that:

- 1- The constant load frequency is achieved by controlling the input of the rotor frequency such that a constant stator frequency is kept constant at any mechanical speed ($\omega_s = \omega_m \mp \omega_r$). The magnitude of the output voltage is controlled by adjusting the rotor input voltage and, hence, current.
- 2- The optimum operating mode of wind turbine, which is connected to the DFIG, is achieved by controlling the system to operate always at maximum power point. The tracking is done by using one of control algorithm used in maximum power point tracking called power signal feedback.
- 3- The capability of the proposed controller is verified and the operation is verified over a wide operating range including sub-synchronous and super-synchronous rotational speeds.

6.2. Future Works

All results on this thesis for MPPT are obtained by using open loop control system. The stability and dynamic performance of stand-alone DFIG can be improved by using closed loop control system.

Also the control method is applied on active power and resistive loads only. The control method could be applied on reactive power and for inductive and non-linear loads.

References

1. W. Qiao, "Integrated Control of Wind Farms, FACTS Devices and the Power Network Using Neural Networks and Adaptive Critic Designs", Georgia Institute of Technology, Ph.D. dissertation, July 2008.
2. H. S. Kim and D. D. Lu, "Wind Energy Conversion System from Electrical Perspective - A Survey", *Smart Grid and Renewable Energy*, vol. 1, no. 3, pp.119-131, Nov. 2010.
3. F. Mei, "Small Signal Modeling and Analysis of Doubly Fed Induction Generator in Wind Power Applications", Ph.D. dissertation, Control and Power Group Dept. of Electrical and Electronic Engineering Imperial College London University of London, 2008.
4. P. Gipe, *Wind Energy Comes of Age*, Johan Wiley & Sons, 1995.
5. www.cleanlineenergy.com
6. www.Wind-science.org
7. <http://centurionenergy.net/generator-types>
8. W. Cao, Y. Xie and Z. Tan, *Wind Turbine Generator Technologies*, ch. 7, *Advances in Wind Power*, 2012.
9. E.H. Camm, M. R. Behnke, O. Bolado, M. Bollen, M. Bradt, C. Brooks, W. Dilling, M. Edds, W. J. Hejdak, D. Houseman, S. Klein, F. Li, J. Li, P. Maibach, T. Nicolai, J. Patiño, S. V. Pasupulati, N. Samaan, S. Saylors, T. Siebert, T. Smith, M. Starke and R. Walling, "Characteristics of Wind Turbine Generators for Wind Power Plants", IEEE PES Wind Plant Collector System Design Working Group, 2009.
10. G. Abad, J. López, M. A. Rodríguez, L. Marroyo, G. Iwanski, *Doubly Fed Induction Machine Modeling and Control for Wind Energy Generation*, IEEE Press 445 Hoes Lane Piscataway, NJ 08854, 2011.
11. B. Pokharel, "Modeling, Control and Analysis of a Doubly Fed Induction Generator Based Wind Turbine System with Voltage Regulation", Tennessee Technological University, Master thesis, December 2011.
12. D. Seyoum, M.F. Rahman and C. Grantham, "Terminal Voltage Control of a Wind Turbine Driven Isolated Induction Generator Using Stator Oriented Field Control", IEEE 2003.
13. M. Rezkallah, A. Chandra, B. Singh, and M. El Kahel, "Vector Control of Squirrel-cage Induction Generator for Stand-Alone Wind Power Generation", IEEE 2012.
14. M. A. Al-Nuaim, "Study of Using Induction Generator in Wind Energy Applications", King Saud University, December 2005.
15. K. Vijayakumar, N. Kumaresan and N. Ammasai Gounden, "Operation and closed-loop control of wind-driven stand-alone doubly fed induction generators using a single inverter-battery system", *IET Electr. Power Appl.*, 2012, Vol. 6, Iss. 3, pp. 162–171.

16. M. G. Simões and F. A. Farret, *Modeling and Analysis with Induction Generators*, Power electronics and applications series, third edition, Taylor and Francis Group, 2015.
17. R.S. Pena, G. M. Asher, J.C. Clare and R. Cardenas, "A Constant Frequency Constant Voltage Variable Speed Stand Alone Wound Rotor Induction Generator", Opportunities and Advances in International Power Generation, 18-20th March 1996, Conference Publication No. 419, 0 IEE, 1996, pp 111-114.
18. T. Mesbahi, T. Ghennam and E.M. Berkouk, "A Doubly Fed Induction Generator for Wind Stand-Alone Power Applications (Simulation and Experimental Validation)", in International Conference on Electrical Machines (ICEM), 2012.
19. P. Ling, L. Yongdong, C. Jianyun and Y. Guofeng, "Vector Control of A Doubly Fed Induction Generator for Stand-Alone Ship Shaft Generator Systems", Proceeding of International Conference on Electrical Machines and Systems 2007, Oct. 8-11, Seoul, Korea, pp 1033-1036.
20. T. Daido, Y. Miura, T. Ise and Y. Sato, "Transient Characteristics for Load Changes of A Doubly-Fed Induction Generator Applied to Gas Engine Cogeneration System in Stand-alone Operation", IEEE 2012.
21. J. G. Slootweg, H. Polinder and W. L. Kling, "Representing Wind Turbine Electrical Generating Systems in Fundamental Frequency Simulations", IEEE transactions on energy conversion, vol. 18, No. 4, December 2003, pp 516-524.
22. S. Heier, *Grid Integration of Wind Energy*, third edition, 2014.
23. R. Bharanikumar, A.C. Yazhini and A. N. Kumar, "Modeling and Simulation of Wind Turbine Driven Permanent Magnet Generator with New MPPT Algorithm", Asian Power Electronics Journal, vol. 4 No. 2 August 2010.
24. H. Soleimani-Bidgoli, S. Afsharnia, M. R. Haqifam and S. V. Khatami, "An Efficient Controller Design of Doubly Fed Induction Generator and Operating Analysis of Isolated Microgrid under Load Variations", IEEE International Conference on Power and Energy (PECon2010), Nov 29 - Dec 1, 2010, Kuala Lumpur, Malaysia, pp 989-994.
25. B. K. Bose, *Modern Power Electronics: Evolution, Technology and Applications*, IEEE Press, January 1992.
26. R. Krishnan, *Electric Motor Drives: Modeling, Analysis, and Control*, Prentice Hall, Feb. 2001.
27. P. C. Krause, O. Wasynczuk, and S. D. Sudhoff, *Analysis of Electric Machinery and Drive Systems*, IEEE Press and Wiley Inter-Science, 2002.
28. C. M. Ong, *Dynamic Simulation of Electric Machinery Using MATLAB/Simulink*, Prentice Hall, 1998.
29. "Sensorless Field Oriented Control (FOC) for Permanent Magnet Synchronous Motors (PMSM)", Microchip Technology Incorporated, 2007.
30. B. Hopfensperger, D.J. Atkinson and R.A. Lakin, "Stator-Flux-Oriented Control of A Doubly-Fed Induction Machine With and Without Position Encoder", IEE Proc. Electr. Power Appl., Vol. 147, No. 4, July 2000.

31. W. Leonhard, *Control of Electrical Drives*, Third Edition, Springer-Verlag, 2001.
32. R. Pena, J. C. Clare and G.M Asher, "Doubly Fed Induction Generator Using Back-to-Back PWM Converter and Its Application to Variable Speed Wind Energy Generation", IEE Proc.-Electr. Power Appl, vol. 143, No. 3, May 1996, pp. 231-241.
33. Y. Tang and L. Xu, "A Flexible Active and Reactive Power Control Strategy for a Variable Speed Constant Frequency Generating System", IEEE Transactions on Power Electronics, Vol. 10, No. 4, July 1995.
34. D.H. Wang, C.V. Nayar and C. Wang, "Modeling of Stand-alone Variable Speed Diesel Generator using Doubly-Fed Induction Generator", 2nd IEEE International Symposium on Power Electronics for Distributed Generation Systems, 2010.
35. S. N. Bhadra, D. Kastha and S. Banerjee, *Wind Electrical Systems*, Oxford University Press 2005.
36. A. P. Varma and K. B. Chakri, "Study of Grid Connected Induction Generator for Wind Power Applications", Bachelor of Technology, National Institute of Technology, Rourkela, 2012.
37. O. Barambones, M. D. L. Sen and P. Alkorta, "A Robust Control of Double-Feed Induction Generator for Wind Power Generation", Industrial Electronics, 2009. IECON '09. 35th Annual Conference of IEEE, pp 94-99.
38. J. S. Thongam and M. Ouhrouche, *MPPT Control Methods in Wind Energy Conversion Systems*", ch. 15, Fundamental and Advanced Topics in Wind Power, 2011.
39. E. Koutroulis and K. Kalaitzakis, "Design of a Maximum Power Tracking System for Wind-Energy-Conversion Applications", IEEE Transactions on Industrial Electronics, Vol. 53, No. 2, April 2006.
40. M. A. Abdullah, A. H. M. Yatim, C. W. Tan and R. Saidur, "Renewable and Sustainable Energy Reviews", Elsevier Ltd., 2012.
41. L. Sun, Z. Mi, Y. Yu, T. Wu and H. Tian, "Active power and reactive power regulation capacity study of DFIG wind turbine", Int. Conf. Sustain. Power Gen. Supply, 2009, pp. 1-6.

الملخص

تعانى المولدات الحثية ذاتية التغذية من بعض المشاكل عندما تستخدم فى أنظمة تحويل طاقة الرياح ذات السرعات المتغيرة القائمة بذاتها. من أهم هذه المشاكل هو تغير قيمة وتردد جهد الخرج مع تغير سرعة الرياح.

تمت مناقشة تلك المشاكل فى هذه الرسالة وقد تبين أنه للتغلب عليها تم إستعمال المولدات الحثية ثنائية التغذية بدلاً من المولدات الحثية ذاتية التغذية فى تطبيقات أنظمة تحويل طاقة الرياح ذات السرعات المتغيرة القائمة بذاتها.

أولاً تمت دراسة ونمذجة الطاقة الهوائية والديناميكا الهوائية لتوربينات الرياح بواسطة المعادلات ومحاكاتها بواسطة الإستعانة ببرنامج MATLAB للتمكن من معرفة خصائص وأداء متغيرات توربينات الرياح مثل السرعة والعزم وقدرة الرياح وذلك عندما يتم توصيلها بالمولدات الكهربية. أيضاً تم إستعراض النمذجة الديناميكية للمولد الحثى ثنائى التغذية بواسطة المعادلات الكهربية ومحاكاتها بواسطة إستخدام برنامج MATLAB وذلك لدراسة أداء وخصائص المولد الكهبرى.

ثانياً تم ربط كلاً من توربينة الرياح والمولد الكهبرى معاً فى نظام واحد. بعد ذلك تمت دراسة أداء النظام فيما يتعلق بسرعة الرياح وما يصاحبه من تغير قيمة وتردد جهد الخرج والقدرة والكميات الكهربية الأخرى للمولد الكهبرى. أتضح أنه لكى يتم التحكم فى قيمة وتردد جهد الخرج وكذا القدرة الخارجة من المولد يجب التحكم دائماً فى جهد الدخل وقيمه وتردده والقدرة الداخلة او الخارجة للعضو الدوار للمحرك الحثى ثنائى التغذية مع التغير المستمر لسرعة الرياح. تم تطبيق التحكم الغير مباشر الإتجاهى على الكميات الكهربية للعضو الدوار وذلك للمحافظة على كلاً قيمة جهد الخرج والتردد ثابت بغض النظر عن تغيرات سرعة الرياح.

أخيراً ولأن سرعة الرياح تتغير هناك قيمة عظمى للقدرة يمكن الحصول عليها من المولد الحثى ثنائى التغذية عند كل قيمة من سرعة الرياح والمناظرة مع قيمة القدرة العظمى لتوربينات الرياح. وللتشغيل الأمثل للمولد الحثى ثنائى التغذية القائم بذاته تم تعقب هذه القيمة. ولقد أظهرت نتائج المحاكاه أن مخطط التحكم المقترح قادر على إبقاء كل من قيمة جهد الحمل وتردده مستقراً بغض النظر عن تغيرات سرعة الرياح.

أما عن أقسام هذه الرسالة فقد تم تقسيمها إلى ستة أبواب بالإضافة إلى المراجع نلخصها فيما يلي:

الباب الأول (المقدمة):

يوضح مراجعة شاملة لأنظمة طاقة توليد الرياح المختلفة الى طاقة كهربية ثم يعرض الدافع الى البحث وأهداف الرسالة والهيكل التنظيمي لها.

الباب الثاني (نمذجة توربينات الرياح):

يعرض مكونات أنظمة تحويل طاقة الرياح ومحاكاة توربينة الرياح لاستعمالها مع المولدات الكهربية لتوليد الطاقة الكهربية بواسطة برنامج MATLAB.

الباب الثالث (نمذجة المولد الحثي ثنائي التغذية):

يوضح شرح وفكرة عمل المولد الحثي ثنائي التغذية ومحاكات المعادلات الكهربية الخاصة به في النظام الديناميكي بواسطة برنامج MATLAB ودراسة الكميات الكهربية والميكانيكية المتعلقة.

الباب الرابع (التحكم وتتبع نقطة القدرة القصوى للمولد الحثي ثنائي التغذية القائم بذاته المستخدم في أنظمة تحويل طاقة الرياح):

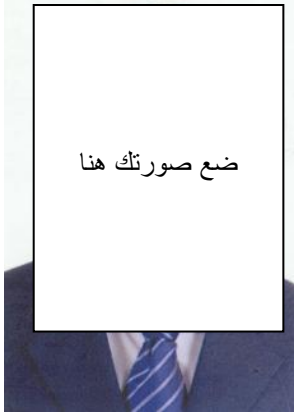
يعرض شرح وفكرة عمل طريقة التحكم الغير مباشر الإتجاهي المستخدمة مع المولد الحثي ثنائي التغذية وذلك عند سرعات متغيره للرياح للتحكم في جهد الخرج والتردد والقدرة للمولد وكيفية تعقب نقطة القدرة القصوى للمولد بإستخدام إحدى طرق تعقب نقطة القدرة القصوى مع الحفاظ في نفس الوقت على جهد الخرج والتردد للمولد ثابت مع التغيرات المصاحبة لسرعة الرياح.

الباب الخامس (المحاكاة بإستعمال برنامج MATLAB ونتائج المحاكاه):

يعرض هذا الباب المحاكاة لطريقة التحكم الغير مباشر الإتجاهي على المولد وتتبع نقطة القدرة القصوى عند سرعات الهواء المختلفة مع عرض النتائج التي تم التوصل اليها بواسطة محاكاة النظام ببرنامج MATLAB.

الباب السادس (الإستنتاجات والعمل المستقبلي):

يبين الإستنتاجات التي تم الحصول عليها من الرسالة والإقتراحات للعمل المستقبلي.



محمد محمود أنور محمد شعراوى

مهندس:

1987 / 12 / 28

تاريخ الميلاد:

مصرى

الجنسية:

2011 / 10 / 1

تاريخ التسجيل:

2016 / /

تاريخ المنح:

هندسة القوى والآلات الكهربائية

القسم:

ماجستير العلوم

الدرجة:

المشرفون:

أ.د. عادل شلتوت

أ.د. ناصر محمد بيومى عبدالرحيم (أستاذ إلكترونيات القوى - قسم الهندسة الكهربائية - كلية الهندسة بشبرا - جامعة بنها)

الممتحنون:

أ.د. فهمى متولى أحمد بندارى (الممتحن الخارجي) (أستاذ نظم القوى الكهربائية والتحكم الآلى - قسم الهندسة الكهربائية - كلية الهندسة بشبرا - جامعة بنها)

أ.د. محمود محمد محمود عبدالحكيم (الممتحن الداخلي)

أ.د. عادل شلتوت (المشرف الرئيسي)

أ.د. ناصر محمد بيومى عبدالرحيم (عضو) (أستاذ إلكترونيات القوى - قسم الهندسة

الكهربائية - كلية الهندسة بشبرا - جامعة بنها)

عنوان الرسالة:

التحكم فى الجهد والتردد للمولدات الحثية ثنائية التغذية القائمة بذاتها لتطبيقات أنظمة تحويل طاقة الرياح ذات السرعات المتغيرة.

الكلمات الدالة:

أنظمة تحويل طاقة الرياح القائمة بذاتها ، نمذجة توربينات الرياح ، نمذجة المولدات الحثية ثنائية التغذية ، التحكم الغير مباشر الإتجاهى ، تتبع نقطة القدرة القصوى.

ملخص الرسالة:

تعانى المولدات الحثية ذاتية التغذية من مشاكل تغير جهد الخرج وتردده عندما تستخدم فى أنظمة تحويل طاقة الرياح ذات سرعات الرياح المتغيرة القائمة بذاتها. تمت مناقشة تلك المشاكل فى هذه الرسالة وللتغلب عليها تم إستعمال المولدات الحثية ثنائية التغذية بدلاً من المولدات الحثية ذاتية التغذية . وقد تم إقتراح طريقة التحكم فى تردد وقيمة جهد التغذية للعضو الدوار بما يمكن من التحكم فى تردد وقيمة جهد الخرج للمولد وقدم أمكن تحقيق ذلك عند كل السرعات التى يعمل عندها المولد. كما تم تطبيق نظام تتبع نقطة القدرة القصوى على المولد كى يتمكن من تشغيله دائماً عند نقطة التشغيل المثالية.

التحكم فى الجهد والتردد للمولدات الحثية ثنائية التغذية القائمة بذاتها لتطبيقات أنظمة
تحويل طاقة الرياح ذات السرعات المتغيرة

إعداد

محمد محمود أنور محمد شعراوى

رسالة مقدمة إلى كلية الهندسة – جامعة القاهرة
كجزء من متطلبات الحصول على درجة ماجستير العلوم
في
هندسة القوى والآلات الكهربائية

يعتمد من لجنة الممتحنين:

الأستاذ الدكتور: عادل شلتوت

المشرف الرئيسى

الأستاذ الدكتور: ناصر محمد بيومى عبدالرحيم

عضو

الأستاذ الدكتور: محمود محمد محمود عبدالحكيم

الممتحن الداخلى

الأستاذ الدكتور: فهمى متولى أحمد بندارى

أستاذ نظم القوى الكهربائية والتحكم الآلى – قسم الهندسة الكهربائية – كلية الهندسة بشبرا – جامعة
بنها.

كلية الهندسة - جامعة القاهرة

الجيزة - جمهورية مصر العربية

2016

التحكم فى الجهد والتردد للمولدات الحثية ثنائية التغذية القائمة بذاتها لتطبيقات أنظمة
تحويل طاقة الرياح ذات السرعات المتغيرة

إعداد

محمد محمود أنور محمد شعراوى

رسالة مقدمة إلى كلية الهندسة – جامعة القاهرة
كجزء من متطلبات الحصول على درجة ماجستير العلوم
في
هندسة القوى والآلات الكهربائية

تحت إشراف

أ.د. ناصر محمد بيومى عبدالرحيم
قسم الهندسة الكهربائية
كلية الهندسة بشبرا – جامعة بنها

أ.د. عادل شلتوت
قسم هندسة القوى والآلات الكهربائية
كلية الهندسة – جامعة القاهرة

كلية الهندسة - جامعة القاهرة
الجيزة - جمهورية مصر العربية

2016



التحكم فى الجهد والتردد للمولدات الحثية ثنائية التغذية القائمة بذاتها لتطبيقات أنظمة تحويل طاقة الرياح ذات السرعات المتغيرة

إعداد

محمد محمود أنور محمد شعراوى

رسالة مقدمة إلى كلية الهندسة – جامعة القاهرة
كجزء من متطلبات الحصول على درجة ماجستير العلوم
في
هندسة القوى والآلات الكهربائية

كلية الهندسة - جامعة القاهرة
الجيزة - جمهورية مصر العربية

2016